

Alma Mater Studiorum – Università di Bologna

DOTTORATO DI RICERCA IN

Scienze Biomediche

Ciclo XXIX

Settore Concorsuale di afferenza: 05/E1

Settore Scientifico disciplinare: BIO/12

Melanopsin retinal ganglion cells in patients with
Leber hereditary optic neuropathy: an fMRI study of brain
activations under monochromatic light stimulations

Presentata da: Dott.ssa Stefania Evangelisti

Coordinatore Dottorato

Relatore

Prof. Lucio Ildebrando Cocco

Prof. Raffaele Lodi

Esame finale anno 2017

Abstract

The current PhD thesis focused on a project that investigated brain responses to monochromatic light stimulation, as assessed by functional magnetic resonance imaging (fMRI), in a population of patients with Leber hereditary optic neuropathy (LHON). In particular, the aim was to explore a possible role of melanopsin retinal ganglion cells (mRGCs) in visual processes and to assess their role in modulating brain responses during cognitive tasks, as in LHON patients it has been shown that mRGCs are relatively spared despite the general RGCs degeneration. Eleven LHON patients, and eleven matched healthy controls, underwent an fMRI protocol (1.5T MR scanner) that included purely visual stimulation and the combination of a sustained attention task and light stimulation, both with blue (480nm) and red (620nm) light exposures of equivalent photon flux ($5 \times 10^{13} \text{ph cm}^{-2} \text{s}^{-1}$).

Overall, lower activations of primary visual cortex in response to purely visual stimuli were observed in LHON compared to healthy subjects, and this is in line with the disease. When considering sustained brain response to monochromatic light stimuli (of 10 and 50s of duration), a higher cortical activity was found in LHON in response to blue rather than to red light, and only when considering blue light no differences between the two groups were observed. Moreover, a prominent modulation of brain responses to a cognitive sustained attention task was found under blue light exposure compared to the red one, both in cortical and subcortical areas.

These results provide support to the relatively new hypothesis of melanopsin role in visual processes, and they give a confirmation of the maintained functionality of mRGCs in modulating brain activity during cognitive engagement for LHON patients, as it was previously shown for healthy subjects.

Contents

1	Introduction	1
1.1	The photopigment melanopsin	1
1.1.1	Discovery of a third photoreceptor system	1
1.1.2	Melanopsin and melanopsin-expressing RGCs	2
1.1.3	Melanopsin-expressing RGCs central projections	3
1.1.4	Melanopsin-expressing RGCs functions	6
1.2	Leber’s hereditary optic neuropathy	7
1.2.1	Melanopsin-expressing RGCs in LHON patients	8
1.3	Functional magnetic resonance imaging	10
1.4	Previous MR studies in LHON patients	11
1.5	Light stimulation and cognitive brain functions	13
1.6	Aim of the study	17
2	Methods	19
2.1	Subjects	19
2.2	Protocol	20
2.3	fMRI paradigms	21
2.3.1	Pure visual paradigm	21
2.3.2	Visual pattern paradigm	22
2.3.3	Visual cognitive paradigm	22
2.4	Light exposure	25
2.4.1	Light exposure hazards	26
2.5	Demographic and behavioural data analysis	27
2.6	fMRI data acquisition	28
2.7	fMRI data analysis	28
2.7.1	Structural evaluation	30

3	Results	31
3.1	Demographic and clinical results	31
3.2	Light exposure setup preliminary measures	33
3.3	Behavioural data	37
3.3.1	Visual 2afc	37
3.3.2	N-back cognitive task	37
3.4	fMRI results	40
3.4.1	Pure visual paradigm	40
3.4.2	Visual pattern paradigm	46
3.4.3	Visual cognitive paradigm	56
3.5	Structural evaluation (VBM)	67
3.6	fMRI results with structural correction	68
3.6.1	Pure visual paradigm	69
3.6.2	Visual pattern paradigm	70
4	Discussion	75
5	Conclusions and future developments	81
	Bibliography	83

Chapter 1

Introduction

1.1 The photopigment melanopsin

1.1.1 Discovery of a third photoreceptor system

The photoreceptor system of the mammalian retina was thought to be made by two classes of photoreceptors, rods and cones. However, between the late 1990s and early 2000s a third mammalian photoreceptor system, that differs considerably from rods and cones, was discovered [1]. The first hypothesis about the existence of some other photoreceptive cells in the retina dates back to the first half of 1900s, when Keeler observed that mice with severe outer retina degeneration, i.e. functionally blind, had functioning pupil constriction in response to light [2, 3]. Although Keeler's prediction of a novel ocular photoreceptor, the explanation for these pupil reflexes to be driven by a small number of rods and cones prevailed, at least until the discovery of a new light-sensitive molecule. This discovery was made by Provencio and colleagues, when studying the photosensitive skin cells of frogs [4]. This novel opsin-like molecule they had cloned, and that they called melanopsin, was then also found to be expressed in a subset of retinal ganglion cells (RGCs) in mouse and human retinas as well [4–6]. Further studies showed that these melanopsin-expressing cells send projections to the suprachiasmatic nucleus (SCN), that is the site of mammalian central circadian clock [7]. Even if these findings supported the hypothesis that mRGCs could be the third photoreceptor system predicted years before, definitive proof that these melanopsin-expressing and SCN-projecting RGCs could be directly sensitive to light was still lacking. This confirmation firstly came from Berson and colleagues, by combining electrophysiology and tracer injections into the SCN [8]. With whole-cell recordings from RGCs (retrogradely labelled by the tracers) they found responses to light from these cells when all rod/cone signalling was eliminated with drugs. The presence of melanopsin in these SCN-projecting

cells was also confirmed with immunohistochemistry performed after whole-cell recording [9].

1.1.2 Melanopsin and melanopsin-expressing RGCs

The capacity of mRGCs to respond directly to light is indeed due to their expression of melanopsin; the melanopsin gene (*opn4*) has been found in many mammalian species, e.g. mice, monkeys, and humans [5].

The physiological characteristics of the intrinsic light response of mRGCs are different from those of rods and cones. Rods and cones hyperpolarize to light, whereas the direct photoresponse of mRGCs is depolarizing. mRGCs have a lower sensitivity to light than the classical photoreceptors, and their signal response have a much slower kinetics [8, 10]. They are also able to maintain very long-lasting light response, therefore encoding light stimuli over relatively long periods of time. A striking feature of mRGCs physiology is that their dendrites contain melanopsin and are able to respond directly to light [8]. These features are in line with mRGCs' role in signalling diffuse environment light levels over long period of time for tonic non-image forming visual functions, such as pupillary reflex and photoentrainment. A further difference between mRGCs and classical photoreceptors is their action spectrum, i.e. their wavelength-sensitivity function. As they utilize melanopsin as photopigment, mRGCs have their maximum sensitivity to light around 480nm, i.e. blue light (Figure 1.1), significantly different (more than 20nm) from the wavelengths of maximum sensitivity of rods and cones [8, 11, 12]. One more difference is in the fact that rods and cones transduce mediated ciliary photoreceptors, typical of vertebrate, whereas melanopsin shares structural homology and signal transduction mechanism typical of invertebrate rhabdometric photopigments. Similarly to fly rhodopsins, melanopsin exhibits a dual-state photosensitive flip-flop behaviour, in which light drives both the phototransduction responses, mainly blue light, and the chromophore photoregeneration, mainly red light [4, 13–16]. This behaviour was also corroborated by *in vivo* studies, in particular More and colleagues explored this hypothesis in humans by investigating pupillary light reflex [17, 18]. The properties of a bistable photopigment were confirmed, and may confer a new form of “photic memory” since information of prior light stimulation is retained and influences subsequent responses to light.

Initially, mRGCs appeared to be homogeneous from the morphological point of view, and were considered as a single cell type. However, subsequent studies, by using various advanced fluorescent labelling techniques, disclosed the existence of at least five distinct morphological types of mRGCs in the mouse retina. The SCN-projecting type originally described is now referred to as “M1”, and the new types are called M2, M3, M4, M5 [19–21]. Beyond

morphology, these five types exhibit different physiological and biophysical properties, such as spiking spontaneously at different frequencies or having different membrane resistance or capacitance [22–25], and this suggest they may perform different functions. Diversity, for example, was observed in responses to moving lights and to light spots of different sizes, and if all five cell types signalled more intensely to moving lights than to static ones, different cells type seemed to be tuned to different speeds of motion [24]. These five types of mRGCs generated melanopsin-based light responses, when the signalling from rods and cones was blocked, that are different in kinetics, amplitude and threshold, and M1 cells exhibited the fastest, largest and most sensitive intrinsic photoresponses [25, 24, 21, 22, 26]. Other species besides mice and rats have been examined, and seemed to have also multiple subtypes of mRGCs, but it is not known yet whether the number of five is confirmed. In primates, including humans, only two types of mRGCs were morphologically identified [11, 27].

Despite the ability of mRGCs to function as photoreceptors, they also receive intra-retinal synaptic input from rod/cone-driven circuits, as revealed by electron microscopy studies [28]. Therefore, it is important to keep in consideration that mRGCs respond to light directly thanks to melanopsin but also indirectly through input from rods and cones that are mediated by synapses [11, 29–31, 24]. Even if the results from rods and cones missing mice or blind people demonstrate that rods and cones are not required for photoentrainment or pupillary reflex, it is not possible to conclude that rods and cones play no role at all. Evidence of rods, cones and mRGCs interaction exists, and recent studies focused on trying to disentangle specific roles played by each photoreceptor system in irradiance detection [32–34], but still further investigations and confirmations are needed.

1.1.3 Melanopsin-expressing RGCs central projections

Hattar and colleagues [36] visualized the axons of M1-type mRGCs in a transgenic line of mouse and managed to better characterized mRGCs projections throughout the brain. They confirmed the already established targets, such as the suprachiasmatic nucleus (SCN), the intergeniculate leaflet (IGL), the olivary pretectal nucleus (OPN), the ventral part of the lateral geniculate nucleus (LGv) and preoptic area, in line with mRGCs contribution to photic synchronization of circadian rhythms and pupillary light reflex. Nevertheless, the comprehensive projections were more widespread, suggesting a diverse array of non-image forming visual functions. They included the lateral nucleus, peri-supraoptic nucleus, subparaventricular area of the hypothalamus, medial amygdala, lateral habenula, posterior limitans nucleus, superior colliculus and periaqueductal gray, and weaker projections were also observed to the dorsal lateral geniculate nucleus (Figure 1.2). More recently, the same group [21] used a more sensitive melanopsin reporter mouse line in order to label all five

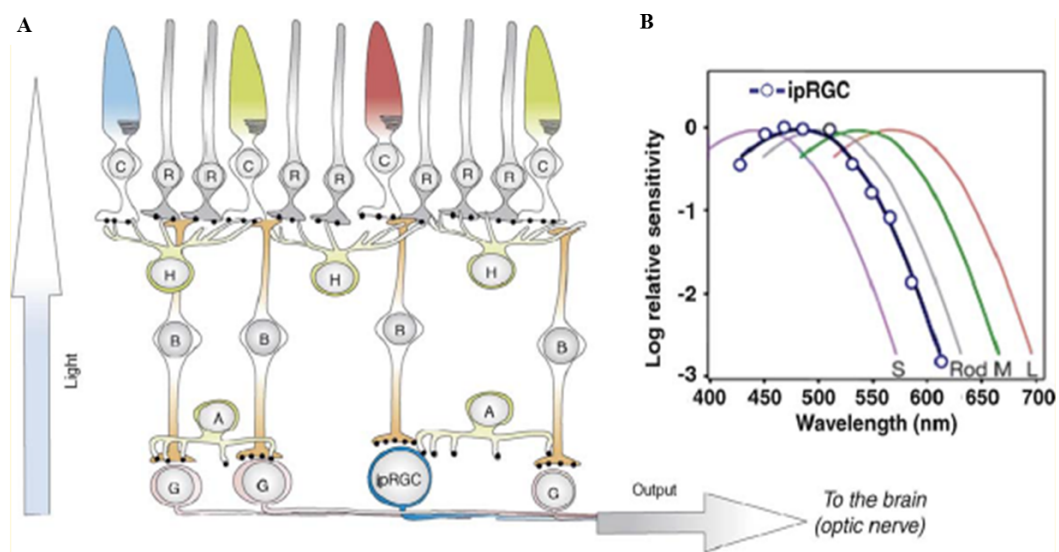


Figure 1.1 A - Schematic representation of retinal cells and their organization (A: amacrine cells, B: bipolar cells, C: cones, G: ganglion cells, H: horizontal cells, ipRGC: intrinsically photosensitive retinal ganglion cells, R: rods,) B - Wavelength sensitivities of short wavelength cones (S), medium wavelength cones (M), long wavelength cones (L), rods (Rod) and melanopsin expressing retinal ganglion cells (ipRGC). (Adapted from [35]).

mRGCs subtypes, and they managed to detect pronounced projections to two more visual nuclei: the dorsal division of the lateral geniculate nucleus (LGN) and the superior colliculus (SC). The former is the primary thalamic relay site of retinal input to the visual cortex, while the latter is a sensorimotor nucleus that detects novel visual stimuli. Moreover, retrograde and anterograde labelling showed that mRGCs projections to LGN and SC exist in primate as well [11, 37]. These results suggest that mRGCs may play a role also in conscious visual perception, in addition to their well-known role in regulating non-image forming visual functions. Electrophysiological and behavioural studies gave strong support to this hypothesis as well (see 1.1.4).

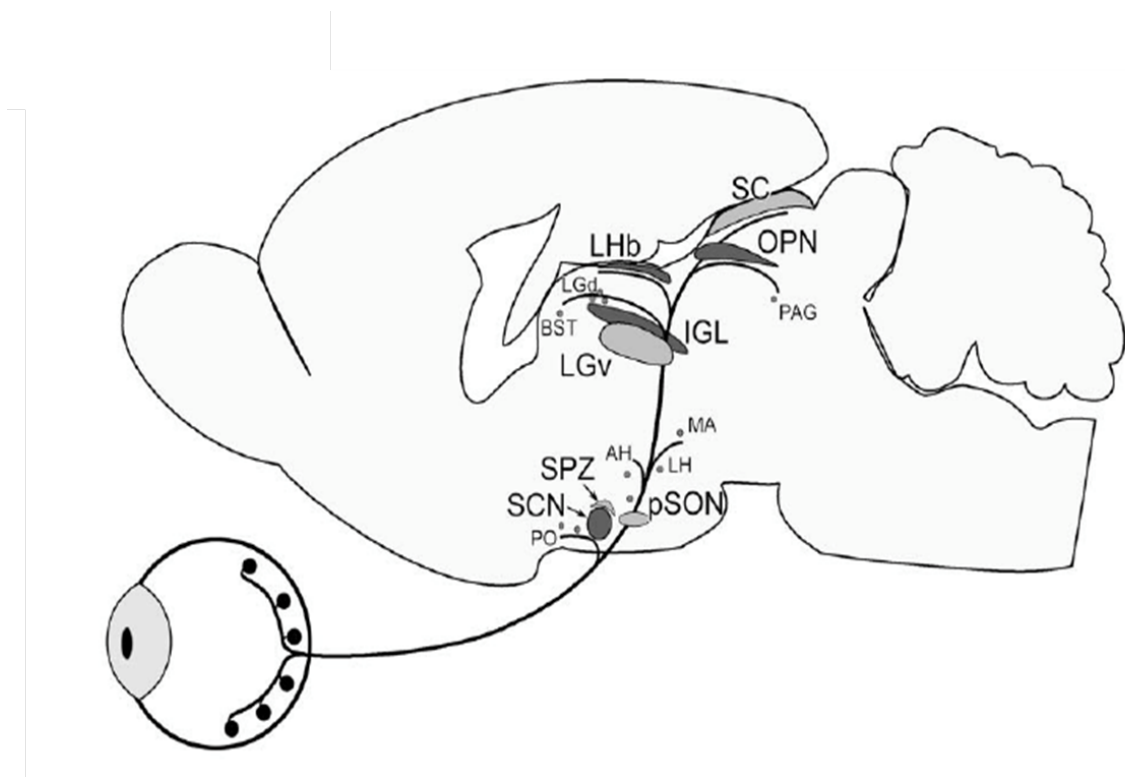


Figure 1.2 Schematic representation of mRGCs projections nuclear targets in mice (AH: anterior hypothalamic nucleus, BST: bed nucleus of the stria terminalis, IGL: intergeniculate leaflet, LGd: lateral geniculate nucleus (dorsal), LGv: lateral geniculate nucleus (ventral), LH: lateral hypothalamus, LHb: lateral habenula, MA: medial amygdaloid nucleus, OPN: olivary pretectal nucleus, PAG: periaqueductal gray, PO: preoptic area, pSON: peri-supraoptic nucleus, SC: superior colliculus, SCN: supra-chiasmatic nucleus, SPZ: subparaventricular zone). (Adapted from [36]).

1.1.4 Melanopsin-expressing RGCs functions

Circadian rhythms, i.e. daily rhythms in mammalian physiology and behaviour, are controlled by cells in the SCN of the hypothalamus and are based on a molecular clock that regulates daily changes in behaviour such as sleep-wake cycles and core body temperature. This clock is adjusted to changes in the environmental light/dark phases, and mRGCs are the primary cells that carry the signal of light as a circadian entrainment cue. Melanopsin-knockout animals are almost insensitive to light pulses in changing their circadian rhythms phase shifts [38]. To regulate circadian rhythms throughout the body, the SCN regulates secretion of melatonin, a hormone involved in sleep promotion that is released from the pineal gland only during subjective night. If exposed to sufficiently intense light, inputs from mRGCs can suppress this release [39–41], and as their photosensitivity remains in the absence of rods and cones, also mice without rod-cone system and some blind patients still exhibit this kind of response [42–44]. Projections of mRGCs to the OPN suggest their responsibility for light-evoked pupil constriction, as the OPN is the retino-recipient site responsible for the pupillary light reflexes. Indeed, when investigating pupillary light reflex in melanopsin-knockout animals it is diminished at high irradiance level, and even in mice with functional rods or cones but melanopsin knockout the ability to constrict pupils in response to light was lost [45–47]. Moreover, various further non-image forming photic response have been shown to be mediated by mRGCs, at least partly. Just to give few examples, suppression of the nocturnal locomotor activity of mice [48], light-induction of sleep [49–52] and maintenance of light-induced sleep in mice [53], modulation of brain response to cognitive stimuli in humans [54, 55], modulation of alertness in humans [56], antidepressant effect in rats [57] and humans [58], light-induced exacerbation of headache in humans [59], light-dependent relaxation of blood vessels [60], and stimulation of the secretion of follicle-stimulating hormone in women [61].

Among the most recent and intriguing evidences of new melanopsin role, there is melanopsin contribution to visual perception [62]. This is presumably mediated by mRGCs projections to LGN and SC [11, 63, 21, 26, 24] and it is supported by a series of studies in mice and humans [64–67]. Blind patients with severe degeneration of the outer retina, but relatively intact mRGCs system, had a basic ability to detect the presence of intense blue light [44]. Mice with normal melanopsin photoreception but lacking rods and cones functionalities were able to distinguish black and white stripes from a uniform gray background of equal mean intensity, supporting the hypothesis that melanopsin can be sufficient for a certain level of pattern vision [21]. A preliminary psychophysical evidence of a direct contribution of melanopsin to colour vision in humans exists [68], and melanopsin-knockout mice were shown to have deficits in contrast sensitivity [69].

1.2 Leber's hereditary optic neuropathy

Leber's hereditary optic neuropathy (LHON) is a mitochondrial genetic disease that manifests preferentially in young adult males with acute or subacute loss of central vision, due to focal degeneration of the retinal ganglion cell layer in the retina and of the optic nerve [70]. Its first description as a distinctive clinical entity dates back to 1871, and it was done by the German ophthalmologist Theodore Leber [71]. Since the earliest studies some of the salient features of the disease became clear: the maternal transmission, the marked gender predilection (with males more likely to become affected than females) and the almost exclusive involvement of the optic nerve. Later, further knowledge about the mitochondrial genome gave the possibility to establish that a mitochondrial DNA mutation was the causative factor in LHON. The first point mutation in mitochondrial DNA in LHON patients was reported in 1988 [72]. Three mitochondrial DNA point mutations have been then identified as primarily cause for LHON (over 95% of cases): G3460A, G11778A and T14484C, which all involve genes encoding complex I subunits of the respiratory chain, and LHON became a paradigm of mitochondrial optic neuropathies [73]. However, about only 50% of males and 10% of females who harbour a pathogenetic mitochondrial DNA mutation actually develop the optic neuropathy. Therefore, additional mitochondrial and/or nuclear generic factors or even environmental factors might be modulating the phenotypic expression of LHON.

The prevalence of the LHON is not fully clearly defined. As for European studies, an estimated prevalence is 1 in 25000 of British population (in the north east of England) has been described [74]. An entire-population-based survey of epidemiology and penetrance of LHON was made in Finland as well, and it showed that LHON prevalence in Finland is 1:50000 and 1 in 9000 Finns is a carrier of one of the three LHON primary mutations [75]. More recently, a meta-analysis [76] of primary reports with LHON prevalence data reported for Europe was carried out, and the estimated prevalence of LHON associated with the combined m.11778G>A, m.14484T>C, m.3460G>A mutations was about 1:45000. Although this meta-analysis, there is still a lack of reliable primary epidemiologic data for this neuropathy.

LHON age of onset is typically between 18 and 35 years. Initially, a painless and rapid central vision loss occurs usually in one eye. This is often associated with fading of colours in the one eye, followed by analogous involvement of the other eye within days, months, or rarely years. The vision loss can be sudden (leading to acuity lower than 20/400 in less than a week) or progressive over 2 or 3 months. Final visual acuity ranges from 20/400 to no light perception. The characteristic field defect in LHON is centrocaecal scotoma. Fundus examination can be normal at the onset of LHON, however in the acute/subacute stages, at the fundus examination the optic disc can appear hyperaemic, occasionally with peripapillar

haemorrhages. Axonal loss in the papillomacular bundle rapidly leads to atrophy of the optic disc [73]. Pupillary reflexes are preserved and no pain on eye movement is usually reported by LHON patients [77, 78]. Typically, at the endpoint of the disease an optic atrophy with permanent severe loss of central vision is present, but with relative preservation of pupillary light responses. Visual loss is often permanent, however, spontaneous improvements have occasionally been observed.

As for the pathophysiology of LHON, it is intriguingly based on the fact that mitochondrial mutations cause defects in several oxidoreductase chain complexes and this is thought to impair glutamate transport and increase reactive oxygen species production. This leads to retinal ganglion cell degeneration through apoptosis, though it is unclear why these cells are particularly vulnerable. Further investigations are needed to clarify LHON pathophysiology, and hopefully the development of faithful animal models (a number of vertebrate and invertebrate disease models that have recently been established) will help to circumvent the lack of human tissues [79]. No generally accepted measures have been shown to prevent or delay blindness onset in LHON, and as for medical treatment, the options are limited, and the only clinically proven treatment is Idebenone, as it leads to improve energy supply and functional recovery of retinal ganglion cells in the acute stage of the disease. Gene therapy trials are currently underway [79, 80].

1.2.1 Melanopsin-expressing RGCs in LHON patients

In the visual system of LHON patients rods and cones are preserved, as the neuropathy degeneration selectively affect retinal ganglion cells. Despite the general loss of RGCs, the subset of melanopsin-expressing RGCs are relatively preserved [81], Figure 1.3. This was assessed by confirming the integrity of retinohypothalamic tract in five LHON patients by investigating the light-induced suppression of nocturnal melatonin secretion. Moreover, also the histologic evaluation of port-mortem eyes from two LHON patients was performed and it showed that in patients mRGCs are relatively spared in comparison with the massive loss of total RGCs. These cells therefore resist the neurodegeneration caused by the mitochondrial dysfunction and their functions in non-image-forming processes are maintained in these visually impaired patients. This is in line with the preservation of pupillary light reaction in LHON patients. In agreement with this findings, a previous study [82] in a case of LHON showed minimal reduction in pupil contraction amplitude to blue light, that specifically stimulate mRGCs. A further study by the same group gave further confirmation of selective preservation of mRGCs by showing that pupillary light reflex in LHON was overall maintained [83].

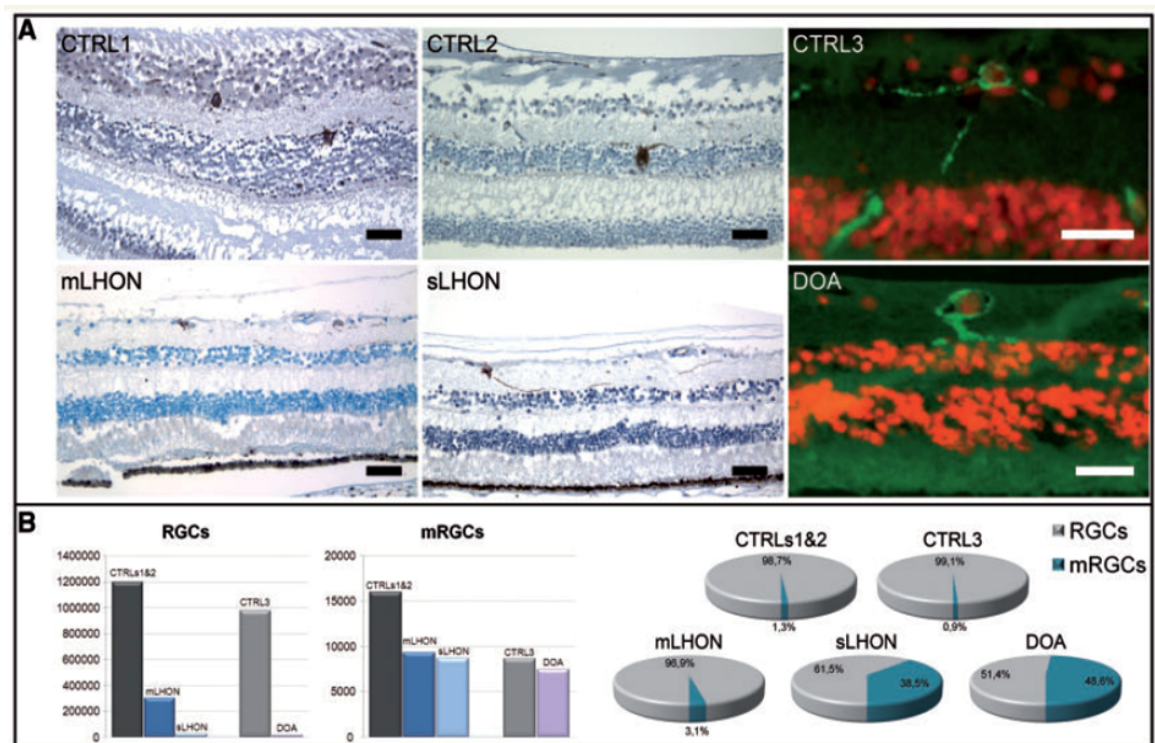


Figure 1.3 Melanopsin cells in healthy controls and optic neuropathy retinas (CTRL: healthy controls, mLHON: mild LHON patient, sLHON: severe LHON patient, DOA: dominant optic atrophy). A - Examples of brown-stained mRGCs (in CTRL1, CTRL2, mLHON, sLHON) and staining by immunofluorescence (CTRL3, DOA). B - From left to right, axonal (RGCs) and mRGC count, and mRGC/RGC ratios. (Adapted from [81]).

1.3 Functional magnetic resonance imaging

Functional magnetic resonance imaging (fMRI) is a non-invasive in vivo advanced MRI technique, that can provide an indirect measure of brain activity [84]. It was introduced for the first time in 1990 [85, 86], and since then it has become a key method for neurosciences thanks to the possibility to give insights into brain activity with a good spatial resolution and whole brain coverage. fMRI can detect blood oxygen level dependent (BOLD) signal change reflecting metabolically active brain areas in relation to a specific stimulus or event and in resting state condition.

A remarkable feature of brain metabolism is that blood flow and energy metabolism are tightly linked to local neuronal activity, therefore maps of local glucose consumption, local oxygen consumption or local blood flow may provide information on neuronal activity. Normal brain energy production depends ultimately on oxidative metabolism (as neural activity is accompanied by ATP, adenosine tri-phosphate, expenditure and by a consequently increased ATP production via glucose consumption), therefore there is greater local demand for delivery of oxygen with increased synaptic activity. To meet this increased metabolic demand, neuronal activation is accompanied by increased local blood flow [84]. This neuro-vascular coupling is the crucial physiological principle fMRI is based on. Image contrast arises as a consequence of the higher ratio of oxy- to deoxyhaemoglobin in local draining venules and veins that accompanies neuronal activation. BOLD signal changes depends on the combined changes in CBF (Cerebral Blood Flow), CMRO₂ (Cerebral Metabolic Rate of Oxygen) and CBV (Cerebral Blood Volume); this complicates the interpretation of BOLD signal in terms of physiological variables. There are also changes in the local oxygen concentration which initially falls due to consumption, and then rises above its baseline value when the increased blood flow brings in more oxygen and, concomitantly, there are changes in the levels of oxygenated and deoxygenated haemoglobin. The different magnetic properties of these molecules provide the basis of the BOLD signal, as the image contrast arises from changes in the local magnetic susceptibility. The MR signal in T2* weighted images is strongly influenced by the oxygenation state of the blood. The rate of loss of proton spin phase coherence is a measure of T2 and local magnetic field homogeneity (T2*) and this can be modulated by the presence of intravoxel deoxyhaemoglobin. When bound to oxygen, haemoglobin is diamagnetic, while deoxygenated haemoglobin is paramagnetic. Magnetic flux is reduced in diamagnetic materials while paramagnetic materials have an increased magnetic flux: a change in haemoglobin oxygenation therefore leads to changes in the local distortions of a magnetic field applied to it, and consequent changes in the rate of loss of proton spin phase coherence. Thus, the size of the BOLD fMRI signal is determined by the difference between the amount of blood flow increase, which increases the signal, and the

use of O₂ by neurons, which reduces the signal. This technique supplies an indirect measure of brain activity as it doesn't measure directly electric activity but it measures a consequence of brain metabolism, with temporal resolution of some seconds, and a spatial resolution in the order of millimetres. As for the acquisition is concerned, a good balance between different factors is required: signal-to-noise ratio, BOLD contrast, whole brain coverage, imaging speed (as a temporal resolution of a few seconds, at maximum, is necessary to properly characterize the haemodynamic response), spatial resolution. As BOLD contrast arises from effects of field inhomogeneity, it is crucial to use a sequence that is sensitive to them, therefore typically a Gradient Echo sequence. To speed up the acquisition, the most used method of acquisition is the Echo Planar Imaging (EPI), which is based on the concept of deriving multiple echoes from a single excitation pulse, altering the pulse sequence such that n-echoes encode n lines of k-space in a single image.

1.4 Previous MR studies in LHON patients

Leber hereditary optic neuropathy is a rare disease, and MR imaging investigation has been relatively limited so far. Mainly, the MR studies that can be found in literature focused on white matter alterations, most often focusing in area specifically involved in the visual pathways.

Inglese and colleagues [87] looked at the integrity of optic radiations and calcarine cortex with magnetization transfer and diffusion tensor MRI, and found no abnormalities at the macroscopic level, nor at the microscopic one, as revealed by MT ratio, average diffusivity and fractional anisotropy. In a different study the same group [88] showed lower values of optic nerve volumes and MT ratio in LHON, as well as mean normal appearing brain tissue MTR histogram peak height and average diffusivity, while no differences were found for any of the cervical cord MTR histogram derived measures.

To describe the topographical pattern of damage to the brain white matter tracts, diffusion tensor model and tract-based spatial statistics have been applied [89] and they revealed lower fractional anisotropy and higher mean diffusivity (and radial diffusivity) exclusively in the optic tracts and optic radiations, and their mean visual acuity correlated with optic tract mean FA, therefore suggesting microstructural alteration of white matter along the entire visual pathways, with a sparing of the other brain white matter tracts.

As the optic nerve is considered the main pathological target for LHON, Rizzo and colleagues [90] investigated the possible involvement of the post-geniculate visual pathway. Mean diffusivity, obtained from diffusion tensor imaging (DTI) for in vivo evaluation within the optic radiations, was higher in the affected patients compared to unaffected mutation

carriers and healthy subjects, and it was related to both disease duration and lack of recovery of visual acuity. They also studied the optic nerve and the lateral geniculate nucleus in post-mortem specimens from a severe case of LHON: atrophy was detected, and, to a lesser extent, degeneration as well in the LHON LGN, associated with extremely severe axonal loss in the optic nerve.

Ogawa and colleagues [91], instead, compared LHON patients to cone-rod dystrophy (CRD) patients, as the former damages the retinal ganglion cell layers, while the latter damages the retinal photoreceptor layer. Therefore, they could compare, by using diffusion MRI and probabilistic tractography, how the two different type of retinal damage affect the optic tract (made of the ganglion cell axons) and the optic radiation (made of geniculo-striate axons). When comparing axial and radial diffusivity at many positions along the two tracts, they found that they were altered in both types of patients. In particular, the optic tract alteration is mainly a decrease in axial diffusivity, while the optic radiation change is mainly an increase in radial diffusivity. This difference in diffusion changes measured in the optic tract and the optic radiation suggests that they are probably caused by different biological mechanisms.

Since brain white matter is often altered in mitochondrial disease, the comparison of brain white matter microstructure as described by DTI between LHON and optic atrophy gene 1-autosomal dominant optic atrophy (ADOA) might be of interest, as these are frequent mitochondrial monosymptomatic optic neuropathies, and it was investigated by Manners and colleagues [92]. For LHON patients, higher mean diffusivity and lower fractional anisotropy were observed in small proportions of the voxels analysed within major white matter tract (0.5% and 5.5%), and the preferential locations were in the optic and acoustic radiations, whereas patients with optic atrophy gene 1-autosomal dominant optic atrophy presented more widespread involvement.

From the structural point of view, as investigated with high resolution T1-weighted MR images, one study [93] focused on the topographical distribution of brain grey matter and white matter damage by using voxel-based morphometry. They found lower grey matter volume in the bilateral primary cortex, and lower white matter volume in the optic chiasm, optic tract and several areas located in the optic radiations, suggesting that brain damage in LHON patients is not limited to the anterior visual pathways, but extends posteriorly to the optic radiations and primary visual cortex. This damage in the posterior part of the visual pathways may be due either to trans-synaptic degeneration secondary to neuroaxonal damage in the retina and optic nerve, or to local mitochondrial dysfunction. Visual cortical plasticity was investigated in carriers of one of LHON mutations, i.e. in a silent model of RGCs loss [94]. Higher cortical thickness was found in the younger carriers, especially in

extrastriate cortex, notably V2 (retinotopic cortical visual areas were defined with a specific fMRI paradigm), suggesting an enhanced plastic developmental mechanism.

Some studies about metabolic alterations, as revealed by MRS (of ^1H and ^{31}P), can be found as well. Ostojic and colleagues [95] wanted to test whether the proton MR spectroscopic profile was different in LHON mutation carriers, when localised in normal appearing white matter. Discriminant analysis showed that decreased absolute concentration of creatine and decreased absolute concentration of N-acetylaspartate have the greatest contribution in discriminating LHON mutation carriers from healthy controls. Lodi and colleagues [96] studied occipital lobe and calf muscle energy metabolism and found that the indices of brain energy metabolism in ^{31}P MRS were abnormal while the muscle oxidative phosphorylation rate was normal, suggesting a tissue specific distribution of the biochemical expression of the specific LHON mutation, along with the fact that extra mitochondrial factors may influence expression of this mutation in vivo. One more study investigated the histoarchitecture of the human optic nerve with post-mortem MRI [97], highlighting that extremely high-resolution MRI can give the possibility to visualize several atrophic lesions (the lamina cribrosa plates seemed collapsed or compressed, the axonal bundles were atrophic and the pial-collagen septae markedly thickened, the entire nerve had shrunk, creating space under the arachnoid, down and around the central ophthalmic artery and vein) normally visible only by histopathological examination.

Only one study exists at the moment in literature about the investigation of brain activity with fMRI in LHON patients, and is relative to functional connectivity measured during resting state condition [98]. They investigated abnormalities within the principal brain resting state networks, and observed that compared to healthy controls, LHON patients had higher resting state fluctuations in the primary visual cortex and auditory cortices bilaterally, while decreased fluctuations were found in the right lateral occipital cortex and right temporal occipital fusiform cortex. A good correspondence to these functional abnormalities was found in structural connectivity when evaluated using a connectivity-based analysis of diffusion weighted data. These findings may suggest that functional and structural abnormalities extend beyond the visual network in LHON patients, and also involve the auditory network, thus corroborating the notion of a cross-modal plasticity between these sensory modalities in patients with severe visual deficits.

1.5 Light stimulation and cognitive brain functions

Light provides visual information and is, obviously, essential for vision. It is also crucial for a series of non-visual functions that are strongly related to the amount of light in the

environment and that vary across the day-night cycle with a circadian (near 24-h) period. They are mainly behavioural and physiological functions, such as sleep-wake control, melatonin secretion and thermoregulation [35]. Moreover, it was shown that light can also be a powerful modulator for other non-visual functions, such as the improvement of alertness and performance on various cognitive tasks [99, 100], and that it can also have an impact on the emotional state, affecting the mood state in long term [101, 102]. In particular, we are now going to focus on recent neuroimaging studies that showed how the exposure to light with specific wavelength, duration and intensity can modulate brain activity in response to cognitive tasks, not necessarily visual tasks.

The first experiments were performed in populations of young and healthy subjects, with regular visual functions, and they aimed to investigate brain activity modulation focusing on different aspects of cognition: auditory perception, executive function and, especially, working memory and updating. The first study [103] used Positron Emission Tomography (PET) to assess possible effects of light during the night, with auditory and visual stimuli in near darkness following light exposure during the biological night. Melatonin was suppressed and alertness was enhanced by the bright polychromatic light. An occipito-parietal attention network was more active in proportion to the duration of light exposure before the scans, while metabolic activity in the hypothalamus decreased in proportion to previous illumination. One of the studies [104] aimed to characterize, by means of fMRI, the neural correlates of the alerting effects of daytime light by evaluating the responses to an auditory oddball task before and after short exposure to a bright white light. An improvement in subjective alertness was observed, and it was related to responses in posterior parts of thalamus. Moreover, light intensified responses in cortical areas involved in attentional oddball effects. Light also prevented the progressive decrease of activity otherwise observed during the darkness, as revealed by fMRI mean parameter estimates in right anterior cingulate cortex, left precuneus and right intraparietal sulcus. These responses to light were dynamic: within minutes after the end of light stimulation they declined. In a later study [54], the same group applied fMRI to investigate how short (18 min) daytime exposure to monochromatic light of different colours (blue 470nm and green 550nm) could influence regional brain response to an auditory working memory task. Their main finding was that blue light tended to enhance brain activity (or at least prevented the decline otherwise observed following green light exposure) within frontal and parietal cortex and in the thalamus. The former is typically involved in working memory, and the latter is implicated in modulation of cognition by arousal. Therefore, the effects of monochromatic light on cognitive functions are almost instantaneous, and, as they are mainly driven by blue light, they suggest a prominent role of the melanopsin-based photoreceptor system. In a similar study [105], the effects of short duration (50s) of

monochromatic light stimulation (violet 430nm, blue 473nm and green 527nm) during a working memory task were explored with fMRI. At light onset, a higher activity was observed with blue light compared to green light in the left hippocampus, left thalamus and right amygdala. Whereas during the task, blue light compared to violet light, seemed to increase brain responses in left middle frontal gyrus, left thalamus and bilateral areas of the brainstem coherent with the locus ceruleus. Considering the key role of blue light, these findings support a prominent role of melanopsin to light within few seconds of an exposure. Moreover, the role of the brainstem in mediating these responses in humans suggests a broad involvement of light in the regulation of brain functions. Similar investigations were performed in three blind subjects in order to better establish the role of rods, cones and mRGCs in the effects of light on cognitive brain functions [55]. In particular, blind subjects that retain non-image-forming photoreception offer a great opportunity to investigate light impacts when no conscious vision is present, and to possibly disentangle the roles of different human retina photoreception systems. Both traditional EEG protocol and fMRI were used, to assess whether brief (2s) exposure to high-intensity blue light could modify EEG activity and to assess whether exposure to high-intensity blue light for less than a minute can modulate brain response to a cognitive auditory task, as previously observed in fully sighted people. Interestingly, the three patients were able to choose nonrandomly about the presence of blue light despite their complete loss of sight. Even 2s of blue light stimulation could modify EEG activity when administered simultaneously to auditory stimuli. FMRI showed that blue light stimulation during an auditory working memory task could increase brain response in prefrontal and thalamic brain regions and in areas of the default mode network. Considering the small number of subjects, these results can just be proof of concepts, but interestingly suggesting that non-image-forming photoreception can trigger some awareness of light and can have a rapid impact on cognition, stimulating higher cognitive brain activity independently of vision. Various aspects have been shown to affect brain responses under light stimulation, such as sleep-wake cycle [99], circadian phase and sleep homeostasis [106], photic memory [107], ageing [108]. Executive functions, as recruited during a working memory task performed in the darkness, were investigated during a normal sleep-wake cycle and during sleep loss in different genotypes, more or less vulnerable, due to a genetic polymorphism that confers vulnerability to sleep loss and circadian misalignment [99]. Dynamic changes in brain responses were observed to evolve across the sleep-wake and circadian cycles, in a regionally specific way, and this supports the existence of individual differences in executive control, in which the allocation of prefrontal resources is constrained by sleep pressure and circadian phase. In the same population, the effects of short stimulation with different lights (blue 473nm and green 527nm) on brain responses to an auditory working memory task while

varying circadian phase and status of the sleep homeostatic were explored [106]. The results indicated that light acts as an activating agent particularly in those individuals in whom brain function is jeopardized by an adverse circadian phase and high homeostatic sleep pressure. It was also shown [107] that a photic memory effect exists in light brain activity modulation as the effect of light on executive brain responses depends on the wavelength of the light to which individuals were exposed prior to each fMRI recording: impact on responses in prefrontal areas and in the pulvinar was higher when the previous exposure (more than 1 hour before) was to the long (589nm, red) wavelength light and not to the short (461nm, blue) one. This is consistent with theories of light-driven melanopsin dual states and gives a stronger evidence for a cognitive role for melanopsin. The analogous approach to investigate brain responses to an auditory working memory task during light stimulation with different colours was also applied in young and older healthy subjects [108] and it showed that the older brains are still capable of sustained responses to light in several brain areas, however compared to young subjects, the effect of blue light is lower in the pulvinar, amygdala, tegmentum and in insular, prefrontal and occipital cortices. Therefore, the effect of blue light on brain activity seems to diminish with aging in key areas for visual functions, alertness regulation and higher executive processes. Interestingly, it was also shown that seasonality and chronotype and time of the day could affect brain responses differently [109, 110]. Seasonal variations in human brain physiology were investigated with fMRI assessing brain responses in two different tasks [109]. Brain responses to both tasks varied across seasons, but the phase of these rhythms were different: for the sustained attention task, the maximum and minimum responses were located, respectively, around summer and winter solstices, whereas for the working memory task maximum and minimum responses were observed around autumn and spring equinoxes. In an fMRI study [110], morning- and evening-type individuals were compared as far as performing different levels of cognitive load/complexity in a N-back paradigm at different time of the day. Neuroimaging data showed an interaction between chronotype, time of day and the modulation of brain responses by working memory load in in the thalamus and in the middle frontal cortex. In the subjective evening hours, evening types exhibited higher thalamic activity than morning types at the highest working memory load condition only, while morning-type individuals show higher recruitment than evening-type participants in the middle frontal gyrus during the morning session in the 3-back condition, suggesting that higher task complexity leads to a chronotype-dependent increase in thalamic and frontal brain activity. These findings emphasized inter-individual differences in time-of-day preferences and underlying cerebral activity, which should be taken into account when investigating vigilance state effects in task-related brain activity.

1.6 Aim of the study

The goal of this study is to examine the role of mRGCs cells in LHON patients, as far as both visual and non-visual (mainly cognitive) processes are concerned. In particular, we aim to study cerebral activations patterns by means of fMRI during light stimulation of different wavelength (specifically, blue and red colours), with particular attention to the system of mRGCs, in order to evaluate their possible contribution in visual system of these patients and their role in modulating brain activity during an attention task. This may give further insights into mRGCs functioning in humans, and it comes in the wider context of the clinical characterization of this neuropathy. Part of the relevance of this project comes along with the possibility to give further insights in highlighting a visual acuity driven by mRGCs as distinct from that provided by rods and cones. The mounting evidence for a direct contribution of mRGCs to vision may have important implications for groups of blind patients where mRGCs are spared.

Chapter 2

Methods

2.1 Subjects

Eleven LHON patients (10 males, mean age \pm sd, 36 \pm 11 years) were included in the study, along with eleven comparable healthy controls (8 males, mean age \pm sd, 36 \pm 13 years). Recruitment of patients was performed on a volunteer basis at the IRCCS Istituto delle Scienze Neurologiche di Bologna, UOC Clinica Neurologica, Department of Biomedical and NeuroMotor Sciences, University of Bologna. The healthy controls were recruited on a volunteer basis among hospital and university co-workers.

Common inclusion criterion for patients and controls was age between 18 and 70 years. For patients, a further inclusion criterion was genetically confirmed diagnosis of Leber's Hereditary Optic Neuropathy (LHON). Exclusion criteria for both patients and healthy controls were contraindications to MR examination, moderate caffeine and alcohol consumption, medication that may affect the sympathetic and parasympathetic influence on pupil response, medication acting on central nervous system (anxiolytics, antidepressant etc.), being shift-workers in the previous year, travels through more than one time zone during the last 2 months, excessive daytime sleepiness as assessed by the Epworth Sleepiness Scale [111], presence of severe sleep disturbances as determined by the Pittsburgh Sleep Quality Index Questionnaire [112], severely abnormal scores in the 21-item Beck Anxiety Inventory [113] and 21-item Beck Depression Inventory [114] tests. Other exclusion criteria for healthy controls were ocular hypertension, lens opacity (cataract etc.), retinal or optic nerve comorbidities including macular degeneration, colour vision abnormalities (Ishihara's Test for Color-Blindness, Kanehara Shupman Co., Tokyo, Japan). The aim of these exclusion criteria was to avoid possible bias, considering melanopsin implication in the regulation of circadian rhythms and pupillary responses. The study gained the consent of the Local Ethical Committees, and all the participants gave their written informed consent.

The baseline assessment for patients before brain functional-MRI evaluation included an ophthalmologic evaluation: visual acuity measurements, tonometry, fundus and anterior chamber examination, retinal nerve fibre layer (RNFL) thickness evaluation by means of optical coherence tomography (OCT) (Stratus OCT, Zeiss, 3.4 protocol), Ishihara's Test for Color-Blindness (Kanehara Shupman Co., Tokyo, Japan). A test for discrimination of red and blue (specifically designed for the purpose of the study) was also performed. During this test, patients were asked to answer for 20 times if the pc screen was red or blue. The colour of the screen was randomly presented. Successively they were asked to answer, for red and blue backgrounds separately, whether the pc screen was lighter or darker than the step before. The brightness of the screen was changed randomly. For both patients and healthy controls, the assessment before brain fMRI included the evaluation of chronotype and concomitant sleep disorders (Horne and Ostberg questionnaire, modified from [115]), Munich questionnaire, Epworth Sleepiness Scale (ESS) [111], Pittsburgh Sleep Quality Index (PSQI) [112], Berlin questionnaire for evaluation of sleep apnoea risk [116], the evaluation of concomitant psychiatric disturbances (Beck Anxiety and Depression Inventory, BDI [113, 114]).

2.2 Protocol

In the 7-day period preceding the laboratory segment of the study participants were asked to follow a regular sleep schedule. Compliance to the schedule was assessed using sleep diaries. Participants were also requested to refrain from all caffeine and alcohol-containing beverages and intense physical activity for 3 days before MRI acquisition. During the week before MR acquisition, participants were instructed to the MR evaluation and trained to the cognitive task. The head circumference of each subject was measured in order to place an appropriate number of small pillows under the head when in the MR scanner, so that the distance between the eyes and the light diffuser was approximately 2 cm for everybody.

On the experimental day, subjects were exposed to white light for 5 minutes, then 1 or 2 drops of tropicamidum 0.5% were administered in the eyes to dilate the pupil and inhibit pupillary constriction, then the subjects were blindfolded and kept in dim light (<5 lux) for one hour before the positioning in the MR scanner. The goal of this preparation phase was to level out the light stimulation, i.e. to avoid possible bias due to photic memory among all participants before starting the acquisitions. During this hour they underwent a short training session for the cognitive task. Then the first part of MRI acquisition was performed. It included the acquisition of the pure visual paradigm (see 2.3.1) and of the visual cognitive paradigm (see 2.3.3), for a total time of about 45 minutes, including the positioning in the

dark. This first session was separated from the second part by approximately 1 hour of rest during which the participant was outside the MR scanner and blindfolded. The second part of MR protocol then included the visual pattern paradigm (with and without 2afc, see 2.3.2) and the high resolution structural brain image, for a total duration of about 35 minutes.

For all the subjects, acquisitions were performed on the same day (Sunday) and at the same time of the day, more precisely starting the MR acquisition 4 hours after subjective habitual awake time, in order to perform, for all the participants, the first light stimulation when melatonin secretion is low in the biological day. The amount of environmental light that was present at the time of acquisition may play a role, for the different light stimulation and the described seasonality in brain responses to working memory task [109], but it was not feasible to perform all the acquisitions in a restricted period of time. Therefore, we kept into consideration this aspect by considering the average number of hours of light per-day at the time of MR session for each subject (data from <https://weatherspark.com/averages>, Bologna Airport Guglielmo Marconi Airport weather station)

2.3 fMRI paradigms

2.3.1 Pure visual paradigm

For this uniform light stimulation paradigm, participants were exposed to 10 s of blue light, 10 s of red light, alternated with 5 s of darkness (<0.01 lux), randomly alternated (Figure 2.1 2.1). The duration of acquisition was 5 minutes. Stimuli were presented with the purpose-built instrumental setup (see 2.4). The aim of this paradigm is to investigate purely visual effects possibly mediated by melanopsin.

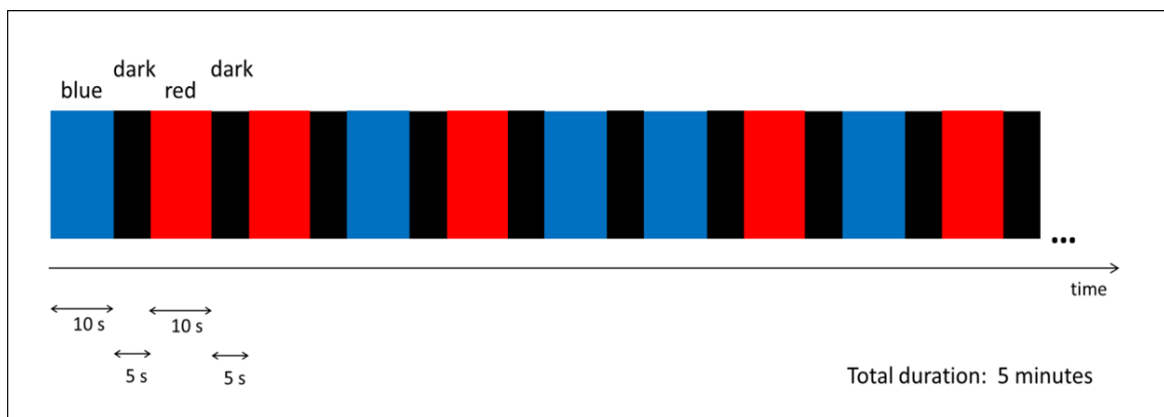


Figure 2.1 Schematic illustration of the pure visual paradigm.

2.3.2 Visual pattern paradigm

In order to investigate visual pattern stimulation, beyond pure uniform light stimulation, this paradigm was included in our investigations. To more specifically activate the visual system, limiting the confounding factor of the cerebral activation (alertness) induced by the light stimuli per se, the subjects were exposed to a visual stimulus consisting of moving (10Hz) vertical or horizontal blue or red bars on a black background with blurred edges (Figure 2.2). The presentation consisted of 40 blocks with pattern light stimuli (10 blocks with horizontal blue bars, 10 blocks with vertical blue bars, 10 blocks with horizontal red bars and 10 blocks with vertical red bars) alternated to dark rest blocks. During each block with pattern light stimulus, the image were presented for 10 s, while each rest block lasted 5 s. The total duration of the paradigm was 10 min. Stimuli were presented with MR compatible projectors (NNL, NordicNeuroLab). In the first session of this paradigm the participants were only asked to look at the screen, then a second session of the same paradigm was acquired, asking in this case the participants to report whether the bars are horizontal or vertical (two alternative forced choice, 2-afc) by pressing buttons on a MR-compatible handgrip (NNL, NordicNeuroLab), so that performances with different colour backgrounds could be compared.

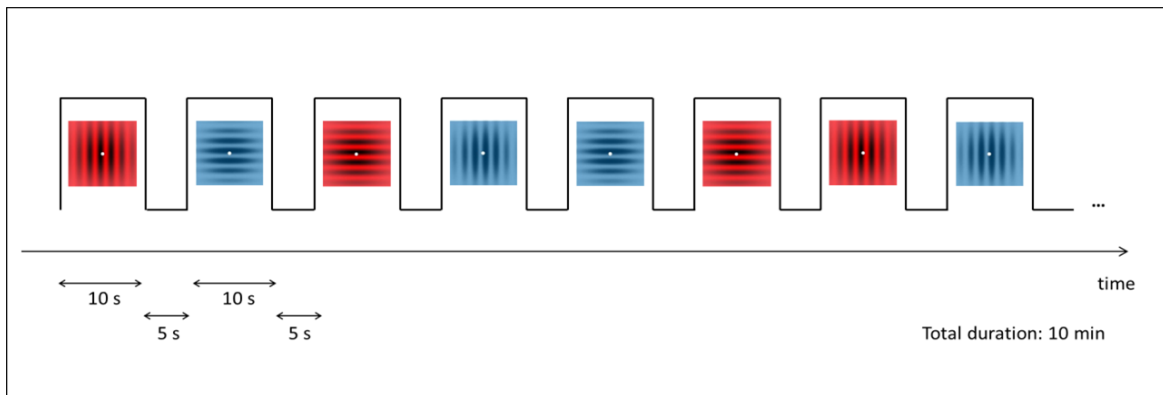


Figure 2.2 Schematic illustration of the visual pattern paradigm.

2.3.3 Visual cognitive paradigm

In order to investigate melanopsin modulation of brain responses during working memory task, this paradigm was constructed (Figure 2.3), based on previous studies [105, 55]. The visual part of the paradigm consisted of alternated illumination periods (50 sec) under uniform diffused blue or red light, alternated to dark period of 20 to 30 s (mean 25 s). Illuminations with one colour (randomly red or blue) was always followed by darkness

periods The blocks made of 50 s of blue light, 20 to 30 s of dark, 50 s of red light and 20 to 30 s of dark were repeated 14 times, and, for the whole acquisition, a mean duration of about 35 minutes resulted (for technical issues, the acquisition was separated into three parts). A 0-back memory cognitive task and a 3-back memory cognitive task were randomly alternated and presented under blue (480nm) and red (620nm) monochromatic light exposure and in the dark. The 0-back task consisted of auditory stimuli, specifically a sequence of consonants, and after hearing each consonant, subjects were requested to state whether or not the consonant was a “r”. The 3-back task consisted of auditory stimuli, specifically a sequence of consonants as well, but after hearing each consonant, subjects were requested to state whether it was identical to the consonant presented three stimuli earlier. In both cases, at the beginning of the consonant sequence subjects were informed with proper instruction whether to perform a 0-back or a 3-back, and they communicated their answer by pressing buttons on a MR-compatible handgrip (NNL, NordicNeuroLab). Stimuli consisted of nine Italian monosyllabic consonants (duration = 0.5 s, Inter-Stimulus Interval= 2 s), produced using COGENT 2000 (www.vislab.ucl.ac.uk/cogent.php), implemented in MATLAB, and transmitted to the participants using MR compatible headphones (NNL, NordicNeuroLab). Series of stimuli were constructed with 30% hits so that difficulty was similar in all blocks, were presented only once, and were randomly assigned to a task block. Each auditory task block consisted of a series of 14 consonants, lasting 35 s, and was alternated to rest periods lasting 10 to 16 s (mean 13 s). A total of 42 blocks were presented, 21 of 0-back and 21 of 3-back, randomly alternated. Each type of task was preceded by a short vocal instruction. This cognitive part of the paradigm was simultaneous, but totally uncorrelated (presentation of task blocks was independent from light changes) to the light stimulation.

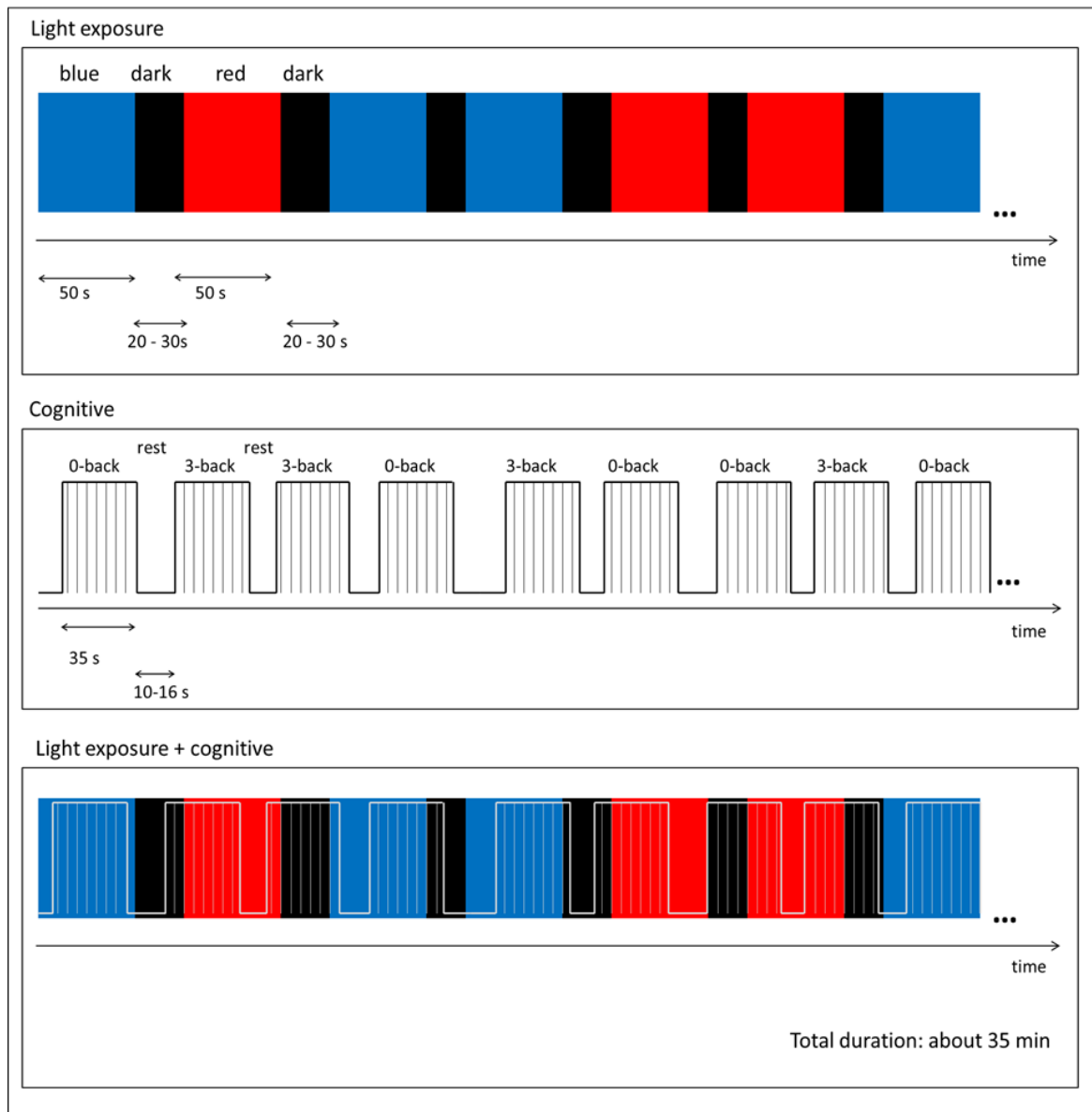


Figure 2.3 Schematic illustration of the visual cognitive paradigm.

2.4 Light exposure

Narrow interference band-pass filters (Full Width at Half Maximum FWHM: 10nm; Edmund Optic, UK) were used to produce the two monochromatic illuminations (480nm and 620nm band-pass filters). A filter wheel (AB301-T, Spectral Products, NM) was computer-controlled to switch band-pass filters and thereby change light wavelength. The light was transmitted by a metal-free optic fibre (Fiberoptics Technology Inc, CT) from a source (DC951H illuminator, EKE lamp, Dolan-Jenner) to two small diffusers placed in front of the subjects' eyes (Ground glass diffuser 220 Grit, Thorlabs). The optic fiber was purpose-built and it was necessary to safely convey monochromatic light inside the MR scanners. A purpose-built Plexiglas support was placed around the chest of the subject to hold up the optic fibre. The diffusers have been designed for the purpose of this study and ensured a uniform illumination of the visual field. They were placed approximately 2 cm away from the subjects' eyes.

In order to characterize the geometry of light stimulation and the uniformity of light after diffusion, measures of light intensity for both colours were performed (Power meter PM100D, Thorlabs with Silicon Power head S120VC) at three different distances from the diffuser glasses (1, 2, 3 cm) thanks to a rigid support, and following a precise sampling scheme: graph paper was used as reference, and the probe was moved by 8 mm at each step, until the whole diffuser surface was covered (Figure 2.4). At the stage of this preliminary assessment of light uniformity, the light intensity was arbitrarily set.

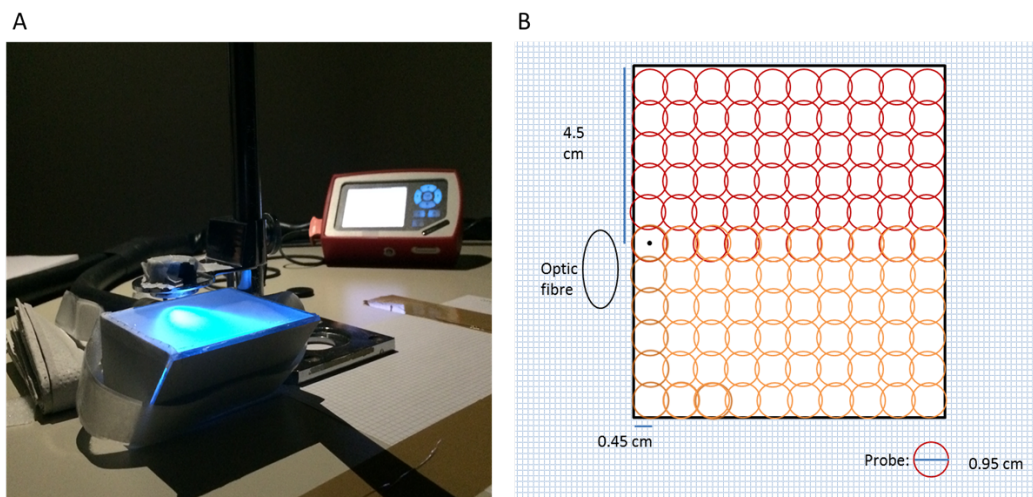


Figure 2.4 Preliminary measures of light intensity outside the diffusers. A - Instrumental setup B - graphic representation of the sampling scheme: the rectangle is the diffusion facet of the diffuser, coloured circles represent the positions where the light intensity was measured with the power meter probe.

Irradiance was not measured directly in the magnet, but the light source was calibrated and photon flux estimated to be $5 \times 10^{13} \text{ ph cm}^{-2} \text{ s}^{-1}$ (Power meter PM100D, Thorlabs with Silicon Power head S120VC), corresponding to an irradiance of 20.7 W/cm^2 for the blue light, wavelength 480 nm, and 16.0 W/cm^2 for the 620nm red light. In accordance with the protocols applied in previous studies of this research area ([105, 99, 55]), the photon densities of the two light exposures were the same to allow the assessment of the relative contribution of the photoreceptors most sensitive to each wavelength. The light device produced no perceptible sounds or temperature change. The total amount of blue light received during the experiment was 4 order of magnitude below the blue-light hazard threshold (see 2.4.1 and [117]). Only the MR-compatible optic fibre, the diffuser glasses and the MR-compatible handgrip, headphones and projectors were inside the scanner room during acquisitions, while all the other instruments were positioned in the control room (Figure 2.5).



Figure 2.5 A participant before entering the MR scanner, after the positioning and the setup of the various devices: the fibre optic, the Plexiglas support and the light diffusers (positioned over the head coil) are visible in this picture, as well as the MR compatible handgrips.

2.4.1 Light exposure hazards

Concerning damages by optical radiation to eyes structures, we considered the thermal damage of the retina and the “blue light” photochemical damage of the retina as other damages (such as thermal damage of the cornea or the near-infrared thermal damage of the crystalline lens) occurring within wavelengths ranges in which the monochromatic lights that we used are not included. For the two mentioned damages, we only report exposure limits

estimation for the blue light since it has lower wavelength and hence higher energy (same photon density) than red light.

As for the Retinal thermal hazards (380-1400nm) according to our stimulation paradigm a radiance of $1.5 \times 10^{-1} \text{ Wm}^{-2}\text{sr}^{-1}$ resulted, and it is well below (6 orders of magnitude) the exposure limit that is set to a radiance of $28 \times 10^4 \text{ Wm}^{-2}\text{sr}^{-1}$. The following assumptions were considered: monochromatic light (wavelength 480 nm), photon density $5 \times 10^{13} \text{ phcm}^{-2}\text{s}^{-1}$ corresponding to an irradiance of 20.7 Wcm^{-2} (wavelength 480 nm), solid angle 1.4 sr (estimated considering 1 inch diameter optic fiber 2 cm away from the eyes, without diffusion, to be more precautionary), retinal thermal hazard function $R(\lambda)$ set at $R(480)=R_{\text{max}}=1$, exposure time $t > 0.25\text{s}$, large sources (subtended angle $> 0.1\text{rad}$).

As for the blue-light photochemical retinal hazard (300-700nm) according to our paradigm an effective dose of $240 \text{ Jm}^{-2}\text{sr}^{-1}$ resulted, and it is well below (4 orders of magnitude) the blue-light limit of effective radiance dose that is set to $10^6 \text{ Jm}^{-2}\text{sr}^{-1}$. The following assumptions were considered: monochromatic light (wavelength 480 nm), photon density $5 \times 10^{13} \text{ phcm}^{-2}\text{s}^{-1}$ corresponding to an irradiance of 20.7 Wcm^{-2} (wavelength 480 nm), solid angle 1.4 sr (estimated considering 1 inch diameter optic fibre 2 cm away from the eyes, without diffusion, to be more precautionary), blue-light hazard function $B(\lambda)$ set at $B_{\text{max}}=1$ (more precautionary), with exposure time $t=1600\text{s}$ obtained taking into account of all the illumination blocks of both visual (uniform light) and visual/cognitive paradigms as if they are all under blue light exposure (more precautionary).

2.5 Demographic and behavioural data analysis

Sex was compared between the two groups with Pearson's 2 test, while age and the average hours of light were compared with a t-test, after that the normality of the data was checked with a Shapiro-Wilk test. Accuracies and reaction times (RT) in the 2afc for the visual pattern with different colour background were compared with a two-way mixed design ANOVA, with group (patients or controls) as independent factor and background colour (blue or red) as the two-level repeated measures. The performances in the two training sessions of the n-back cognitive task were compared between sessions with a paired t-test, and between patients and controls with a t-test. As for the performance of the cognitive task during MR acquisitions, a two-way mixed design ANOVA was performed, with group (patients or controls) as independent factor and light conditions (blue, red, darkness) as the three-level repeated measures.

2.6 fMRI data acquisition

MRI acquisitions were performed with a 1.5 T system (GE Medical System Signa HDx 15), equipped with an 8-channel brain phased array coil GE (1.5T HD 8 Channel High Res Head Array for the GE HDx MR System). Functional MR images were acquired with a multislice T2*-weighted gradient-echo-planar sequence using pure axial slice orientation (34 slices, thickness 4 mm, field of view FOV=240x240 mm, matrix size=98x98x34, repetition time TR=3000 ms, echo time TE=40 ms, flip angle=90°). A high-resolution volumetric structural MRI was acquired using a T1-weighted fast spoiled gradient echo (FSPGR) sequence, (TR=12.4 ms, TE=5.2 ms, inversion time TI=600 ms, flip angle=10°, matrix size=256x256 mm, FOV=256x256 mm, slice thickness=1 mm, yielding axial slices with a voxel size of 1x1x1 mm).

2.7 fMRI data analysis

The analyses of fMRI data were performed with the software FSL (<https://fsl.fmrib.ox.ac.uk/fsl/> [118]).

The image pre-processing included motion correction through rigid body registration (MCFLIRT, Motion Correction FMRIB's Linear Image Registration Tool, [119]), high-pass filtering (cut-off 90s), spatial smoothing (gaussian FWHM 5mm) and slice timing correction.

At the single subject level, changes in brain responses were estimated by using a general linear model, in which for each run of each paradigm blocks were modelled using boxcar functions and convolved with a double-gamma hemodynamic response function. In particular, for the pure visual paradigm boxcar functions modelled blue light stimulation periods and red light stimulation periods. Stick functions were added to separately model light onsets and offsets. The regressors described so far were also added to the design after a linear parametric modulation, to describe any linear change of response amplitude with time. The modulated version of each regressor was orthogonalized with respect to the original regressor. Light onset and offset regressors were considered as covariate of no interest. Movement parameters derived from realignment for motion correction of functional volumes were added as covariate of no interest. Contrasts then tested the effects of interest, generating statistical parametric maps. The contrasts of interest included: blue and red light mean effect (with and without modulation), comparison between blue and red (with and without modulation), mean effect of light (irrespective of colour, with and without modulation). In order to also describe transient effects in brain activity, i.e. the brain response to light onset, functions describing light onset were also considered as effects of interest in specific contrasts,

looking at mean blue/red effect separately, comparing the two colours and considering light irrespectively of colour. As for the visual pattern paradigm, boxcar functions were used to model period of time when horizontal bars were shown on blue background, vertical bars on blue background, horizontal bars on red background and vertical bars on red background. Also in this case the time-modulated and orthogonal versions of these regressors were added, such as stick functions describing onsets and offsets, and movement parameters derived from motion correction were added as covariate of no interest. The contrasts of interest aimed to describe mean response to blue and to red backgrounds (with and without modulation), comparison between blue and red backgrounds (with and without modulation), mean response to horizontal and vertical lines (with and without modulation) and comparison between horizontal and vertical orientations (with and without modulation). In this case as well, stick functions describing image onsets and offset were considered as effects of no interest, a part from specific contrast where image onset was considered as an effect of interest. Regarding the visual cognitive paradigm, boxcar functions were used to describe 0-back task blocks, 3-back task blocks, blue illumination periods and red illumination periods. Stick functions for light onset and offset were added, and considered as covariate of no interest. In order to describe different task blocks performed under different light exposure, interactions, i.e. multiplication of the original boxcar functions together, were considered. All these regressors were also added in the time-modulated version, orthogonal to the original regressor. Movement parameters were added as covariate of no interest as well. The contrasts of interest consisted of: mean effect of task (3-back vs 0-back), mean effect of blue and red light separately, and comparison between the two, mean effect of light irrespectively of colours, interactions between task and light conditions [(3-back-blue – 0-back-blue) vs (3-back-red – 0-back-red)]. All these contrast were carried out both with and without time modulated regressors. Movement parameters and stick functions for light onset and offset were considered covariate of no interest. Contrasts to investigate brain responses at light onsets, as effect of interest, were added as well. Each so obtained statistical parametric map was then corrected for multiple comparisons across the whole brain with a cluster approach (clusters were determined in Z-statistic images with a threshold of $Z=2.3$ and a family-wise-error corrected cluster significance threshold of $p=0.05$ was applied). The results from the three separate runs that were acquired for the visual cognitive paradigm were then averaged at the single subject level, with a fixed effect analysis.

At the group level, comparisons among the LHON patients group and the healthy controls group were carried out with a mixed effect analysis (FLAME 1 in fsl), accounting for inter-subject variance in the effects of interest. Age, sex and the average numbers of hours of light per day at the moment of MRI acquisitions were added as covariate of no interest.

Comparisons were performed within a group-specific grey matter mask. Statistical inferences were made from statistical maps that were corrected for multiple comparisons over the whole brain grey matter with a cluster approach: clusters were determined in Z-statistic images ($Z=2.3$) and a family-wise-error corrected cluster significance threshold of $p=0.05$ was applied.

2.7.1 Structural evaluation

In addition to fMRI data analyses, we explored possible differences in grey matter (GM) density by applying a voxel based morphometry (VBM) approach. This can be useful within fMRI analyses as potential alterations in grey matter could be taken into account when performing functional analysis. Moreover, this is also of interest, as this aspect in LHON have not been particularly investigated in literature so far. Even if VBM for white matter is controversial and white matter integrity can be better assessed with other MRI techniques, such as diffusion weighted imaging, we performed VBM analyses for white matter as well considering the exploratory nature of the investigation, and to compare with a single previous study which is present in the poor literature about VBM in LHON [93]. The software SPM 12.0 (<http://www.fil.ion.ucl.ac.uk/spm>) was used. First, structural images were segmented into grey matter, white matter and CSF components. Grey and white matter were then aligned and registered to an iteratively-created study specific template, by using the tool DARTEL (Diffeomorphic Anatomical Registration Through Exponentiated Lie algebra, [120]). The resulting images were then registered to the MNI-152 template with an affine transformation and they were spatially smoothed (Gaussian kernel, FWHM 8mm). In order to take into account the amount of deformation, volumes were intensity normalized by the local jacobian maps of the deformation map. Whole brain grey and white matter and CSF concentrations were evaluated and then summed to get total intracranial volume (TIV). Comparisons between groups were then performed over the whole brain on GM density, applying a voxel-wise general linear model (GLM) by using a nonparametric permutation approach (randomise FSL). For each contrast, 5000 permutations were performed and for the multiple comparisons problem, the family-wise error rate was controlled ($p<0.05$) and TFCE was applied (threshold-free cluster enhancement).

Chapter 3

Results

3.1 Demographic and clinical results

The two groups did not differ significantly in age, sex and average number of hours of light at the time of MR acquisitions (Table 3.1). Overall, the participants had not an excessive morning-evening chronotype nor presented particularly severe sleep disturbances, and their daytime sleepiness was in general normal. The sleep apnoea risk was high only in two of the patients. As for psychiatric disturbances, scores were normal in all participant, a part from two patients that presented mild to moderate levels of anxiety and depression. Results of patients ophthalmologic evaluations are reported in Table 3.2. Fundus examination revealed a diffuse optic atrophy for all LHON participants, and Ishihara's Test score was 0/12 for all of them. Essentially, all patients were able to distinguish blue from red when randomly displayed on a computer screen. Some of them had more difficulties in distinguishing the different shade and intensities (Table 3.3).

Table 3.1 Demographic features of the study sample

		LHON	HC
Age (years)	<i>mean</i>	36.2	36.3
	<i>sd</i>	11.4	13.3
	<i>min</i>	22	25
	<i>max</i>	59	69
Sex	<i>M</i>	10	8
	<i>F</i>	1	3
Average light (hours/day)	<i>mean</i>	12.8	12.8
	<i>sd</i>	2.1	2.3
	<i>min</i>	9.6	9.2
	<i>max</i>	15.3	15.3

Table 3.2 Demographics and ophthalmologic evaluations for LHON patients.

Patient	Sex	Age	DD	VA		description	VF				RNFL										
				LE	RE		LE		RE		RE					LE					
							MD	fovea	MD	fovea	avg	T	S	N	I	avg	T	S	N	I	
LHON 1	M	29	4	0.005	0.01	n.e.	n.e.	n.e.	n.e.	n.e.	n.e.	44	38	56	46	37	47	32	60	42	54
LHON 2	M	34	17	0.032	0.05	generalized defect	-31.78	not active	-27.14	not active	n.e.	48	40	67	35	52	47	40	54	52	41
LHON 3	M	40	13	0.063	0.01	generalized defect	-32.96	n.e.	n.e.	n.e.	n.e.	51	30	73	52	47	56	45	73	43	61
LHON 4	M	22	5	0.025	0.01	generalized defect	-33.03	not active	-34.1	not active	n.e.	45	31	55	44	51	47	31	59	45	54
LHON 5	M	29	12	0.01	0.005	generalized defect right eye central scotoma	n.e.	not active	-34.03	not active	n.e.	41	44	35	45	41	32	27	40	34	25
LHON 6	M	27	10	0.016	0.05	right eye; generalized defect left eye	-30.95	not active	-16.95	18	n.e.	39	27	5	2	36	39	27	62	33	33
LHON 7	F	54	24	0.01	0.003	n.e.	n.e.	n.e.	n.e.	n.e.	n.e.	40	27	54	36	43	41	36	53	33	42
LHON 8	M	59	32	0.04	0.01	generalized defect	-30.99	not active	-31.45	not active	n.e.	50	29	49	60	61	43	27	56	39	51
LHON 9	M	36	20	0.02	0.16	generalized defect	n.e.	n.e.	-32.04	20	n.e.	38	29	43	36	42	37	32	39	39	39
LHON 10	M	39	9	0.016	0.02	generalized defect	n.e.	n.e.	-33.42	not active	n.e.	50	38	57	50	57	48	40	63	51	38
LHON 11	M	29	13	0.032	0.032	generalized defect	-27.33	<0	-27.72	<0	n.e.										n.e.

DD: disease duration; LE: left eye; RE: right eye; VA: visual acuity; VF: visual field; MD: mean defect; RNFL: retinal nerve fibre layer; T: temporal; S: superior; N: nasal; I: inferior; n.e.: not executed, due to unfeasibility.

Table 3.3 Results of the test for discrimination of red and blue.

Patient	Accuracy red vs blue (%)	Accuracy blue intensity (%)	Accuracy red intensity (%)
LHON 1	70	32	84
LHON 2	100	88	80
LHON 3	100	84	76
LHON 4	100	44	36
LHON 5	70	84	84
LHON 6	100	100	100
LHON 7	100	72	72
LHON 8	100	84	80
LHON 9	100	96	92
LHON 10	100	96	100
LHON 11	100	92	96
LHON 12	100	96	92

3.2 Light exposure setup preliminary measures

Results of the measures of light irradiance outside the diffuser glasses are reported in Table 3.4 for both blue and red lights at the three considered distances (1, 2, 3 cm). Each box of the tables corresponds to a position in the sampling scheme. Visual representation of these measures are in Figure 3.1 and Figure 3.2, in 2D and 3D representations. As the sensitivity of the power meter was very high (approximately 10^{-3} W/cm²), our measures were not repeatable within the instrumental uncertainty. Therefore, for a representative condition (blue light at a distance of 2 cm) we performed repeated measures (6 times), in order to have an estimation of the measure variability. Results are in Table 3.5 and Figure 3.3. The illumination we administered was relatively uniform over the field of view, but not entirely. Considering the available space inside the MR scanner gantry above the head coil, the rigidity and dimensions of the optic fibre and the light diffusion system, this was the best uniformity we could reach, and it is, however, reasonably good.

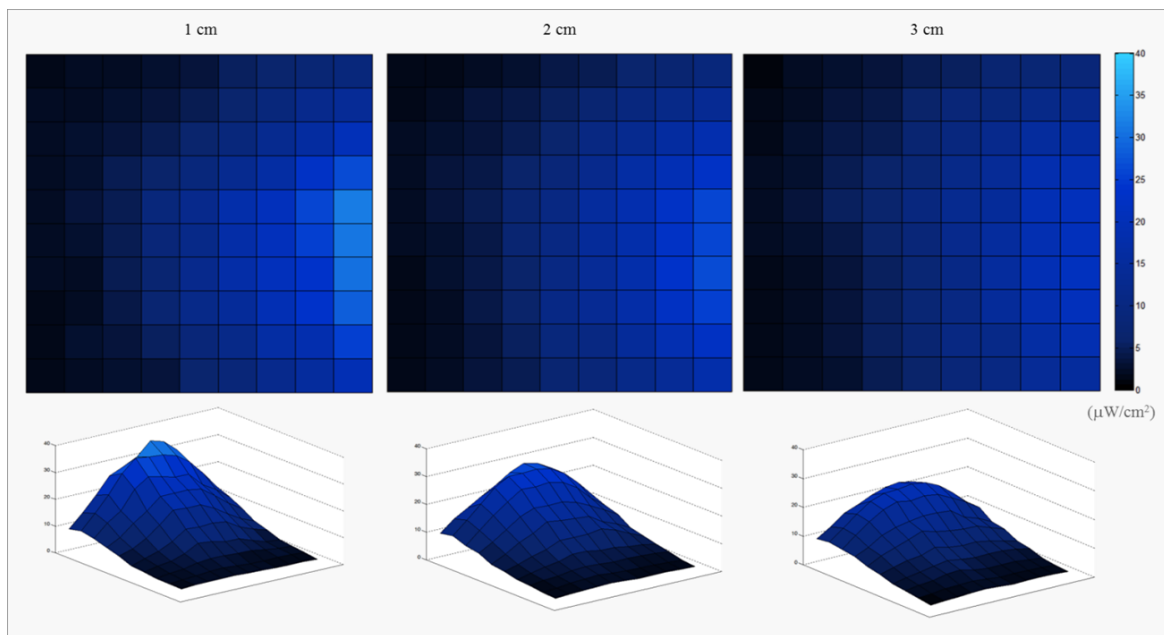


Figure 3.1 Measure of blue light irradiance outside the diffuser glasses, at distances of 1, 2, 3 cm.

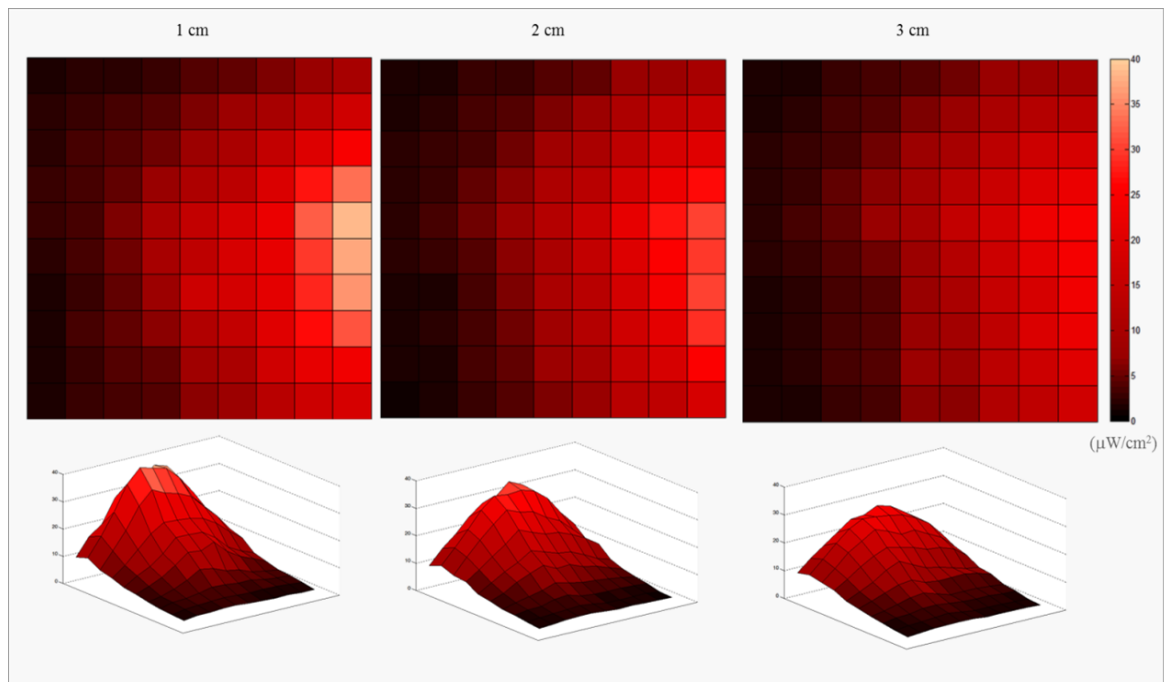


Figure 3.2 Measure of red light irradiance outside the diffuser glasses, at distances of 1, 2, 3 cm.

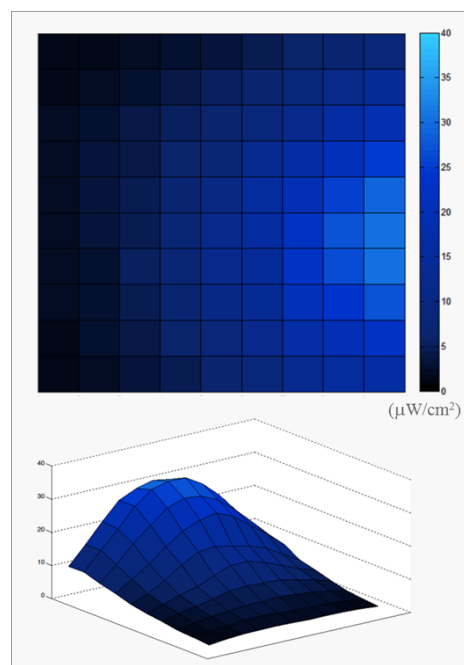


Figure 3.3 Measures of blue light irradiance outside the diffuser glasses at a distance of 2 cm. The mean values are represented in 2D and 3D.

Table 3.4 Measure of light irradiance outside the diffuser glasses, at distances of 1, 2, 3 cm for blue (on the left) and red (on the right) light. Each box in the tables corresponds to a position in the sampling scheme.

Blue light										Red light									
Irradiance at 1 cm ($\mu\text{W}/\text{cm}^2$)										Irradiance at 1 cm ($\mu\text{W}/\text{cm}^2$)									
1.86	2.02	2.06	2.63	3.17	5.07	6.38	7.85	8.85	7.77	1.65	1.97	2.34	2.97	3.96	4.68	6.21	7.43	9.95	8.51
2.18	2.39	2.84	3.74	4.75	6.53	8.95	12.50	14.20	12.50	2.23	2.78	3.50	3.89	5.82	7.85	9.89	13.40	16.90	14.80
2.31	2.71	3.39	4.45	6.29	9.25	12.90	15.80	20.00	18.00	2.31	3.13	3.81	5.34	7.85	10.10	14.50	19.50	24.60	18.30
2.32	3.11	4.50	6.06	8.78	13.10	16.50	22.70	26.80	24.10	2.65	3.44	4.57	7.45	11.10	13.70	19.10	27.40	33.70	26.80
2.34	3.30	4.88	8.86	12.30	17.50	20.80	26.20	31.30	26.30	2.60	3.61	5.70	10.40	14.70	18.30	22.10	32.20	38.50	29.50
2.00	2.91	4.82	8.28	11.80	17.00	20.80	25.20	30.70	28.90	2.13	3.35	5.34	9.41	14.10	18.30	21.80	29.90	37.20	30.80
1.91	2.46	4.60	7.01	12.20	17.00	20.80	23.70	30.20	33.60	1.87	3.08	4.83	7.50	16.30	18.00	21.10	28.50	36.10	35.30
1.58	2.35	4.37	6.98	11.50	14.70	19.90	23.70	28.70	32.10	1.65	3.20	4.74	6.69	11.60	14.80	20.00	26.30	31.50	33.90
1.45	2.55	3.53	5.19	8.29	11.40	16.40	18.60	25.10	27.80	1.77	3.05	3.81	4.68	8.57	10.20	17.10	21.30	23.30	28.10
1.57	2.37	2.91	3.51	6.31	8.42	12.30	15.50	19.80	21.50	1.40	2.68	3.22	3.93	6.62	7.60	12.90	16.60	18.40	21.80
1.28	2.02	2.57	3.20	4.92	6.33	9.13	11.80	13.70	14.70	1.41	2.25	2.84	3.17	4.49	5.72	9.32	10.90	13.40	14.00
Irradiance at 2 cm ($\mu\text{W}/\text{cm}^2$)										Irradiance at 2 cm ($\mu\text{W}/\text{cm}^2$)									
1.35	1.68	2.30	2.65	3.79	4.52	6.72	7.49	9.32	8.31	1.31	1.86	2.55	2.86	4.02	4.78	7.39	8.03	9.73	7.87
1.74	2.10	3.13	3.82	5.12	7.09	9.47	11.80	13.70	12.40	1.67	2.38	3.38	4.13	5.74	7.76	10.70	13.40	15.10	13.20
1.95	2.72	3.50	4.91	6.75	10.00	12.90	16.20	18.50	15.30	2.17	2.68	3.52	5.26	8.55	10.60	14.30	18.60	20.60	17.00
2.03	3.13	4.19	5.65	8.13	12.10	16.30	19.90	23.10	18.30	2.24	3.02	4.82	6.31	10.68	12.90	17.70	23.10	26.50	22.20
2.19	3.32	4.52	7.22	10.20	15.10	18.30	23.10	25.90	21.20	2.27	3.25	5.27	8.00	12.44	15.90	21.70	27.10	30.50	26.10
1.91	2.87	4.23	7.00	10.10	14.50	18.00	22.80	25.90	24.20	1.94	2.67	3.92	6.79	10.14	14.40	19.70	25.30	29.90	27.20
1.51	2.51	3.83	6.19	10.20	14.00	18.10	23.30	26.30	26.50	1.51	1.86	3.22	5.71	10.51	12.80	17.90	24.30	30.20	31.50
1.50	2.38	4.06	6.11	10.90	13.60	16.90	22.20	25.20	25.30	1.55	1.88	3.17	5.28	8.52	12.00	17.30	21.00	28.80	29.40
1.52	2.26	3.66	5.19	9.29	10.40	14.50	19.10	22.40	22.50	1.38	1.84	3.14	4.68	7.56	9.90	15.40	18.60	25.00	24.90
1.29	2.01	3.41	4.69	6.98	8.56	11.90	14.20	17.90	17.70	1.21	1.83	2.90	4.00	5.70	7.35	12.90	14.20	18.60	19.40
1.18	1.70	2.88	3.76	4.89	6.04	8.94	10.40	12.50	12.20	1.03	1.39	2.42	3.12	4.20	5.80	9.63	9.47	13.40	13.50
Irradiance at 3 cm ($\mu\text{W}/\text{cm}^2$)										Irradiance at 3 cm ($\mu\text{W}/\text{cm}^2$)									
1.17	1.91	2.67	3.18	4.52	5.59	7.07	7.90	8.52	7.86	1.44	1.84	2.72	3.24	4.26	5.22	7.17	8.07	9.09	8.01
1.58	2.28	3.38	4.14	5.98	8.15	9.19	11.60	12.30	10.90	1.78	2.47	3.46	4.09	5.83	7.34	10.00	12.00	13.50	12.00
1.66	2.76	3.83	4.93	7.18	9.67	12.20	15.10	16.00	14.40	2.14	2.71	3.70	5.20	7.52	9.58	13.40	16.50	18.20	15.50
2.03	2.98	4.90	5.80	7.80	11.40	13.90	18.20	19.30	16.20	2.24	3.09	4.55	6.48	9.31	12.70	15.90	19.60	22.10	18.90
2.10	3.17	5.11	6.66	9.44	13.10	14.80	19.80	20.90	18.40	2.23	3.46	4.60	7.05	9.85	14.90	17.90	22.50	24.50	22.60
1.91	2.69	3.98	5.88	8.27	11.90	15.50	18.90	21.00	19.90	2.10	2.78	4.01	5.54	7.99	12.40	16.70	20.70	24.10	22.90
1.53	2.20	3.42	5.28	7.61	11.03	15.40	19.50	21.80	20.50	1.66	2.09	3.45	4.05	7.25	10.20	15.50	18.50	23.50	25.20
1.55	2.31	3.45	5.44	7.74	10.40	14.90	18.70	21.00	19.50	1.63	2.15	3.25	4.22	7.24	9.08	13.80	18.90	22.40	23.80
1.65	2.23	3.46	5.31	6.96	10.30	11.50	16.40	18.80	17.40	1.57	1.98	3.25	4.08	7.51	7.87	13.20	16.30	20.20	20.70
1.56	1.99	2.95	4.78	5.79	8.44	10.00	13.90	15.10	14.20	1.47	1.82	2.72	3.64	6.46	6.31	11.60	13.70	17.10	17.30
1.28	1.66	2.28	3.67	4.54	6.84	7.53	10.70	10.90	10.90	1.21	1.58	2.70	3.17	5.01	5.58	8.13	9.44	11.90	11.90

Table 3.5 Measures of blue light irradiance outside the diffuser glasses at a distance of 2 cm. Top: mean over the 6 repetitions, middle: standard deviation over the 6 repetitions, bottom: relative error of each measure. Each box in the tables corresponds to a position in the sampling scheme.

Mean irradiance at 2 cm ($\mu\text{W}/\text{cm}^2$)									
1.28	1.67	2.1	2.8	3.4	4.4	5.8	7	8.6	8.5
1.7	2.4	3	4.04	5	6.5	8.9	11.4	14.1	13.9
2.1	2.9	3.8	5.1	6.6	9.3	12.2	16.7	19.2	19.7
2.2	3.4	4.3	6.1	8.1	12.8	16.4	21.1	24.9	25
2.2	3.7	4.7	7.4	10.1	15.6	19.9	25.2	28.8	27.4
2.1	3.3	4.9	7.7	12	16	22.1	26.9	30.1	28.6
1.97	2.8	5.1	7.5	12.1	14.9	23.1	26.3	30.07	27.8
1.96	2.8	4.7	7.3	10.7	13.7	20.9	24.1	27.1	24.3
1.84	2.6	4.2	6.1	8.6	11.9	17	19.9	22.5	19.3
1.56	2.24	3.4	4.9	6.5	9	13.1	15.1	16.7	14.6
1.18	1.66	2.4	3.4	4.9	6.1	8.8	10.1	11.2	9

Standard deviation of irradiance at 2 cm ($\mu\text{W}/\text{cm}^2$)									
0.18	0.16	0.17	0.2	0.4	0.7	0.3	0.4	0.5	0.3
0.2	0.2	0.2	0.11	0.5	0.8	0.5	0.6	0.8	0.2
0.2	0.3	0.4	0.2	0.6	0.8	0.4	1.1	1.2	0.3
0.3	0.4	0.4	0.3	0.7	1.3	0.5	1.7	1.4	0.4
0.3	0.5	0.5	0.4	0.6	0.9	1	1.8	1.4	0.9
0.1	0.4	0.5	0.7	0.7	1	1.7	1.3	0.9	0.8
0.07	0.2	0.5	0.6	0.7	1	0.9	1	0.8	0.6
0.14	0.3	0.3	0.5	0.8	0.8	1.2	0.9	0.3	0.9
0.15	0.2	0.4	0.5	0.8	0.4	0.9	0.5	0.2	0.8
0.16	0.16	0.3	0.4	0.3	0.7	0.3	0.3	0.11	0.2
0.15	0.11	0.2	0.2	0.2	0.7	0.2	0.4	0.2	0.6

Relative error (%)									
14	10	8	8	11	16	5	6	6	4
12	9	7	3	10	12	5	6	5	1
9	11	10	4	9	8	4	7	6	2
12	11	10	4	9	10	3	8	5	2
12	13	10	6	6	6	5	7	5	3
7	12	10	9	6	6	8	5	3	3
4	9	10	9	6	7	4	4	3	2
7	9	7	7	7	6	6	4	1	4
8	8	8	7	9	3	5	2	1	4
10	7	9	8	5	8	2	2	1	1
13	6	9	6	4	12	3	4	2	6

3.3 Behavioural data

3.3.1 Visual 2afc

A significant effect of background colour was not found in the accuracies and RT (reaction time) of 2afc task (accuracy: $F=0.776$ $p=0.389$; RT: $F=0.503$ $p=0.486$), nor was a significant interaction between group and background colour (accuracy: $F=0.086$ $p=0.772$; RT: $F=0.012$ $p=0.913$). Instead, a significant effect of group was found for RT ($F=4.673$ $p=0.043$), but not for accuracies ($F=2.716$ $p=0.115$). Average RT for healthy subjects, irrespectively of background colour, was 1507ms, while for patients it was 2640ms (Table 3.6).

3.3.2 N-back cognitive task

At the second training session, all the participant reached at least 75% of accuracy (Table 3.7). Over the whole study cohort, there was a significant improvement of performances between the first training, during the week before MR acquisition, and the second one, just before MR acquisition, in the 3-back task (paired t-test, $p=0.027$, mean first training: 86.3%, mean second training 90.0%). As for the accuracy of n-back tasks during fMRI acquisition (Table 3.7), there was no significant main effect of group (0-back: $F=1.357$ $p=0.258$; 3-back: $F=0.574$ $p=0.457$), nor light condition (0-back: $F=2.268$ $p=0.117$; 3-back: $F=2.597$ $p=0.087$) and no significant interaction between group and light condition (0-back: $F=0.932$ $p=0.402$; 3-back: $F=2.178$ $p=0.126$). These negative results ensure that fMRI results were not biased by possible differences in the cognitive task performances.

Table 3.6 Performances in 2afc task for each participant, with blue and red background separately.

	Blue					Red				
	corr	err	ng	RT (mean, ms)	RT (std, ms)	corr	err	ng	RT (mean, ms)	RT (std, ms)
HC 1	20	0	0	2018	767	20	0	0	2365	819
HC 2	20	0	0	2020	1392	20	0	0	2128	855
HC 3	20	0	0	1173	428	20	0	0	1225	427
HC 4	20	0	0	815	150	20	0	0	917	218
HC 5	20	0	0	1009	169	20	0	0	974	155
HC 6	20	0	0	1157	594	20	0	0	1295	189
HC 7	20	0	0	999	313	20	0	0	1090	233
HC 8	20	0	0	1198	233	20	0	0	1178	265
HC 9	20	0	0	1396	654	19	0	1	1408	580
HC 10	15	5	0	4064	3540	14	5	1	1964	1910
HC 11	20	0	0	1351	281	20	0	0	1410	838
mean	19.5			1564		19.4			1450	
std	1.5			915		1.8			485	
LHON 1	9	7	4	4975	2587	7	8	5	3444	1488
LHON 2	18	0	2	3273	2411	19	0	1	2807	1926
LHON 3	20	0	0	1182	303	20	0	0	1479	668
LHON 4	20	0	0	1390	549	20	0	0	1305	434
LHON 5	2	1	17	4476	2558	1	1	18	4734	1940
LHON 6	20	0	0	1207	531	20	0	0	1710	1868
LHON 7	20	0	0	1393	149	20	0	0	1371	207
LHON 8	20	0	0	1931	701	19	1	0	2700	2338
LHON 9	19	1	0	1488	523	20	0	0	1605	468
LHON 10	15	1	4	6325	1961	15	1	4	5646	1975
LHON 11	17	0	3	1865	1201	18	0	2	1791	1668
mean	16.4			2682		16.3			2599	
std	5.8			1803		6.4			1466	

Corr: number of correct responses; *err*: number of errors; *ng*: number of not given answers; *RT*: reaction time.

Table 3.7 Performances in 0-back and 3-back tasks for each participant in the first training session, second training session and during the fMRI acquisition (irrespective of light condition, under blue light, under red light and in the darkness).

Subject	Training 1 (%)		Training 2 (%)		fMRI (%)		fMRI - blue (%)		fMRI - red (%)		fMRI - dark (%)	
	<i>0-back</i>	<i>3-back</i>	<i>0-back</i>	<i>3-back</i>	<i>0-back</i>	<i>3-back</i>	<i>0-back</i>	<i>3-back</i>	<i>0-back</i>	<i>3-back</i>	<i>0-back</i>	<i>3-back</i>
HC 1	99.1	99.7	100.0	100.0	100.0	97.3	100.0	98.0	100.0	95.4	100.0	100.0
HC 2	99.6	89.2	100.0	90.8	100.0	91.5	100.0	93.7	100.0	91.2	100.0	88.6
HC 3	100.0	98.9	100.0	100.0	98.6	97.3	94.0	98.5	100.0	98.7	99.1	94.1
HC 4	99.3	87.1	100.0	91.1	99.7	88.0	99.2	91.5	100.0	87.8	100.0	84.6
HC 5	97.4	92.9	98.2	89.3	100.0	89.3	100.0	97.8	100.0	84.1	100.0	87.3
HC 6	99.5	76.8	98.8	97.3	98.6	96.3	100.0	96.5	96.7	97.5	99.0	94.9
HC 7	97.1	95.2	97.6	92.9	95.9	85.7	89.3	84.0	100.0	89.7	99.0	85.1
HC 8	97.6	80.8	100.0	97.6	99.7	97.3	78.0	95.6	100.0	98.6	98.9	98.2
HC 9	97.6	97.6	100.0	94.0	93.5	96.3	92.3	97.5	94.5	94.1	93.3	95.2
HC 10	98.8	80.1	98.2	75.0	99.3	69.7	99.2	78.3	98.7	63.8	100.0	68.0
HC 11	97.1	84.3	100.0	87.9	99.7	83.7	100.0	84.3	100.0	87.2	99.4	65.5
mean	98.5	89.3	99.4	92.4	98.6	90.2	95.6	92.3	99.1	89.8	99.0	87.4
sd	1.0	7.8	0.9	6.8	2.0	8.1	6.6	6.7	1.7	9.5	1.9	10.9
LHON 1	99.1	92.1	100.0	91.7	99.7	89.8	100.0	90.5	99.2	90.3	100.0	88.9
LHON 2	95.8	84.6	91.1	82.1	97.3	86.1	96.9	88.4	99.2	88.0	95.0	82.8
LHON 3	80.2	81.0	75.7	88.6	81.3	77.6	78.3	77.9	85.7	80.6	81.1	77.3
LHON 4	96.8	89.6	100.0	90.8	98.3	91.2	98.0	88.8	100.0	93.1	96.3	95.6
LHON 5	100.0	90.7	100.0	91.4	100.0	93.5	100.0	93.0	100.0	91.9	100.0	94.8
LHON 6	99.5	84.4	100.0	90.5	95.9	86.4	91.7	85.8	100.0	86.6	94.0	86.8
LHON 7	100.0	79.5	100.0	82.1	100.0	86.7	100.0	87.9	100.0	83.3	100.0	88.6
LHON 8	47.4	60.3	98.6	77.9	95.6	77.9	96.5	76.4	100.0	79.6	93.0	75.6
LHON 9	98.1	86.5	100.0	89.3	100.0	86.7	100.0	86.8	100.0	89.6	100.0	83.7
LHON 10	99.4	85.2	100.0	83.5	97.3	86.1	99.0	87.8	94.8	86.2	97.9	84.5
LHON 11	91.8	83.0	98.4	96.1	97.3	97.1	98.3	97.7	94.5	96.0	98.1	100.0
mean	91.6	83.3	96.7	87.6	96.6	87.2	96.2	87.4	97.6	87.7	95.9	87.1
sd	15.1	8.2	7.1	5.2	5.1	5.6	6.2	5.8	4.2	4.9	5.3	7.2

3.4 fMRI results

The results for the fMRI paradigms are not presented following the same order as the acquisition, but with a more conceptual one: starting with the more simple and controlled purely visual stimulation (pure visual paradigm), following with a slightly more complex and less controlled visual stimulation (visual pattern paradigm, without and with 2afc) and finishing with the combination of visual and cognitive stimulation (visual cognitive paradigm).

3.4.1 Pure visual paradigm

Regarding brain responses to monochromatic sustained light in the pure visual paradigm, we observed a group effect within visual areas in HC for both light colours and, clearly, also when considering light stimulation with no colour distinction. As for patients, probably the effect was not strong enough to come out as a significant group mean effect (Figure 3.4, Table 3.8). A significant lower recruitment of the occipital pole was found for LHON patients compared to HC, especially with red light. When comparing the two different wavelengths, under blue light stimulation compared to red a lower brain activation of visual areas, but also subcortical and other cortical areas, were found in HC. This effect is in general due to stronger positive activations under red light compared to blue (Figures 3.4, 3.5, Table 3.8). Instead, a higher response to blue light compared to red was found within the insular cortex and the precentral gyrus for LHON patients, as a positive brain response to blue light was present along with a negative response to red light. A stronger brain activity in LHON compared to HC when considering the contrast blue > red was found, and this is probably related to the lower activation with blue light stimulation which was observed on average in HC and not in LHON. Specifically, for the cluster in the occipital pole, a strong positive response to red light was present in HC but absent in LHON, while smaller positive responses to blue light were observed in both groups; a part from the cluster in the frontal pole (with a negative response to blue for HC), for the other clusters the observed significant effect was due to a deactivation with red light in LHON combined with an activation with red light in HC, and the opposite situation with blue light, i.e. positive response for LHON while negative for HC (Figures 3.4, 3.6, Table 3.8). The time modulated regressors gave no significant results. For all the 22 subjects, the mean displacement estimated by MCFLIRT during the fMRI acquisition was less than 2mm.

As for the brain response to light onset (transient effects), a significant group effect of visual areas recruitment was observed in both HC and LHON, with a lower activation in LHON, and this is confirmed by the significant results in the comparisons, especially

for blue light. Considering the stronger visual stimulation at light onset, compared to a uniform sustained light, in this case probably the effect was strong enough to come up as an average group effect for patients as well (Figure 3.7, Table 3.9). No significant differences were observed when comparing the two colours. The time modulated regressors gave no significant results.

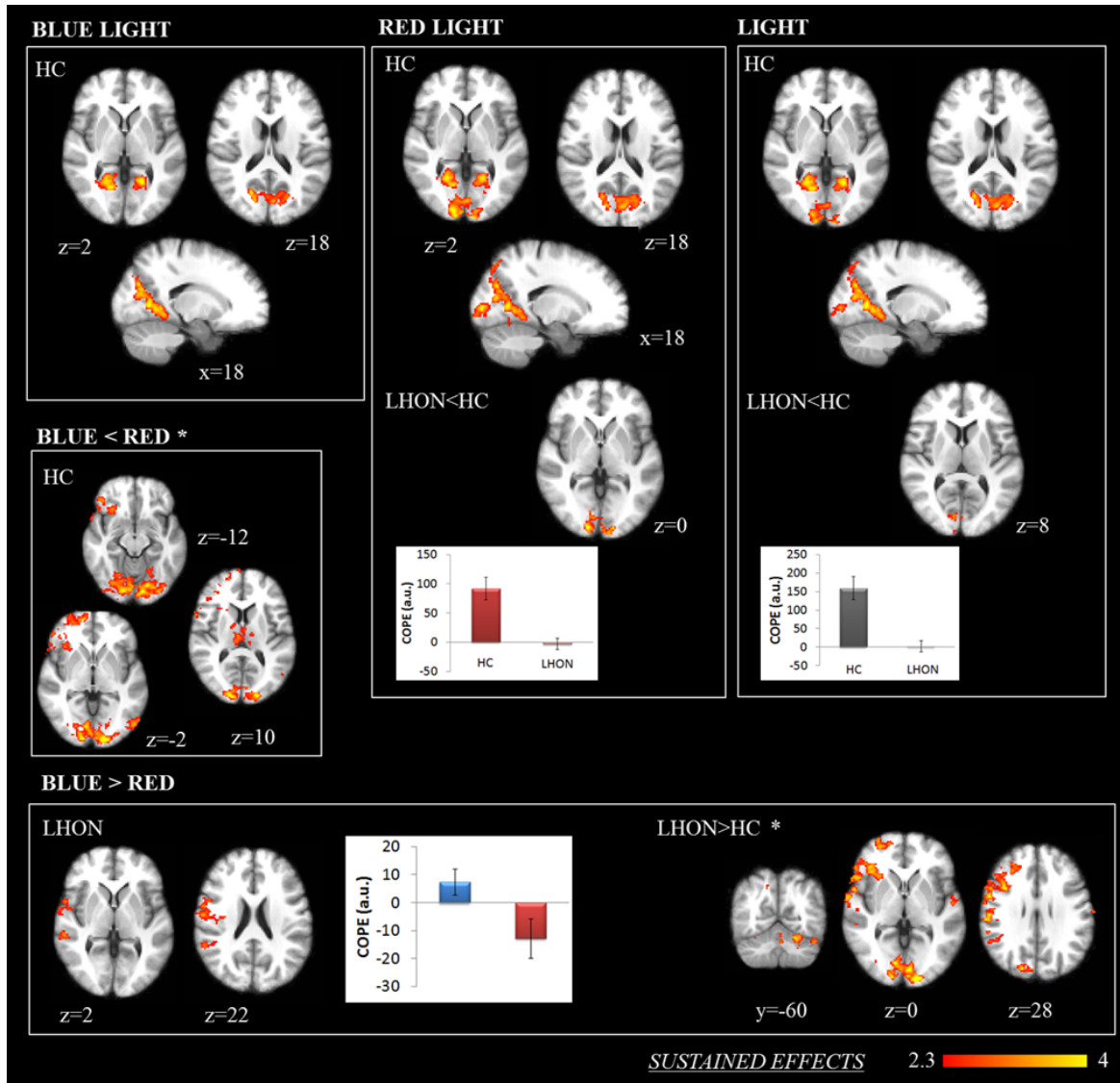


Figure 3.4 Group-level results for sustained effects in pure visual paradigm (FWE corrected, $p < 0.05$). Statistical maps of z-values are shown. The background is an average of individual T1-w scans, images are in radiological convention. For comparisons between light conditions and/or groups, histograms are shown and they report mean and standard error of the estimated activity (COPE: contrast parameter estimates; *: for these contrast, histograms for each separate cluster are in Figures 3.5 and 3.6); bars are coloured according to the colour of light, and they are grey when no distinction between colours is taken into consideration.

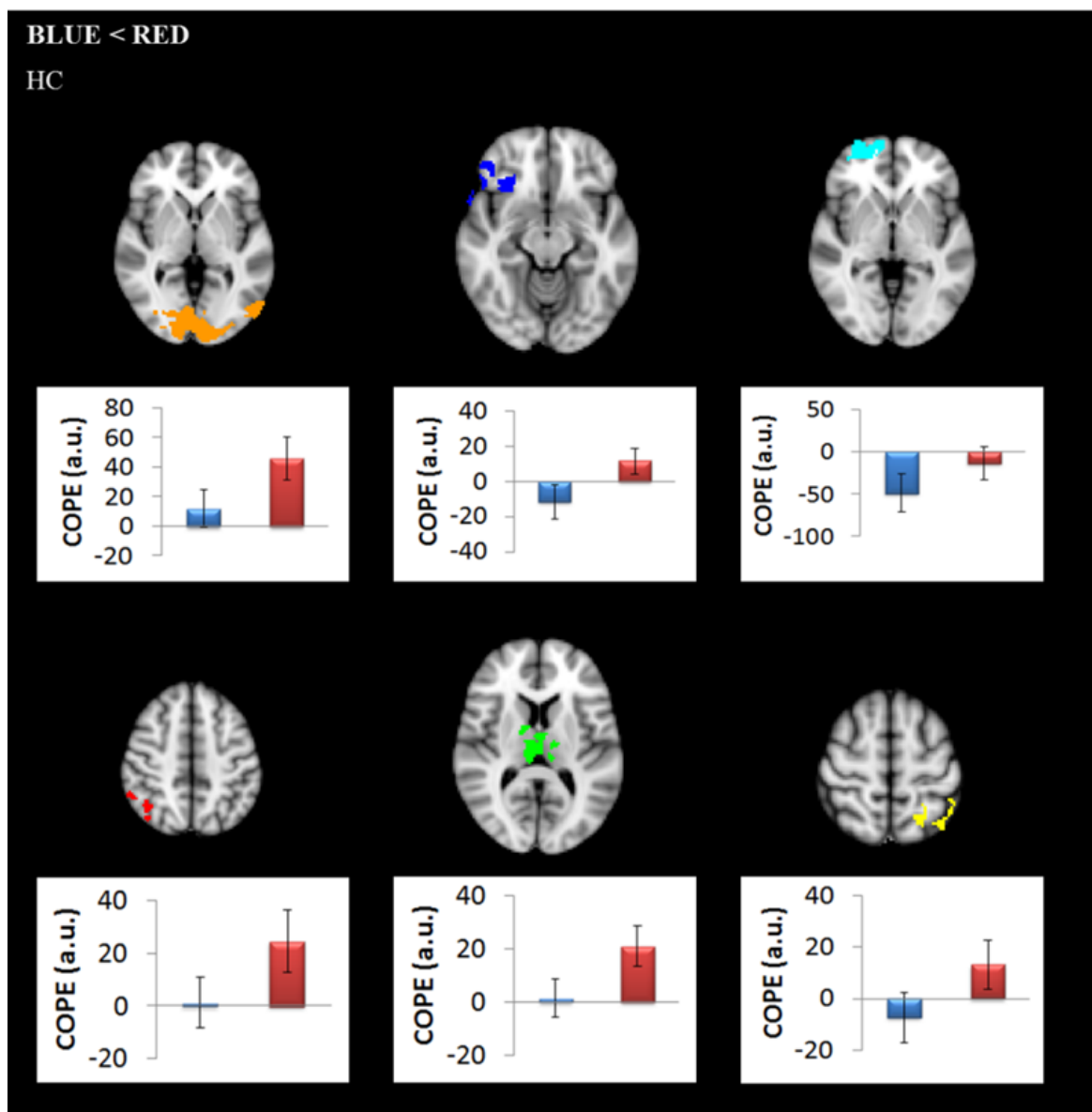


Figure 3.5 Histograms of mean estimated activity for each cluster of the contrast blue<red in HC for sustained effects of pure visual paradigm (COPE: contrast parameter estimates). Bars are coloured according to the colour of light.

Table 3.8 Cluster data for group-level results for sustained effects in pure visual paradigm.

		Volume (mm ³)	z-stat max	p-value	Coordinates (mm)			Area	
					x	y	z		
Blue light	HC	14792	4.23	1.77E-14	18	-64	4	Intracalcarine Cortex (r)	
Red light	HC	32792	4.54	1.05E-24	16	-92	4	Occipital Pole (r)	
	LHON < HC	7200	3.95	5.96E-08	16	-94	2	Occipital Pole (r)	
Light	HC	25256	4.31	3.43E-21	20	-62	6	Intracalcarine Cortex (r)	
	LHON < HC	1856	3.32	2.06E-02	16	-94	2	Occipital Pole (r)	
Blue < Red	HC	46040	4.55	6.99E-28	-18	-96	4	Occipital Pole (l)	
		16536	3.48	2.38E-13	44	38	-12	Frontal Pole (r)	
		6152	3.72	3.46E-06	12	62	-2	Frontal Pole (r)	
		5992	3.34	4.71E-06	62	-46	42	Angular Gyrus (r)	
		4832	3.21	4.82E-05	6	-20	8	Thalamus (r)	
		2280	3.83	1.79E-02	-38	-64	60	Lateral Occipital Cortex (l)	
		LHON	11912	3.57	1.96E-10	62	8	10	Precentral Gyrus (r)
		37856	4.07	2.74E-24	62	10	10	Precentral Gyrus (r)	
Blue > Red	LHON > HC	27816	4.17	1.68E-19	-8	-88	-8	Lingual Gyrus (l)	
		3008	3.55	2.84E-03	44	-42	20	Supramarginal Gyrus (r)	
		2816	3.63	4.55E-03	8	-32	54	Precentral Gyrus (r)	
		2152	3.28	2.52E-02	28	56	-2	Frontal Pole (r)	
		1984	3.52	3.98E-02	-68	-16	16	Postcentral Gyrus (l)	

Coordinates are in the standard MNI space; brain areas are referred to the Harvard-Oxford Cortical and Subcortical Structural Atlases; (l): left, (r): right.

Table 3.9 Cluster data for group-level results for transient effects in pure visual paradigm.

		Volume (mm ³)	z-stat max	p-value	Coordinates (mm)			Area	
					x	y	z		
Blue light	HC	103232	4.93	2.61E-35	14	-66	2	Lingual Gyrus (r)	
		6312	3.42	5.96E-08	38	-2	56	Precentral Gyrus (r)	
		3232	3.36	2.13E-04	-32	-52	50	Superior Parietal Lobule (l)	
		1920	3.58	1.23E-02	-4	-76	-36	Cerebellum (Crus II,l)	
		1792	3.3	1.90E-02	26	-14	62	Precentral Gyrus (r)	
		1560	3.24	4.27E-02	60	-48	14	Angular Gyrus (r)	
		1536	3.91	4.65E-02	2	10	50	Paracingulate Gyrus (r)	
		LHON	4824	3.75	3.10E-06	10	-66	12	Intracalcarine Cortex (r)
		2176	3.47	5.25E-03	-20	-66	4	Intracalcarine Cortex (l)	
		LHON < HC	4104	3.65	1.95E-05	20	-52	0	Lingual Gyrus (r)
		2984	3.29	4.36E-04	12	-86	12	Intracalcarine Cortex (r)	
		2040	3.27	8.20E-03	-20	-64	-12	Lingual Gyrus (l)	
		Red Light	HC	52408	4.94	1.66E-35	-4	-76	16
LHON	1896		3.5	1.79E-02	-40	-80	14	Lateral Occipital Cortex (l)	
	LHON	15016	3.78	1.56E-14	16	-80	32	Cuneal Cortex (r)	
Light	HC	89848	5.21	4.89E-38	-4	-76	16	Intracalcarine Cortex (l)	
		3880	3.31	3.11E-05	52	-6	56	Precentral Gyrus (r)	
		1504	3.29	4.91E-02	-28	-64	58	Lateral Occipital Cortex (l)	
		LHON	15616	3.97	1.01E-15	22	-58	4	Lingual Gyrus (r)
	LHON < HC	2928	3.72	4.62E-04	20	-52	0	Lingual Gyrus (r)	

Coordinates are in the standard MNI space; brain areas are referred to the Harvard-Oxford Cortical and Subcortical Structural Atlases; (l): left, (r): right.

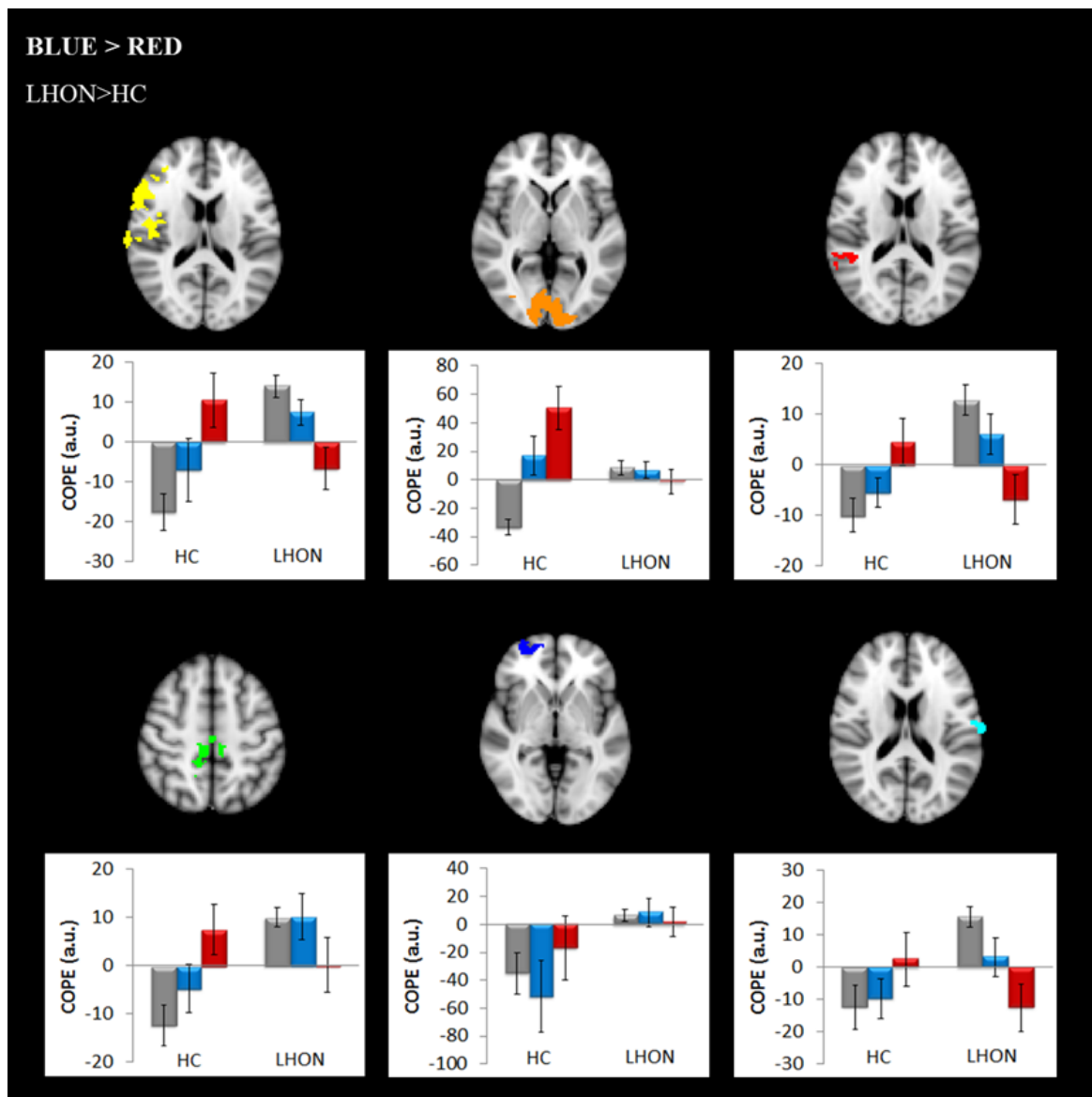


Figure 3.6 Histograms of mean estimated activity for each significant cluster of the contrast blue > red in LHON > HC for sustained effects of pure visual paradigm (COPE: contrast parameter estimates). Grey bars represent COPEs for the contrast blue > red, that resulted significantly different between LHON and HC, while blue and red bars represent COPE for blue and red light respectively within the same cluster and are shown for interpretation purposes.

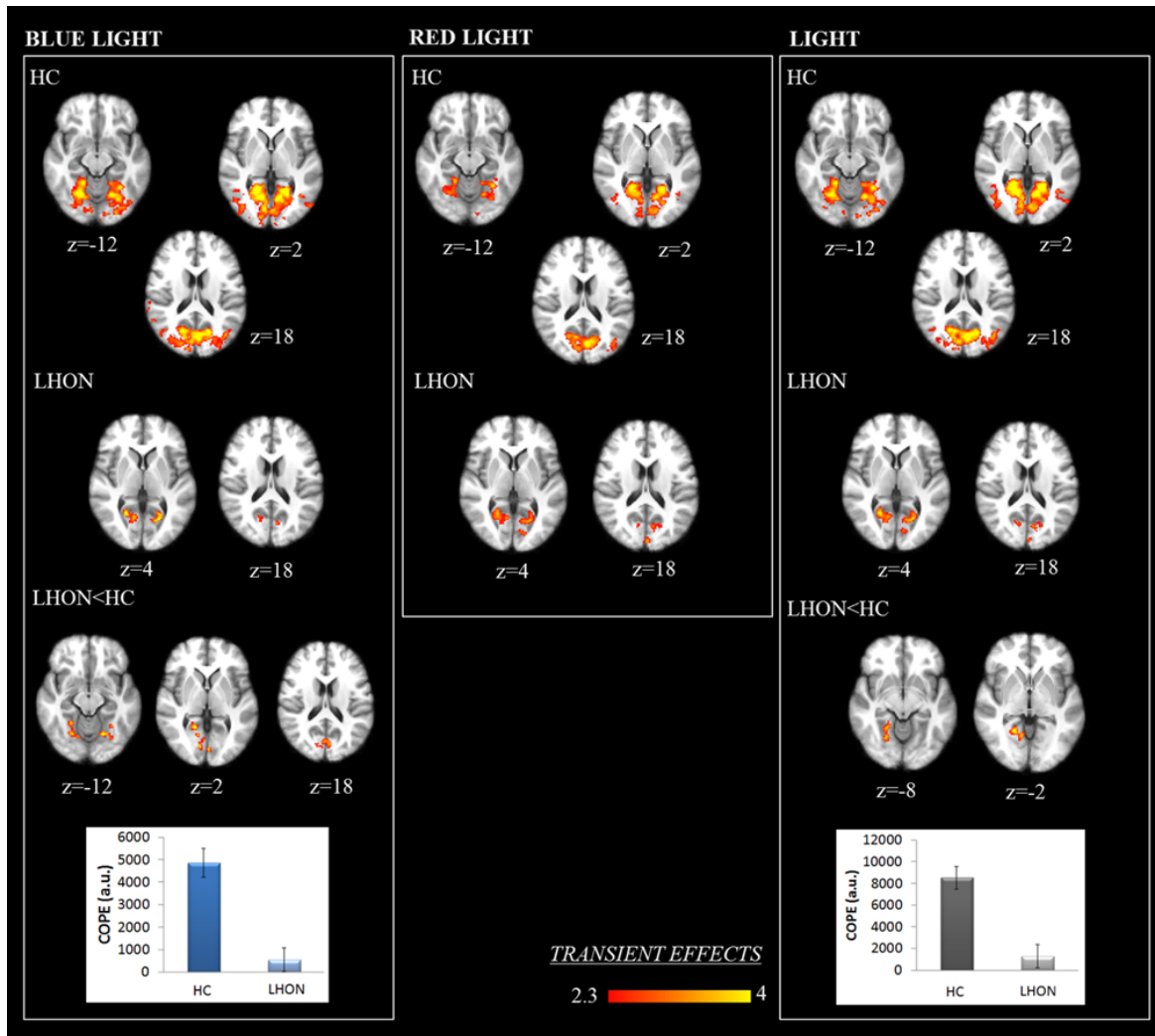


Figure 3.7 Group-level results for transient effects in pure visual paradigm (FWE corrected, $p < 0.05$). Statistical maps of z-values are shown. The background is an average of individual T1-w scans, images are shown in radiological convention. For comparisons between groups, histograms are shown and they report mean and standard error of the estimated activity (COPE: contrast parameter estimates); bars are coloured according to the colour of light, and they are grey when no distinction between colours is taken into consideration.

3.4.2 Visual pattern paradigm

Brain responses to sustained stimulation in the visual pattern paradigm involved visual areas in both groups for both blue and red backgrounds. For LHON the activations were more in the lateral visual cortex and involved areas within the thalamus as well. When comparing the two groups, the activation was lower in occipital pole and lingual gyrus for LHON patients, while it was higher in the thalamus, that was indeed recruited only by the patients (Figure 3.8, Table 3.10). When comparing the two background colours, lower activations in visual areas were observed in both groups for the blue background. It is however important to keep in mind that blue and red are, in this paradigm, just colours on a screen, and there is no control on the wavelength of the light.

As for the transient effects, i.e. brain responses to visual paradigm stimulation onsets, visual areas are recruited in both LHON and HC, but with a significantly lower activation for patients. Compared to the sustained effects, no activation in the thalamus are observed (Figure 3.9, Table 3.11).

Considering the exploratory nature of the investigation, we also explored brain activation related to different lines orientations. Comparably to the results for the sustained effects, visual areas are significantly recruited in both groups, even if more laterally and together with thalamus for LHON. A difference between stimulation with horizontal and vertical lines was observed within the occipital pole for LHON (Figure 3.10, Table 3.12).

As for the visual paradigm with 2afc, visual areas were significantly active in both HC and LHON, but to a lower extent for LHON (Figure 3.11, Table 3.13). Brain responses to stimulation onset showed broad activation of subcortical and cortical areas, a part from the visual system: frontal, insular, parietal cortices were recruited, along with thalamus, in both groups but less in LHON (Figure 3.12, Table 3.14). When evaluating brain responses to different lines orientations, brain responses resulted very similar to those for the sustained effects. Differently from the visual pattern paradigm, no recruitment of the thalamus in LHON nor differences between orientations were observed (Figure 3.13, Table 3.15). For all participants, the mean displacement estimated by MCFLIRT during the fMRI acquisition was less than 2.5 mm.

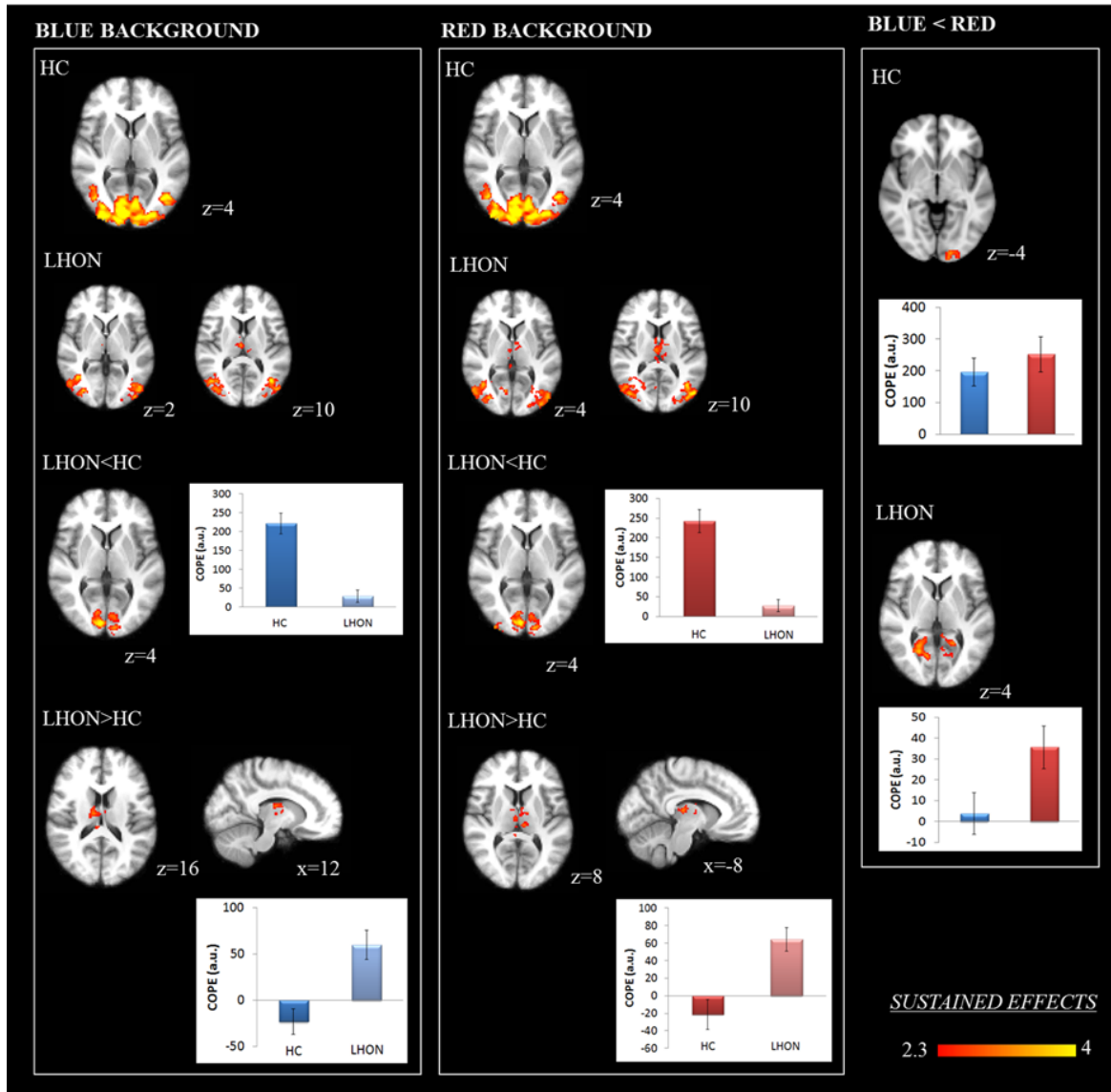


Figure 3.8 Group-level results for sustained effects in visual pattern paradigm (FWE corrected, $p < 0.05$). Statistical maps of z -values are shown. The background is an average of individual T1-w scans, images are shown in radiological convention. For comparisons between different backgrounds and/or groups, histograms are shown and they report mean and standard error of the estimated activity (COPE: contrast parameter estimates); bars are coloured according to the background colour.

Table 3.10 Cluster data for group-level results for sustained effects in visual pattern paradigm.

		Volume (mm ³)	z-stat max	p-value	Coordinates (mm)			Area
					x	y	z	
Blue background	HC	82048	5.75	1.63E-40	10	-84	-6	Lingual Gyrus (r)
		17744	4.4	1.20E-13	28	-80	22	Lateral Occipital Cortex (r)
	LHON	9992	4.2	7.83E-09	-40	-68	10	Lateral Occipital Cortex (l)
		3384	3.24	1.58E-03	4	-16	8	Thalamus (r)
		2744	3.66	7.11E-03	-36	-62	-14	Temporal Occipital Fusiform Cortex (l)
	LHON < HC	13344	4.45	5.00E-11	10	-90	6	Occipital Pole (r)
LHON > HC	2192	3.1	2.84E-02	4	-24	10	Thalamus (r)	
Red background	HC	84112	6.08	3.93E-41	10	-84	-6	Lingual Gyrus (r)
		15496	4.3	2.59E-12	-50	-80	12	Lateral Occipital Cortex (l)
	LHON	13776	4.14	2.85E-11	28	-80	24	Lateral Occipital Cortex (r)
		5424	3.16	2.28E-05	4	-14	8	Thalamus (r)
	LHON < HC	15568	4.62	2.35E-12	10	-84	-6	Lingual Gyrus (r)
LHON > HC	3704	3.17	7.89E-04	-8	-24	10	Thalamus (l)	
Blue < red	HC	2768	3.27	8.45E-03	-12	-84	-16	Occipital Fusiform Gyrus (l)
	LHON	9048	3.92	5.96E-08	22	-64	6	Intracalcarine Cortex (r)
		3392	3.09	2.04E-03	6	-58	42	Precuneous Cortex (r)

Coordinates are in the standard MNI space; brain areas are referred to the Harvard-Oxford Cortical and Subcortical Structural Atlases; (l): left, (r): right.

Table 3.11 Cluster data for group-level results for transient effects in visual pattern paradigm.

		Volume (mm ³)	z-stat max	p-value	Coordinates (mm)			Area
					x	y	z	
Blue background	HC	40048	5.4	4.61E-29	-8	-80	-2	Lingual Gyrus (l)
		2584	4.44	2.44E-03	46	-70	6	Lateral Occipital Cortex (r)
		1752	3.46	3.21E-02	-30	-56	50	Superior Parietal Lobule (l)
	LHON	24472	4.4	1.75E-20	26	-70	-8	Occipital Fusiform Gyrus (r)
		13968	4.3	1.35E-13	-28	-62	-10	Temporal Occipital Fusiform Cortex (l)
	LHON < HC	2504	3.64	3.09E-03	64	-38	22	Supramarginal Gyrus (r)
LHON > HC	4024	4.48	4.94E-05	-10	-90	-12	Lingual Gyrus (l)	
Red background	HC	77560	5.92	2.80E-45	-8	-80	-2	Lingual Gyrus (l)
	LHON	18576	4.59	1.62E-16	28	-70	-8	Occipital Fusiform Gyrus (r)
		5944	4.16	7.15E-07	-28	-86	24	Lateral Occipital Cortex (l)
		5192	4.03	3.76E-06	-28	-60	-10	Temporal Occipital Fusiform Cortex (l)
LHON < HC	6928	4.37	5.96E-08	-12	-90	-14	Occipital Pole (l)	

Coordinates are in the standard MNI space; brain areas are referred to the Harvard-Oxford Cortical and Subcortical Structural Atlases; (l): left, (r): right.

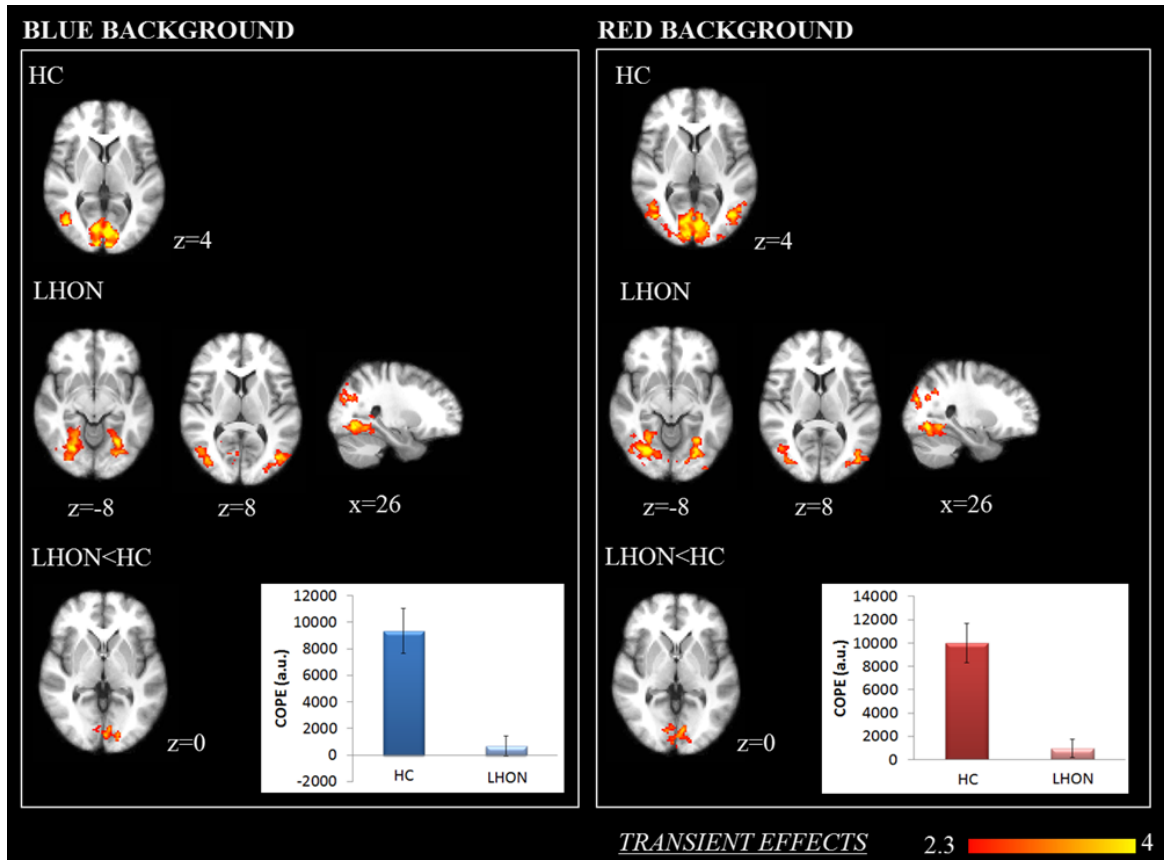


Figure 3.9 Group-level results for transient effects in visual pattern paradigm (FWE corrected, $p < 0.05$). Statistical maps of z-values are shown. The background image is an average of individual T1-w scans, images are shown in radiological convention. For comparisons between groups, histograms are shown and they report mean and standard error of the estimated activity (COPE: contrast parameter estimates); bars are coloured according to the background colour.

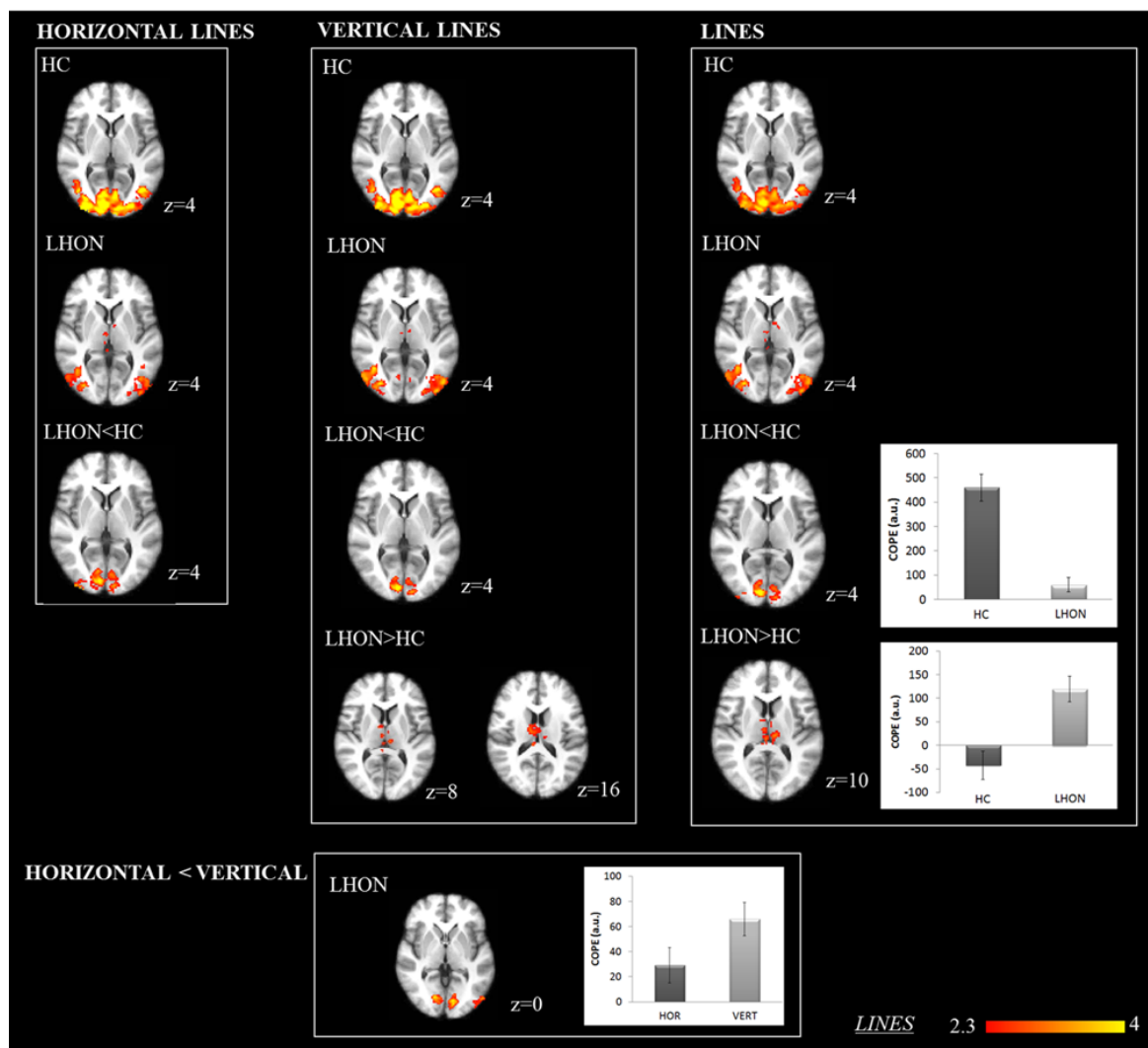


Figure 3.10 Group-level results for responses to lines (irrespective of the background colour) in visual pattern paradigm (FWE corrected, $p < 0.05$). Statistical maps of z-values are shown. The background image is an average of individual T1-w scans, images are shown in radiological convention. For comparisons between lines orientations and/or groups, histograms are shown and they report mean and standard error of the estimated activity (COPE: contrast parameter estimates); bars are coloured in grey as no distinction between colours is taken into consideration. For brevity, only group comparison histograms for lines, irrespectively of orientation, are shown.

Table 3.12 Cluster data for group-level results for responses to lines (irrespective of the background colour) in visual pattern paradigm.

		Volume (mm ³)	z-stat max	p-value	Coordinates (mm)			Area
					x	y	z	
Horizontal lines	<i>HC</i>	85968	5.9	4.62E-44	10	-84	-6	Lingual Gyrus (r)
		11656	4.17	1.65E-10	28	-80	22	Lateral Occipital Cortex (r)
	<i>LHON</i>	9136	4.17	1.05E-08	-42	-68	10	Lateral Occipital Cortex (l)
		4640	3.22	5.45E-05	4	-16	10	Thalamus (r)
	<i>LHON < HC</i>	20064	4.52	9.30E-16	20	-82	-6	Occipital Fusiform Gyrus (r)
Vertical lines	<i>HC</i>	81224	6.16	4.50E-38	10	-84	-6	Lingual Gyrus (r)
		21744	4.31	5.76E-15	28	-80	22	Lateral Occipital Cortex (r)
	<i>LHON</i>	20632	4.14	2.11E-14	-50	-78	0	Lateral Occipital Cortex (l)
		3280	3.19	3.35E-03	4	-14	10	Thalamus (r)
	<i>LHON < HC</i>	11424	4.62	3.08E-09	10	-84	-6	Lingual Gyrus (r)
	<i>LHON > HC</i>	3416	3.09	2.50E-03	6	-14	18	Thalamus (r)
Lines	<i>HC</i>	85992	6.13	7.97E-42	10	-84	-6	Lingual Gyrus (r)
		17344	4.32	2.08E-13	28	-80	22	Lateral Occipital Cortex (r)
	<i>LHON</i>	15392	4.12	2.86E-12	-40	-68	10	Lateral Occipital Cortex (l)
		4928	3.26	5.96E-05	4	-16	10	Thalamus (r)
	<i>LHON < HC</i>	15096	4.66	4.30E-12	10	-84	-6	Lingual Gyrus (r)
	<i>LHON > HC</i>	3512	3.14	1.19E-03	-8	-24	10	Thalamus (r)

Coordinates are in the standard MNI space; brain areas are referred to the Harvard-Oxford Cortical and Subcortical Structural Atlases; (l): left, (r): right.

Table 3.13 Cluster data for group-level results for sustained effects in visual pattern paradigm with 2afc.

		Volume (mm ³)	z-stat max	p-value	Coordinates (mm)			Area
					x	y	z	
Blue background	<i>HC</i>	80312	5.39	3.17E-42	10	-94	0	Occipital Pole (r)
		3872	4.49	2.85E-04	50	-70	2	Lateral Occipital Cortex (r)
	<i>LHON</i>	2128	3.5	2.28E-02	30	-66	64	Lateral Occipital Cortex (r)
		2008	3.03	3.18E-02	28	-92	32	Occipital Pole (r)
	<i>LHON < HC</i>	35144	4.78	1.08E-23	10	-94	0	Occipital Pole (r)
Red background	<i>HC</i>	85384	5.58	1.40E-45	-6	-82	-2	Lingual Gyrus (l)
	<i>LHON</i>	2968	4.33	1.80E-03	42	-68	6	Lateral Occipital Cortex (r)
	<i>LHON < HC</i>	43168	4.92	2.45E-28	10	-86	6	Intracalcarine Cortex (r)

Coordinates are in the standard MNI space; brain areas are referred to the Harvard-Oxford Cortical and Subcortical Structural Atlases; (l): left, (r): right.

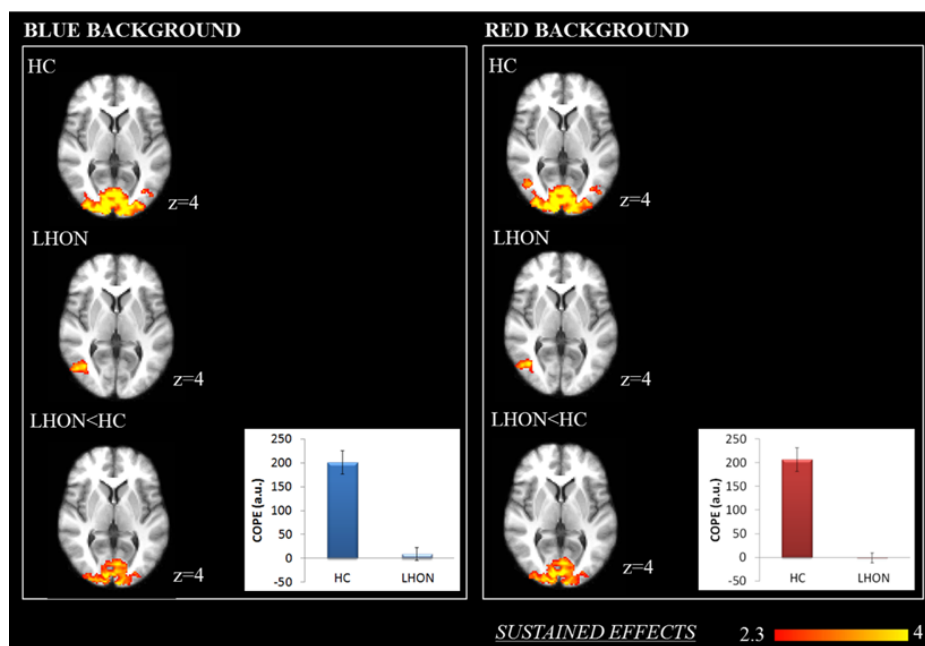


Figure 3.11 Group-level results for sustained effects in visual pattern with 2afc paradigm (FWE corrected, $p < 0.05$). Statistical maps of z-values are shown. The background image is an average of individual T1-w scans, images are shown in radiological convention. For comparisons between groups, histograms are shown and they report mean and standard error of the estimated activity (COPE: contrast parameter estimates); bars are coloured according to the background colour.

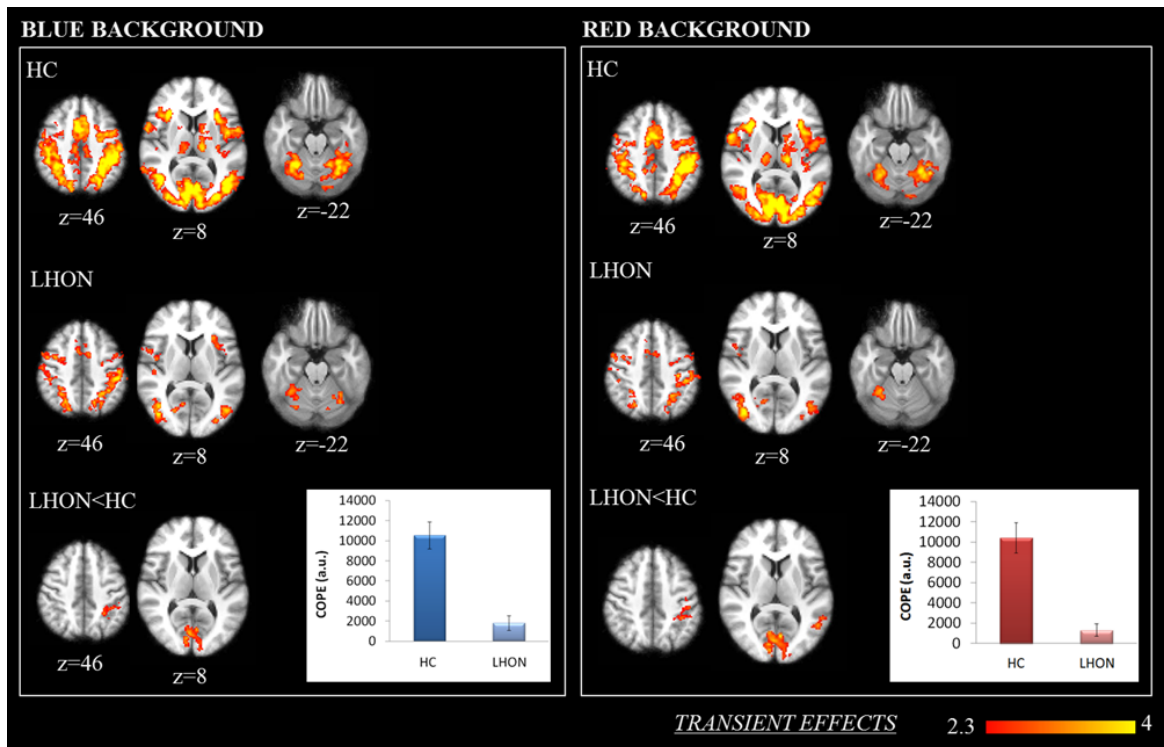


Figure 3.12 Group-level results for transient effects in visual pattern with 2afc paradigm (FWE corrected, $p < 0.05$). Statistical maps of z-values are shown. The background image is an average of individual T1-w scans, images are shown in radiological convention. For comparisons between groups, histograms are shown and they report mean and standard error of the estimated activity (COPE: contrast parameter estimates); bars are coloured according to the background colour.

Table 3.14 Cluster data for group-level results for transient effects in visual pattern paradigm with 2afc.

		Volume (mm ³)	z-stat max	p-value	Coordinates (mm)			Area
					x	y	z	
Blue background	HC	364520	6.13	1.37E-38	-8	-80	-4	Lingual Gyrus (l)
		9656	3.86	3.27E-09	-12	-22	8	Thalamus (l)
		4120	3.73	1.47E-04	-38	34	30	Middle Frontal Gyrus (l)
	LHON	63240	4.93	4.53E-36	26	-72	-6	Occipital Fusiform Gyrus (r)
		55576	4.65	5.74E-33	-54	6	36	Precentral Gyrus (l)
		10552	4.07	7.24E-10	8	2	54	Juxtapositional Lobule Cortex (r)
		2904	3.55	2.71E-03	-30	28	2	Frontal Orbital Cortex (l)
	LHON < HC	18688	4.82	3.75E-15	-8	-80	-4	Lingual Gyrus (l)
		3312	3.37	9.83E-04	-34	-44	44	Superior Parietal Lobule (l)
	Red background	HC	289680	5.68	3.12E-40	-6	-74	4
15616			4.93	1.15E-13	34	22	10	Frontal Operculum Cortex (r)
7400			4.12	1.19E-07	-14	-22	8	Thalamus (l)
4016			3.7	1.32E-04	-2	-32	26	Cingulate Gyrus (l)
3984			3.99	1.43E-04	14	-28	4	Thalamus (l)
LHON		28512	4.59	3.52E-21	-34	-8	70	Precentral Gyrus (l)
		24016	4.72	1.01E-18	28	-70	-6	Occipital Fusiform Gyrus (r)
		12552	3.8	1.32E-11	44	-4	14	Central Opercular Cortex (r)
		11176	4.38	1.26E-10	-20	-84	22	Lateral Occipital Cortex (l)
		9136	4.25	4.28E-09	0	2	52	Juxtapositional Lobule Cortex (l)
LHON < HC		3664	3.4	3.06E-04	34	-66	52	Lateral Occipital Cortex (r)
		21008	4.61	5.41E-17	-6	-76	-6	Lingual Gyrus (l)
		2504	3.49	6.05E-03	-50	-60	10	Middle Temporal Gyrus (l)
		2360	3.39	9.02E-03	-48	-24	38	Postcentral Gyrus (l)

Coordinates are in the standard MNI space; brain areas are referred to the Harvard-Oxford Cortical and Subcortical Structural Atlases; (l): left, (r): right.

Table 3.15 Cluster data for group-level results for responses to lines (irrespectively of the background colour) in visual pattern paradigm with 2afc.

		Volume (mm ³)	z-stat max	p-value	Coordinates (mm)			Area
					x	y	z	
Horizontal lines	HC	83944	5.47	8.84E-43	10	-94	0	Occipital Pole (r)
		5016	4.54	2.95E-05	42	-66	6	Lateral Occipital Cortex (r)
	LHON	2016	3.57	3.51E-02	30	-66	64	Lateral Occipital Cortex (r)
		1976	3.15	3.92E-02	28	-92	32	Occipital Pole (r)
	LHON < HC	37256	4.91	2.94E-24	10	-94	0	Occipital Pole (r)
Vertical lines	HC	80704	5.6	5.61E-44	10	-86	6	Intracalcarine Cortex (r)
	LHON	2656	4.27	3.97E-03	40	-68	6	Lateral Occipital Cortex (r)
	LHON < HC	40312	4.84	4.12E-27	12	-92	2	Occipital Pole (r)
Lines	HC	84520	5.45	1.68E-44	-4	-78	-4	Lingual Gyrus (l)
	LHON	3456	4.42	6.27E-04	50	-70	2	Lateral Occipital Cortex (r)
	LHON < HC	39648	4.83	2.93E-26	12	-92	0	Occipital Pole (r)

Coordinates are in the standard MNI space; brain areas are referred to the Harvard-Oxford Cortical and Subcortical Structural Atlases; (l): left, (r): right.

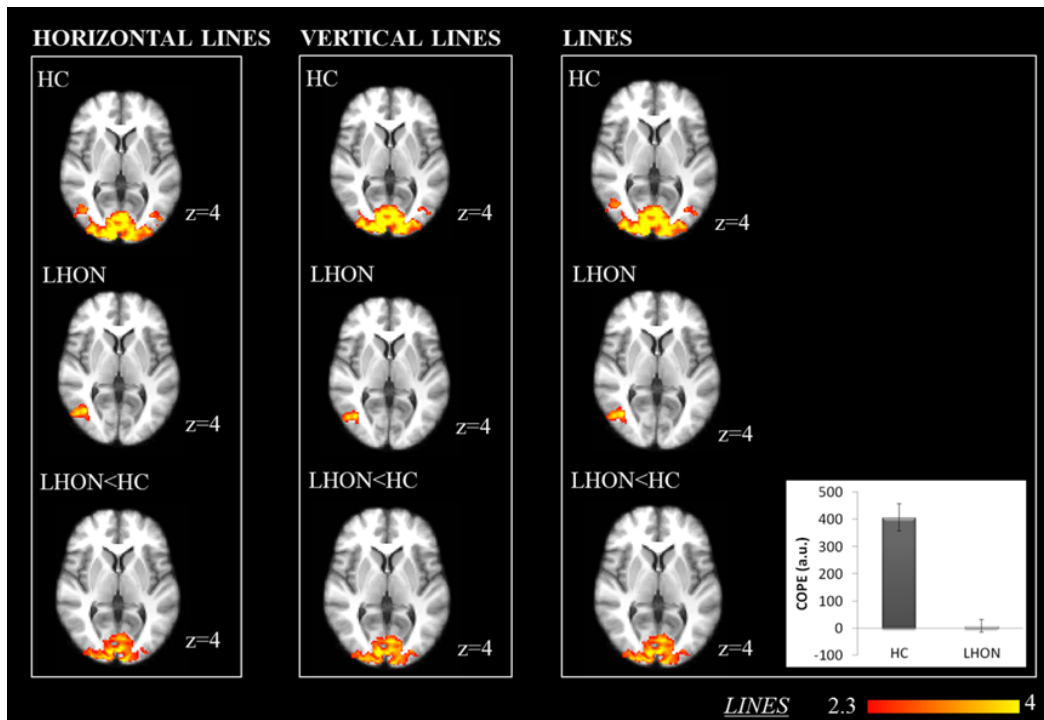


Figure 3.13 Group-level results for responses to lines (irrespective of the background colour) in visual pattern with 2afc paradigm (FWE corrected, $p < 0.05$). Statistical maps of z-values are shown. The background image is an average of individual T1-w scans, images are shown in radiological convention. For comparisons between groups, histograms are shown and they report mean and standard error of the estimated activity (COPE: contrast parameter estimates); bars are coloured in grey as no distinction between colours is taken into consideration. For brevity, only group comparison histograms for lines, irrespectively of orientation, are shown.

3.4.3 Visual cognitive paradigm

As for the fMRI paradigm that combines monochromatic light stimulation and cognitive task, we focused on the brain activation due to the n-back task (ignoring light stimulation), on the purely visual sustained response to light stimulation (as the duration of light periods was longer than in the pure visual paradigm and therefore a comparison between the two cases could be of interest) and on the interactions between cognitive task and light stimulation, i.e. the different brain responses when the task was performed under different light conditions.

When the 3-back task was compared to the control condition, that is the 0-back task, average group responses involved, for both HC and LHON, prefrontal cortex, in particular dorso-lateral prefrontal cortex (DLPFC) and mid-ventro-lateral prefrontal cortex (mid-VLPFC), frontal pole, premotor cortex bilaterally and medial premotor cortex, insular cortex, posterior parietal cortex, both medially and bilaterally, cerebellar cortex. In HC also a recruitment of structures in the basal ganglia, such as thalamus and caudate, was observed. Overall, no significant differences between the two groups were found (Figure 3.14, Table 3.16).

Regarding the sustained response to visual stimulation, areas of the visual cortex were recruited, in average, in both HC and LHON. No significant differences were found between the two groups for the blue light, while higher activations for the healthy controls were observed in the occipital pole, the parietal cortex and prefrontal areas with the red light. When visual stimulation irrespectively of colour was considered, a combination of the two outlined effects was found. Moreover, within the LHON group a more intense activation was observed within the occipital pole with blue light compared to red light (Figure 3.15, Table 3.17).

As for the interactions between task and light colours, no significant group effects was observed for HC, while significant responses were found for LHON in temporo-occipital areas, frontal pole, middle frontal gyrus, insular cortex, paracingulate cortex and bilateral putamen. Within these different clusters, typically a small and positive effect was observed with blue light, while a deactivation was present under red light stimulation (Figures 3.16, 3.17, Table 3.18). The difference of this effect between LHON and HC was significant in particular in the lateral occipital cortex, inferior, middle and superior frontal gyri, frontal pole and precuneus (Figures 3.16, 3.18, Table 3.18). In general in these clusters, for red light a strong negative response was present in LHON while a small and positive one was observed in HC, whereas for blue light stimulation the estimated responses tended to be smaller but positive in both groups (Figure 3.18). When considering the time modulated response, i.e. a response that linearly increases with time, for the interactions between task and light colours, again no significant group effects were highlighted for HC, differently from LHON, that instead showed significant activations in frontal and prefrontal areas, cuneal cortex, cingulate

gyrus, cerebellum and brainstem, in particular in areas that are compatible with the location of the locus ceruleus (Figure 3.19, Table 3.19). Within these clusters, the observed effects was essentially due to a positive brain response to the task under blue light versus a negative one with red light (Figures 3.19, 3.20). These effects resulted in a significant differences from the HC in particular in the lateral occipital cortex, the frontal operculum, superior frontal gyrus, precuneus cortex and cerebellum, where typically brain responses were negative under both blue and red light for HC, while they were negative for red and positive for blue in LHON (Figures 3.19, 3.21). With the time modulation, the estimated parameters were far smaller than those for the uniform response in time, suggesting a smaller effect for this regressor. The modulation of brain activity with different wavelengths that we described with the interactions between task and light conditions was in part within brain areas that were recruited by the task in itself, and in part within brain areas that were not significantly activated in response to the task.

As we did not find significant brain modulation by light in subcortical areas that were instead highlighted in previous literature (Vandewalle et al., 2007b), results after less stringent corrections for multiple comparisons were also considered, in order to make a comparison with previously reported data. Statistical inferences were performed after multiple comparison correction within small spherical volume (small volume correction, radius of 10 mm) at $p_{sv} < 0.05$ located around a-priori locations of activation as known from previously published works (coordinates are reported in standard MNI space): hippocampus (-28, -38, -2), (-30, -30, 2), amygdala (16, -4, -18), (22, -6, -15) and LGN (-22, -22, -10) (-23, -21, -3). Even after this focused analysis, no significant results were observed in these areas.

Task and sustained visual effects with time modulation gave no significant results. Transient responses to light onset were essentially the same as for the pure visual paradigm, both conceptually and regarding the results (data not shown). For all the 22 subjects, the mean displacement estimated by MCFLIRT during the fMRI acquisition of the present paradigm was less than 2.5 mm.

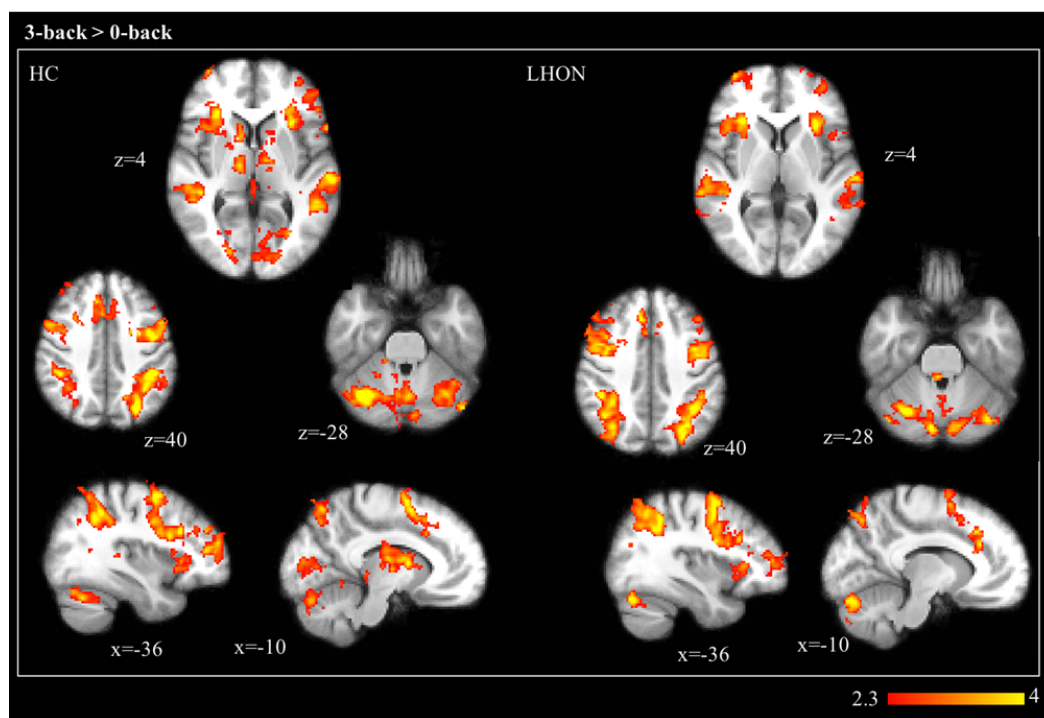


Figure 3.14 Group-level results for responses to 3-back task compared to the control condition (0-back task) in visual cognitive paradigm (FWE corrected, $p < 0.05$). Statistical maps of z-values are shown. The background image is an average of individual T1-w scans, images are shown in radiological convention.

Table 3.16 Cluster data for group-level for responses to 3-back task compared to the control condition (0-back task) in visual cognitive paradigm.

	Volume (mm ³)	z-stat max	p-value	Coordinates (mm)			Area	
				x	y	z		
HC	125352	5.14	2.30E-45	26	-10	48	Precentral gyrus (r)	
	107552	5.52	8.13E-44	34	-68	-26	Cerebellum (Crus I, r)	
	6312	4.39	1.97E-05	48	-30	-10	Middle temporal gyrus (r)	
	94144	5.41	5.61E-40	-2	8	62	SMA (l)	
	27016	4.84	1.33E-16	22	-66	56	Lateral occipital cortex (r)	
3-back > 0-back	23432	5.12	5.65E-15	-38	-52	38	Angular gyrus (l)	
	18856	5.11	9.11E-13	8	-78	-24	Occipital fusiform gyrus (r)	
	LHON	9912	4.69	5.96E-08	56	-42	-6	Middle temporal gyrus (r)
		7680	4.21	2.21E-06	-64	-44	12	Supramarginal gyrus (l)
	3864	4.15	1.58E-03	-32	52	8	Frontal pole (l)	
	3168	4.18	6.44E-03	-30	22	4	Insular cortex (l)	

Coordinates are in the standard MNI space; brain areas are referred to the Harvard-Oxford Cortical and Subcortical Structural Atlases; (l): left, (r): right.

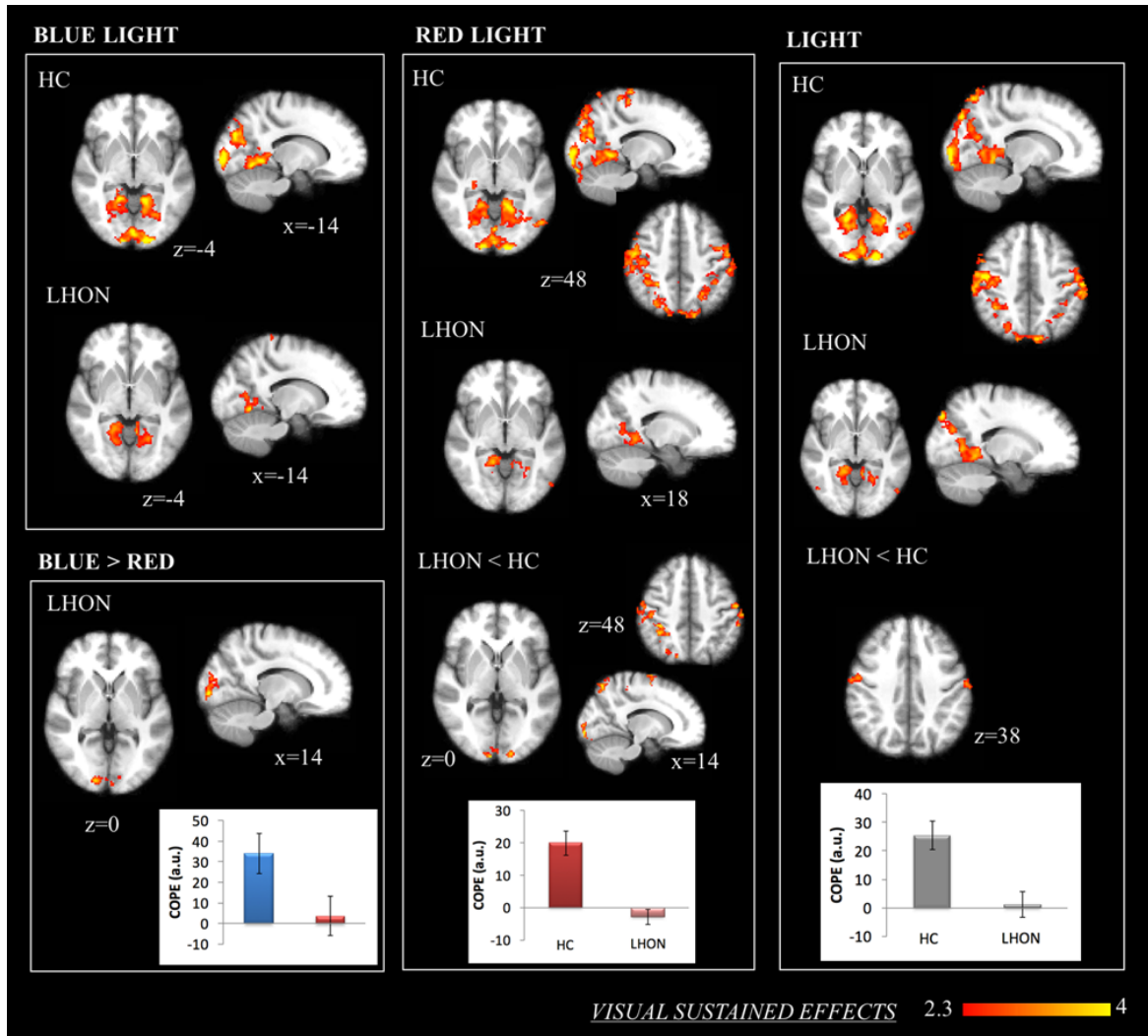


Figure 3.15 Group-level results for visual sustained effects for visual cognitive paradigm (FWE corrected, $p < 0.05$). Statistical maps of z-values are shown. The background image is an average of individual T1-w scans, images are shown in radiological convention. For comparisons between groups or light conditions histograms are shown and they report mean and standard error of the estimated activity (COPE: contrast parameter estimates); bars are coloured according to the background colour, and they are grey when no distinction between colours is taken into consideration.

Table 3.17 Cluster data for group-level for visual sustained effects in visual cognitive paradigm.

		Volume (mm ³)	z-stat max	p-value	Coordinates (mm)			Area		
					x	y	z			
Blue light	HC	41048	4.82	2.00E-21	2	-86	-8	Lingual gyrus (r)		
		6520	4.62	2.57E-05	-16	-62	-8	Lingual gyrus (l)		
		5160	3.82	2.37E-04	-26	-62	66	Lateral occipital cortex (r)		
		3208	3.77	8.44E-03	60	-6	40	Postcentral gyrus (r)		
		23136	4.39	3.48E-14	22	-62	6	Intracalcarine cortex (r)		
	LHON	5832	4.34	7.73E-05	-16	-62	-8	Lingual gyrus (l)		
		3712	3.52	3.17E-03	-26	-68	60	Lateral occipital cortex (l)		
		3216	3.61	8.30E-03	-6	-40	72	Postcentral gyrus (l)		
		Red light	HC	147888	5.18	4.20E-19	14	-96	-4	Occipital pole (r)
			LHON	6120	3.79	9.48E-06	24	-62	8	Intracalcarine cortex (r)
3976	3.85			5.94E-04	-36	-80	12	Lateral occipital cortex (l)		
LHON < HC	2128		3.64	4.02E-02	-24	-58	0	Lingual gyrus (l)		
	24856		4.12	7.21E-17	54	-26	56	Postcentral gyrus (r)		
	7096	4.17	1.73E-06	-62	8	12	Precentral gyrus (l)			
5032	4.45	7.18E-05	8	-100	0	Occipital pole (r)				
Blue > Red	LHON	4800	4.26	2.28E-04	16	-92	-2	Occipital pole (r)		
Light	HC	107872	4.96	7.01E-45	14	-98	-6	Occipital pole (r)		
		22456	4.05	7.40E-15	-64	-18	44	Postcentral gyrus (l)		
	LHON	12416	4.11	1.51E-09	30	-52	-12	Temporal occipital fusiform cortex (r)		
		9608	4.73	5.96E-08	14	-84	42	Lateral occipital cortex (r)		
		5504	3.77	5.83E-05	-16	-84	46	Lateral occipital cortex (l)		
		5408	3.88	6.92E-05	-22	-58	-2	Lingual gyrus (l)		
		2280	3.37	3.87E-02	-32	-68	58	Lateral occipital cortex (l)		
		2408	3.69	2.88E-02	-64	-18	46	Postcentral gyrus (l)		
	LHON < HC	2312	3.29	3.59E-02	64	-8	40	Postcentral gyrus (r)		

Coordinates are in the standard MNI space; brain areas are referred to the Harvard-Oxford Cortical and Subcortical Structural Atlases; (l): left, (r): right.

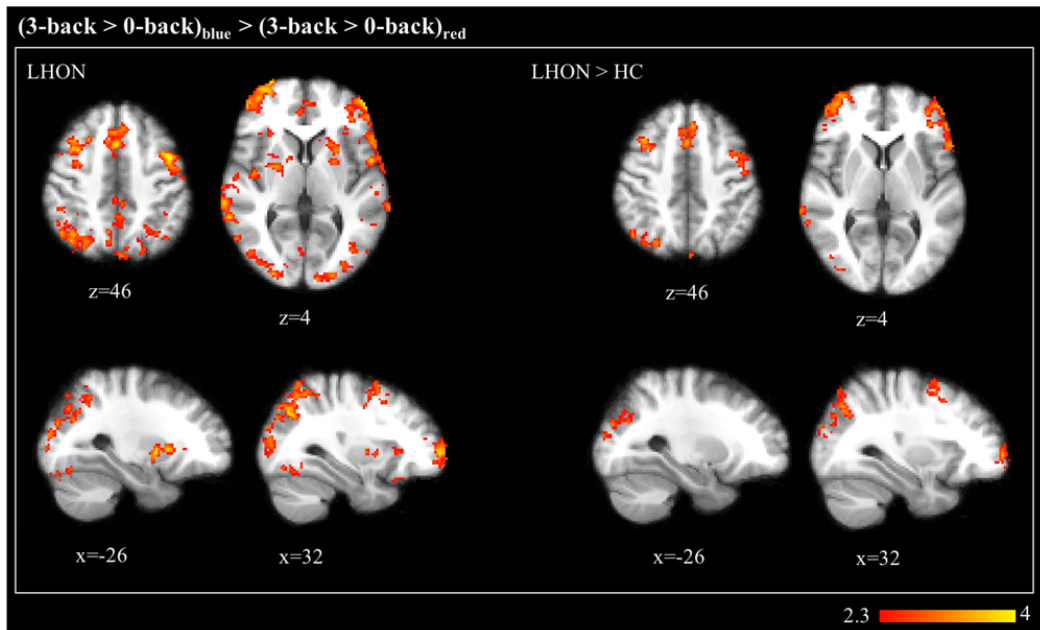


Figure 3.16 Group-level results for the interaction between cognitive tasks and light conditions for visual cognitive paradigm (FWE corrected, $p < 0.05$). Statistical maps of z-values are shown. The background image is an average of individual T1-w scans, images are shown in radiological convention. Histograms for each separate cluster are reported in Figures 3.17, 3.18

Table 3.18 Cluster data for group-level for the interaction between tasks and light conditions in visual cognitive paradigm.

	Volume (mm ³)	z-stat max	p-value	Coordinates (mm)			Area
				x	y	z	
(3-back > 0-back) _{blue} > (3-back > 0-back) _{red}	61720	3.9	7.63E-38	36	-60	-12	Temporal occipital fusiform cortex (r)
	13320	3.89	1.26E-12	-44	58	-10	Frontal pole (l)
	10072	4.31	3.24E-10	-46	6	44	Middle frontal gyrus (l)
	9368	3.91	1.16E-09	2	16	46	Paracingulate gyrus (r)
	7088	3.94	1.19E-07	36	12	48	Middle frontal gyrus (r)
	5696	4.08	1.67E-06	34	64	2	Frontal pole (r)
	5616	3.35	2.03E-06	-52	-70	-10	Lateral occipital cortex (l)
	3824	3.38	1.28E-04	44	-8	4	Insular cortex (r)
	2584	3.78	3.34E-03	-26	12	2	Putamen (l)
	2456	3.5	4.80E-03	-64	-44	-4	Middle temporal gyrus (l)
	2216	3.46	9.65E-03	-20	-86	-20	Occipital fusiform gyrus (l)
	2136	3.89	1.22E-02	38	24	-22	Frontal orbital cortex (r)
	2112	3.52	1.32E-02	56	30	30	Middle frontal gyrus (r)
	1720	3.38	4.40E-02	26	-2	4	Putamen (r)
	LHON > HC	11104	3.66	5.25E-11	30	-72	42
7568		3.9	5.96E-08	-56	22	8	Inferior frontal gyrus (l)
4200		3.37	5.11E-05	-34	-82	28	Lateral occipital cortex (l)
4032		3.75	7.67E-05	34	64	0	Frontal pole (r)
2704		3.41	2.39E-03	-4	-58	70	Precuneus cortex (l)
2424		3.56	5.27E-03	-4	32	46	Superior frontal gyrus (l)
2392		3.78	5.77E-03	40	20	46	Middle frontal gyrus (r)
1848		3.31	2.95E-02	-40	8	48	Middle frontal gyrus (l)

Coordinates are in the standard MNI space; brain areas are referred to the Harvard-Oxford Cortical and Subcortical Structural Atlases; (l): left, (r): right.

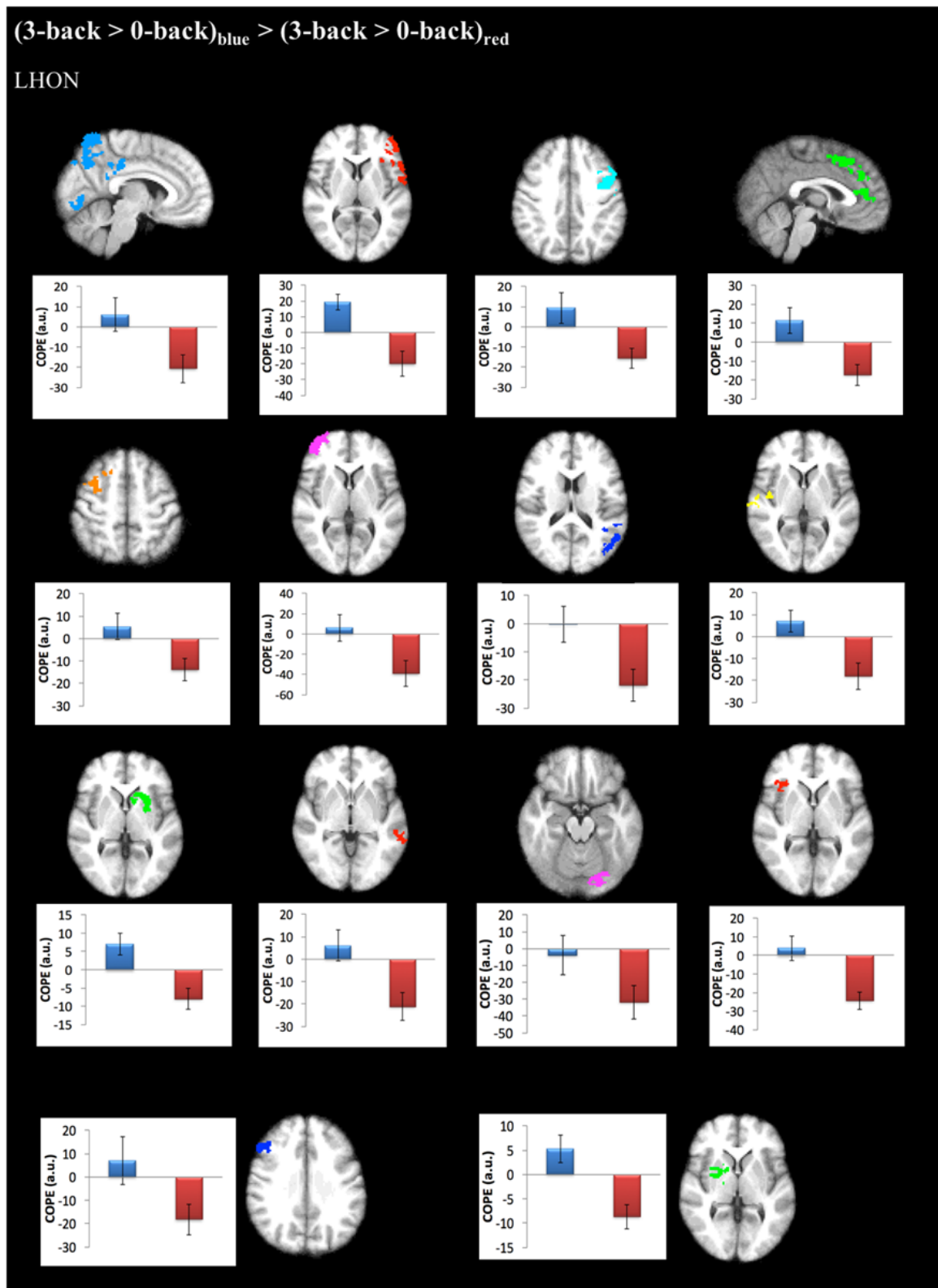


Figure 3.17 Histograms of mean estimated activity for each cluster of the interaction between tasks and light conditions in LHON of visual cognitive paradigm (COPE: contrast parameter estimates). Grey bars represent COPEs for the contrast on interest, that resulted significantly different between LHON and HC, while blue and red bars represent COPE for blue and red light respectively within the same cluster and are shown for interpretation purposes.

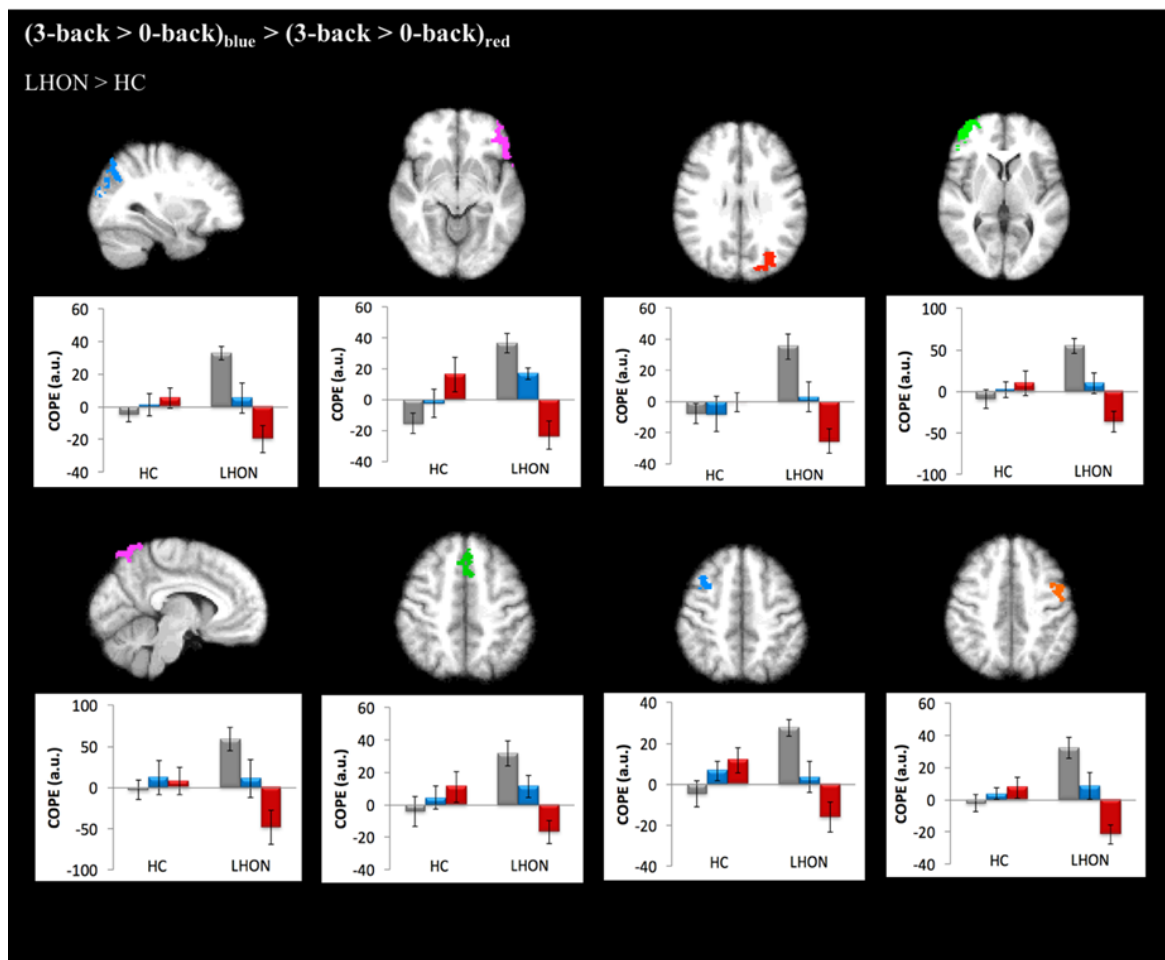


Figure 3.18 Histograms of mean estimated activity for each cluster of the interaction between tasks and light conditions in the contrast LHON > HC of visual cognitive paradigm (COPE: contrast parameter estimates). Grey bars represent COPEs for the contrast of interest, that resulted significantly different between LHON and HC, while blue and red bars represent COPE for blue and red light respectively within the same cluster and are shown for interpretation purposes.

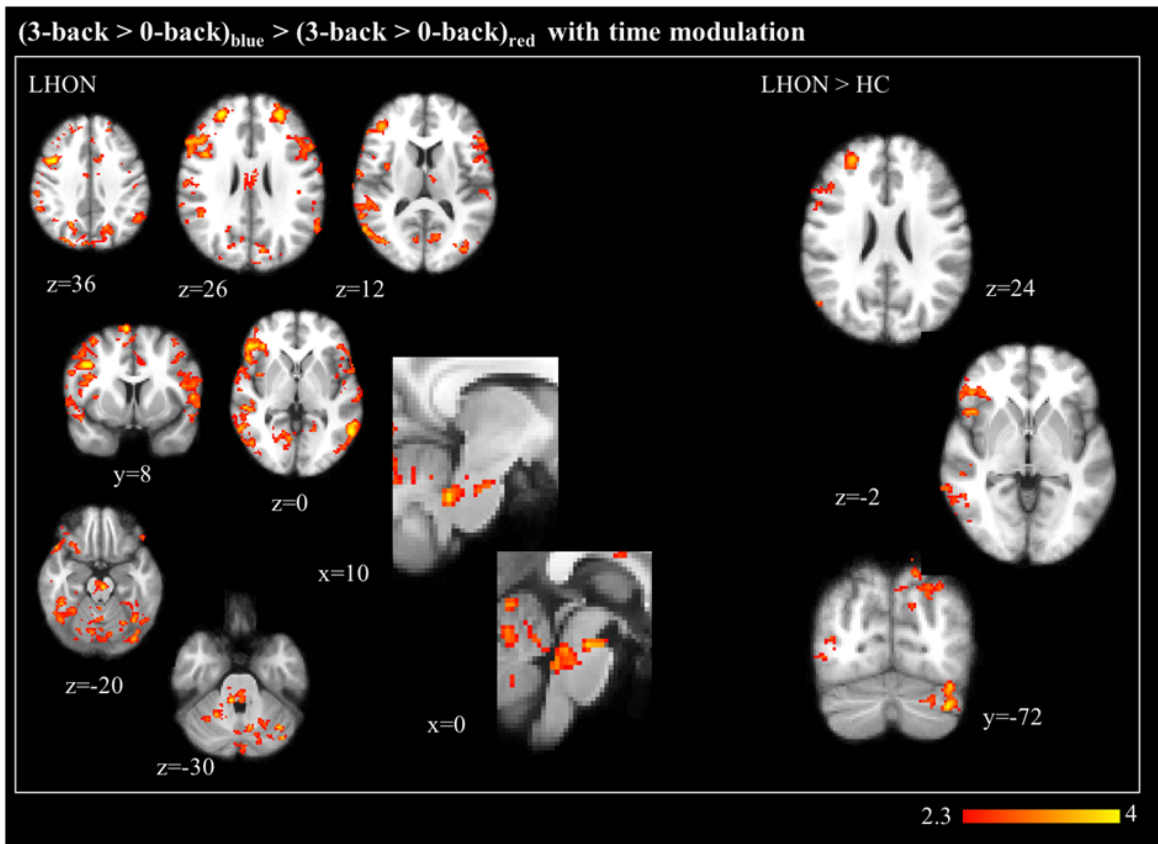


Figure 3.19 Group-level results for the interaction between cognitive tasks and light conditions with time modulation for visual cognitive paradigm (FWE corrected, $p < 0.05$). Statistical maps of z-values are shown. The background image is an average of individual T1-w scans, images are shown in radiological convention. Histograms for each separate cluster are reported in Figures 3.20, 3.21.

Table 3.19 Cluster data for group-level for the interaction between tasks and light conditions with time modulation in visual cognitive paradigm.

	Volume (mm ³)	z-stat max	p-value	Coordinates (mm)			Area
				x	y	z	
(3-back > 0-back)_{blue} > (3-back > 0-back)_{red} with time modulation	92224	4.31	4.12E-21	44	10	36	Middle frontal gyrus (r)
	21648	3.8	1.38E-16	-10	-80	24	Cuneal cortex (l)
	16032	3.94	2.64E-13	-48	26	18	Inferior frontal gyrus (l)
	5952	3.67	3.76E-06	56	-40	48	Supramarginal gyrus (r)
	3368	4.1	9.80E-04	-26	46	28	Frontal pole (l)
	3304	3.67	1.14E-03	-40	-4	60	Precentral gyrus (l)
	2704	3.81	5.04E-03	8	-38	-30	Brainstem
	2512	3.67	8.29E-03	6	-12	30	Cingulate gyrus (r)
	6792	3.51	7.75E-07	46	18	-2	Frontal operculum cortex (r)
	4664	3.46	5.29E-05	44	-76	16	Lateral occipital cortex (r)
	3376	3.87	9.61E-04	4	52	40	Superior frontal gyrus (r)
	3136	3.55	1.71E-03	-16	-68	38	Precuneus cortex (l)
	2824	3.94	3.72E-03	-40	-72	-36	Cerebellum (Crus I, l)
2768	3.41	4.28E-03	42	-54	-14	Temporal occipital fusiform cortex (r)	
LHON > HC							

Coordinates are in the standard MNI space; brain areas are referred to the Harvard-Oxford Cortical and Subcortical Structural Atlases; (l): left, (r): right.

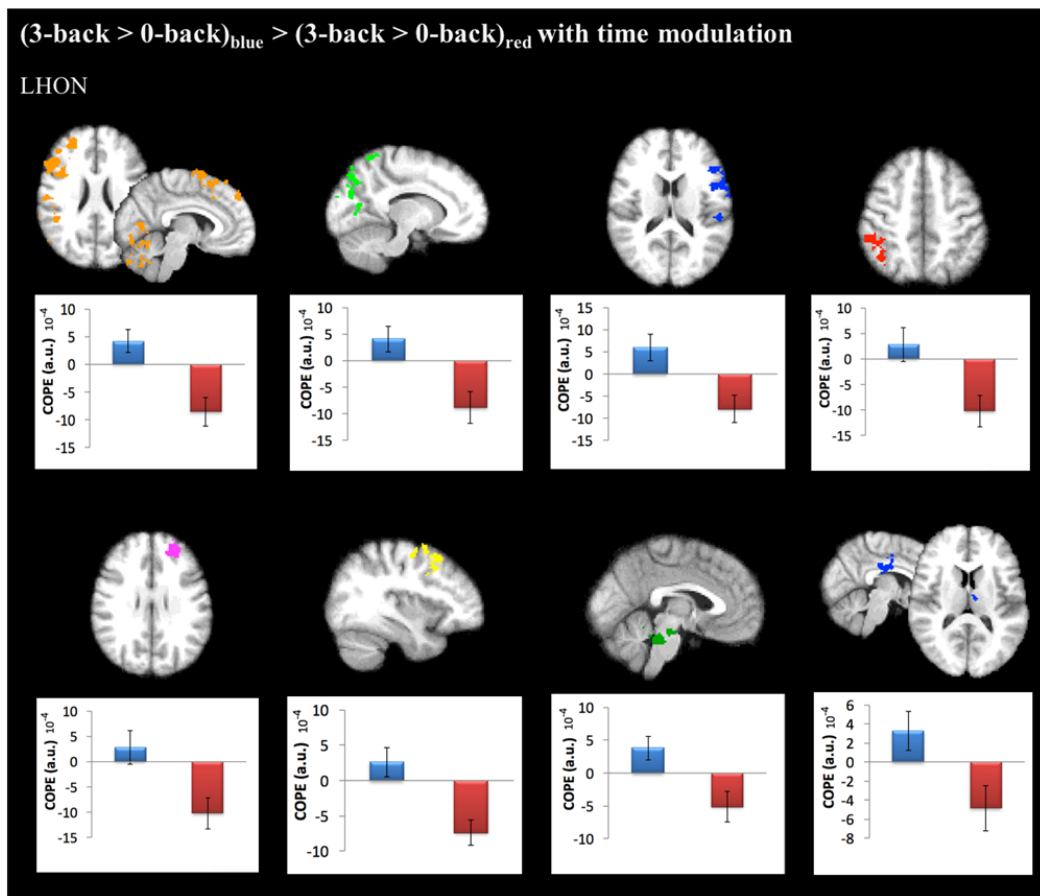


Figure 3.20 Histograms of mean estimated activity for each cluster of the interaction between tasks and light conditions with time modulation in LHON for visual cognitive paradigm (COPE: contrast parameter estimates). Bars are coloured according to the colour of light.

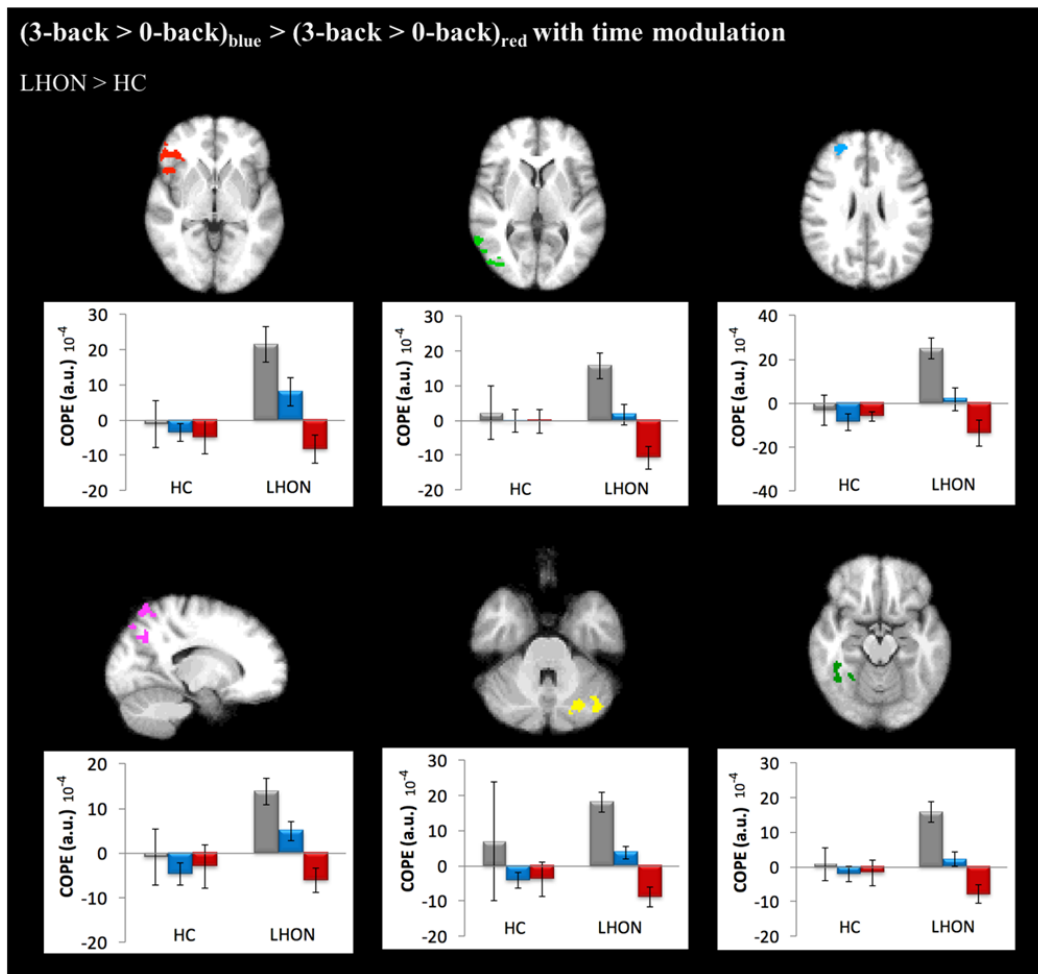


Figure 3.21 Histograms of mean estimated activity for each cluster of the interaction between tasks and light conditions with time modulation in the contrast LHON > HC of visual cognitive paradigm (COPE: contrast parameter estimates). Bars are coloured according to the colour of light.

3.5 Structural evaluation (VBM)

Whole brain VBM analysis of grey matter showed that, compared to healthy subjects, LHON patients had a significantly lower GM density in the primary visual cortex (Figure 3.22); the maximum of the cluster in the statistic map is located in the occipital pole, as long as most part of local maxima, Table 3.20). White matter VBM gave no significant results.

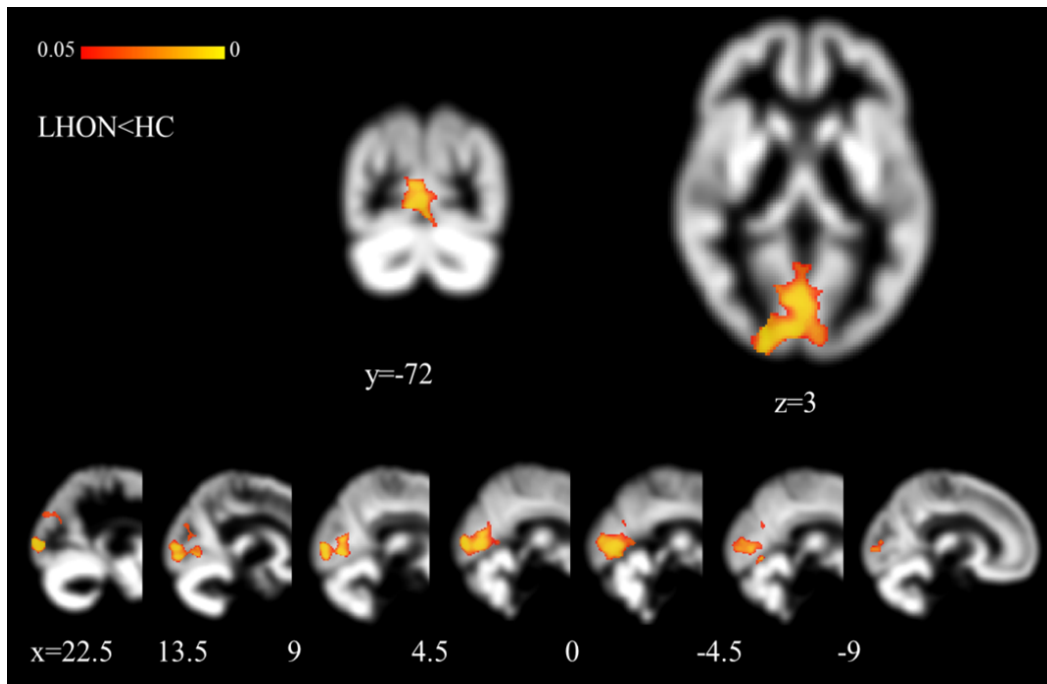


Figure 3.22 VBM analysis results. Statistical results from the comparison LHON < HC are shown over the study-specific grey matter template. Images are shown in radiological convention.

Table 3.20 VBM analysis results: cluster data for the comparison LHON<HC.

<u>Cluster</u>	Volume (mm ³)	t-stat value	p-value	Coordinates (mm)			Area
				x	y	z	
	16099	6.33	0.005	21	-96	3	<i>Occipital pole (r)</i>
		t-stat value	p-value	Coordinates (mm)			Area
		6.25	0.006	21	-99	4.5	<i>Occipital pole (r)</i>
<u>Local maxima</u>		5.89	0.007	6	-91.5	3	<i>Occipital pole (r)</i>
		5.88	0.007	21	-94.5	0	<i>Occipital pole (r)</i>
		5.43	0.008	12	-91.5	4.5	<i>Occipital pole (r)</i>
		5.39	0.008	10.5	-75	0	<i>Lingual gyrus (r)</i>

Coordinates are in the standard MNI space; brain areas are referred to the Harvard-Oxford Cortical Structural Atlas, (r): right.

3.6 fMRI results with structural correction

Our VBM results raised the issue of a possible role of GM atrophy in the differences we observed between HC and LHON in visual areas for fMRI activation, especially as far as the pure visual and the visual pattern paradigms are concerned.

Even if one of the first studies investigating the relationship between fMRI activation and atrophy dates back to 2000 [121], the role of GM atrophy in fMRI is still controversial [122–125]. Structural differences may give rise to partial volume effects, and, from one side, these effects may be ignored in fMRI analyses with the assumption that they are controlled for as fMRI group differences are evaluated after that within-subject statistical maps had been computed, and the fMRI signal might be strong enough to make these differences in noise levels between groups negligible. However, considering the relatively low spatial resolution of fMRI and the thickness of cortical structures of interest, even small structural differences between groups may lead to different partial volume effects contributing to the signal in fMRI voxels and therefore differences in the measured signal and in the observed results [126]. Mean grey matter density can be used as a covariate to take into account cortical atrophy, but this parameter does not consider local differences in cortical areas. To be more specific, grey matter maps of each subject can be added to the analyses as a regressor for structural damage, in a voxel-wise setting [122].

In order to assess a possible role of structural damage in our fMRI results, especially in group comparisons, we repeated all the comparisons between LHON and HC for all the

paradigms including each subject modulated GM maps (as constructed for VBM analysis) as a voxel-wise covariate of no interest.

3.6.1 Pure visual paradigm

When adding GM maps as covariate of no interest in group comparisons, for sustained effects in the pure visual paradigm the results are confirmed for the lower activation in occipital pole for LHON with red light and for the higher cortical recruitment for LHON in the contrast blue>red (Figure 3.23, Table 3.21). Similarly, the lower activation in visual areas for LHON in response to transient stimuli of blue light and light irrespectively of colour remains (Figure 3.24, Table 3.21).

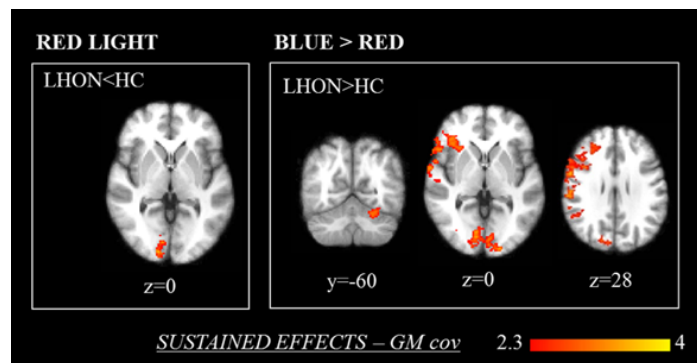


Figure 3.23 Group comparisons results for sustained effects in pure visual paradigm with GM maps as covariate of no interest (FWE corrected, $p < 0.05$). Statistical maps of z-values are shown, the background image is an average of individual T1-w scans. Images are shown in radiological convention.

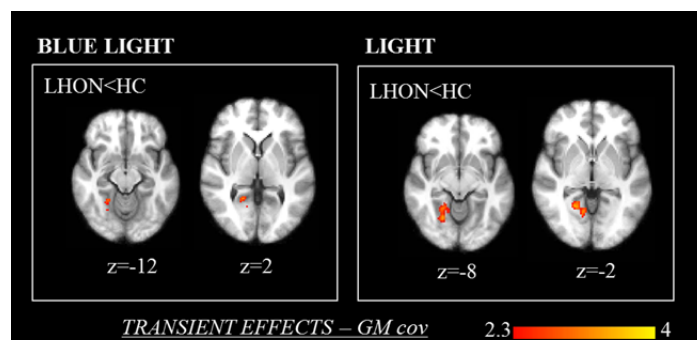


Figure 3.24 Group comparisons results for transient effects in pure visual paradigm with GM maps as covariate of no interest (FWE corrected, $p < 0.05$). Statistical maps of z-values are shown, the background image is an average of individual T1-w scans. Images are shown in radiological convention.

Table 3.21 Cluster data for group comparisons results for sustained (top) and transient (bottom) effects in pure visual paradigm with GM maps as covariate of no interest.

		<i>Sustained effects</i>						
		Volume (mm ³)	z-stat max	p-value	Coordinates (mm)			Area
					x	y	z	
Red light	<i>LHON < HC</i>	2184	4.14	6.75E-03	14	-94	2	Occipital Pole (r)
		31984	3.82	1.81E-22	62	10	10	Precentral Gyrus (r)
Blue > Red	<i>LHON > HC</i>	17968	4.35	8.20E-15	-6	-90	-6	Lingual Gyrus (l)
		2816	3.44	3.14E-03	44	-42	20	Supramarginal Gyrus (r)

		<i>Transient effects</i>						
		Volume (mm ³)	z-stat max	p-value	Coordinates (mm)			Area
					x	y	z	
Blue light	<i>LHON < HC</i>	3176	3.62	1.56E-04	20	-52	0	Lingual Gyrus (r)
Light	<i>LHON < HC</i>	2248	3.65	2.55E-03	20	-52	0	Lingual Gyrus (r)

Coordinates are in the standard MNI space; brain areas are referred to the Harvard-Oxford Cortical Structural Atlas; (l): left, (r): right.

3.6.2 Visual pattern paradigm

As for the group comparisons results of the visual pattern paradigm with GM maps as covariate of no interest, for the sustained effects it is confirmed the lower activation for LHON in visual areas with both blue and red background, while the higher recruitment of thalamus in LHON remains significant only for the red background (Figure 3.25, Table 3.22). All the results for transient effects, i.e. lower activation within the occipital pole for LHON with both backgrounds, remain significant (Figure 3.26, Table 3.22). Similarly, also the results of group comparisons for lines orientations are confirmed (Figure 3.27, Table 3.22). Regarding the visual pattern paradigm with 2afc, all the results of comparisons, that were essentially a lower visual areas activation for LHON), were observed also after adding individual GM maps to the model (Figures 3.28 3.29 3.30, Table 3.23).

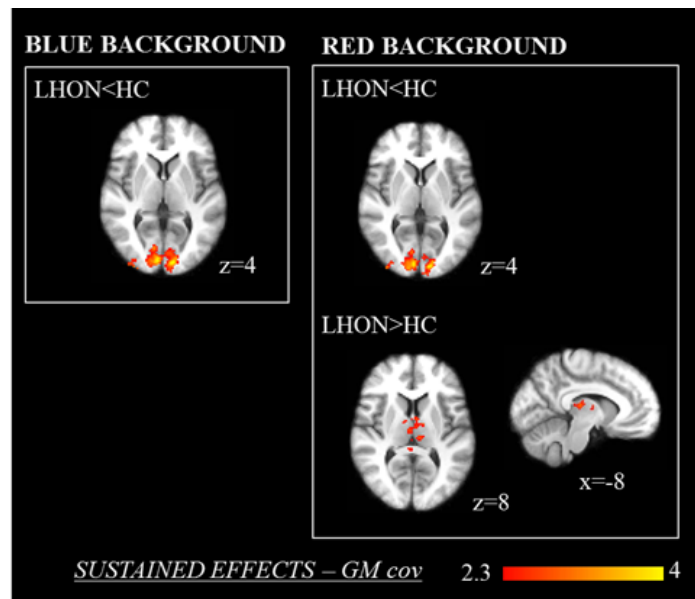


Figure 3.25 Group comparisons results for sustained effects in visual pattern paradigm with GM maps as covariate of no interest (FWE corrected, $p < 0.05$). Statistical maps of z-values are shown, the background image is an average of individual T1-w scans. Images are shown in radiological convention.

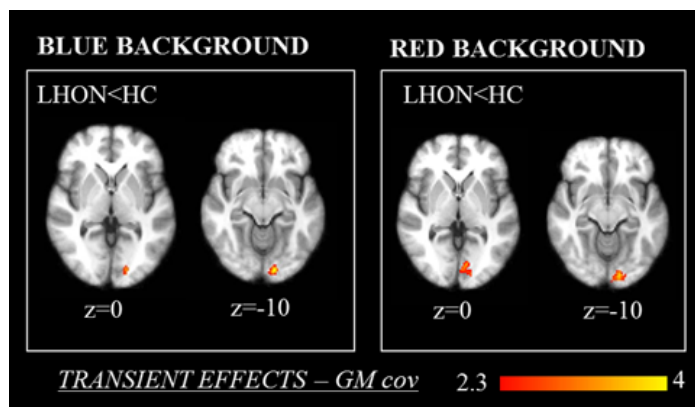


Figure 3.26 Group comparisons results for transient effects in visual pattern paradigm with GM maps as covariate of no interest (FWE corrected, $p < 0.05$). Statistical maps of z-values are shown, the background image is an average of individual T1-w scans. Images are shown in radiological convention.

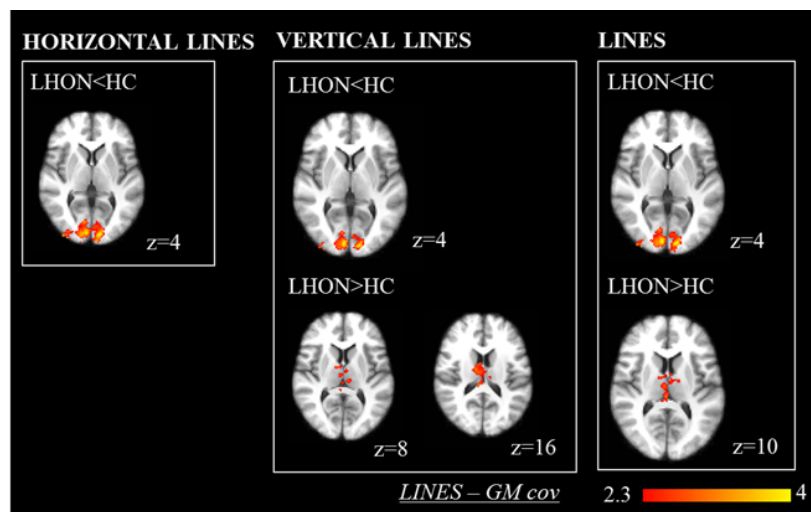


Figure 3.27 Group comparisons results for responses to lines (irrespective of the background colour) in visual pattern paradigm with GM maps as covariate of no interest (FWE corrected, $p < 0.05$). Statistical maps of z-values are shown, the background image is an average of individual T1-w scans. Images are shown in radiological convention.

Table 3.22 Cluster data for group comparisons results for sustained (top), transient (middle) and lines (bottom) effects in visual pattern paradigm with GM maps as covariate of no interest.

Sustained effects

		Volume (mm ³)	z-stat max	p-value	Coordinates (mm)			Area
					x	y	z	
Blue background	<i>LHON < HC</i>	15616	4.71	5.33E-13	10	-84	-6	Lingual Gyrus (r)
Red background	<i>LHON < HC</i>	15664	4.57	5.79E-13	-18	-88	-8	Occipital Fusiform Gyrus (l)
	<i>LHON > HC</i>	4032	3.07	2.40E-04	10	-12	6	Thalamus (r)

Transient effects

		Volume (mm ³)	z-stat max	p-value	Coordinates (mm)			Area
					x	y	z	
Blue background	<i>LHON < HC</i>	1864	4.49	1.68E-02	-10	-90	-12	Lingual Gyrus (l)
Red background	<i>LHON < HC</i>	4328	4.29	1.63E-05	-12	-90	-14	Occipital Pole (l)

Lines

		Volume (mm ³)	z-stat max	p-value	Coordinates (mm)			Area
					x	y	z	
Horizontal lines	<i>LHON < HC</i>	21928	4.67	1.56E-17	-8	-102	0	Occipital Pole (l)
Vertical lines	<i>LHON < HC</i>	11184	4.56	1.56E-09	10	-84	-6	Lingual Gyrus (r)
	<i>LHON > HC</i>	3720	3.07	8.30E-04	12	-10	16	Thalamus (r)
Lines	<i>LHON < HC</i>	15608	4.66	5.75E-13	10	-84	-6	Lingual Gyrus (r)
	<i>LHON > HC</i>	3184	3.04	1.67E-03	10	-14	16	Thalamus (r)

Coordinates are in the standard MNI space; brain areas are referred to the Harvard-Oxford Cortical and Subcortical Structural Atlases; (l): left, (r): right.

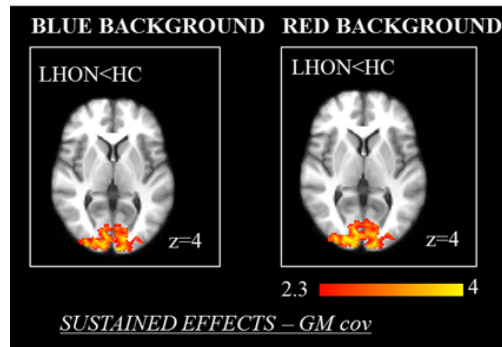


Figure 3.28 Group comparisons results for sustained effects in visual pattern paradigm with 2afc with GM maps as covariate of no interest (FWE corrected, $p < 0.05$). Statistical maps of z-values are shown, the background image is an average of individual T1-w scans. Images are shown in radiological convention.

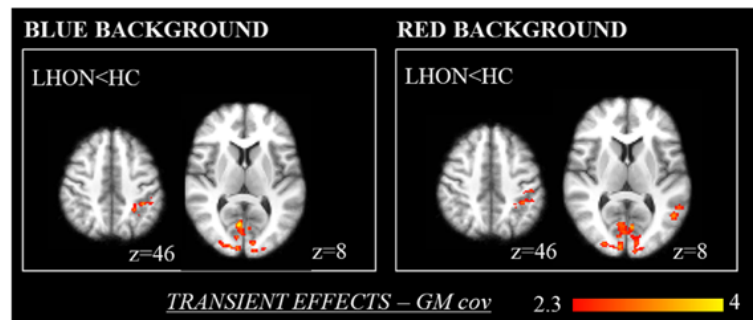


Figure 3.29 Group comparisons results for transient effects in visual pattern paradigm with 2afc with GM maps as covariate of no interest (FWE corrected, $p < 0.05$). Statistical maps of z-values are shown, the background image is an average of individual T1-w scans. Images are shown in radiological convention.

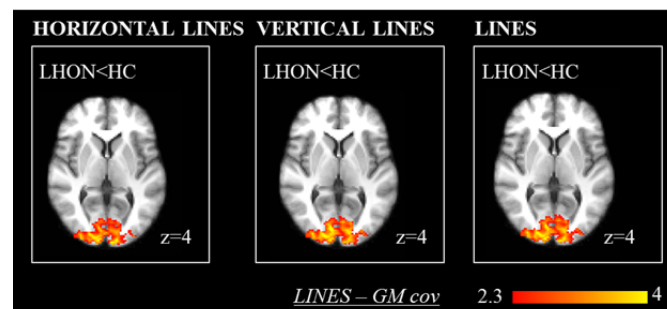


Figure 3.30 Group comparisons results for responses to lines (irrespective of the background colour) in visual pattern paradigm with 2afc with GM maps as covariate of no interest (FWE corrected, $p < 0.05$). Statistical maps of z-values are shown, the background image is an average of individual T1-w scans. Images are shown in radiological convention

Table 3.23 Cluster data for group comparisons results for sustained (top), transient (middle) and lines (bottom) effects in visual pattern paradigm with 2afc with GM maps as covariate of no interest.

Sustained effects

		Volume (mm ³)	z-stat max	p-value	Coordinates (mm)			Area
					x	y	z	
Blue background	<i>LHON < HC</i>	36400	5.18	3.37E-25	-10	-98	0	Occipital Pole (l)
Red background	<i>LHON < HC</i>	44120	5.37	6.56E-30	-10	-98	0	Occipital Pole (l)

Transient effects

		Volume (mm ³)	z-stat max	p-value	Coordinates (mm)			Area
					x	y	z	
Blue background	<i>LHON < HC</i>	13208	4.36	3.31E-12	-8	-80	-4	Lingual Gyrus (l)
		3152	3.6	9.70E-04	-38	-42	42	Superior Parietal Lobule (l)
Red background	<i>LHON < HC</i>	17216	4.3	2.41E-15	-8	-78	-4	Lingual Gyrus (l)
		2104	3.48	1.35E-02	-50	-60	10	Middle Temporal Gyrus (l)
		2024	3.39	1.72E-02	-48	-26	38	Postcentral Gyrus (l)

Lines

		Volume (mm ³)	z-stat max	p-value	Coordinates (mm)			Area
					x	y	z	
Horizontal lines	<i>LHON < HC</i>	37240	5.43	3.68E-25	-10	-98	0	Occipital Pole (l)
Vertical lines	<i>LHON < HC</i>	41544	5.13	8.87E-29	-10	-98	0	Occipital Pole (l)
Lines	<i>LHON < HC</i>	40872	5.34	7.54E-28	-10	-98	0	Occipital Pole (l)

Coordinates are in the standard MNI space; brain areas are referred to the Harvard-Oxford Cortical Structural Atlas; (l): left, (r): right.

Chapter 4

Discussion

In the present study we investigated brain responses in LHON patients and healthy subjects when three different fMRI paradigms were administered, in order to investigate pure visual effects of monochromatic light, visual effects of a pattern stimulation and the combined effects of visual monochromatic stimulation and a sustained attention cognitive task.

As for the pure visual paradigm, overall, our finding of lower activation of primary visual cortex in LHON compared to HC is quite a predictable result: it is in line with this pathology and with previous findings of structural, microstructural, metabolic and functional alterations in this brain area [87, 88, 96, 93, 98, 89–92]. For both blue and red light a significant group effect in LHON did not come up, probably due to low statistical power. But, when comparing the two groups, brain response to blue light resulted not significantly different between LHON and HC, while it was lower in LHON compared to HC for red light stimulation. This could be a very first element supporting the suggestive hypothesis of a visual role of the photopigment melanopsin, that due to its sensitivity power spectrum would give its main contribution with blue light stimulation. It is intriguing that we found significant differences in brain activations between different wavelengths when the sustained response to the whole period of light stimulation was considered (10 seconds), while such differences were not observed when the transient effects of light onsets were investigated. This can be interestingly related to the fact that the kinetics of melanopsin in response to a light stimulus is much slower than the response of rods and cones [8, 10] and it could be of support to the hypothesis that these differences in brain stimulation between different light colours might be, at least partially, related to a role of melanopsin. In a study investigating melanopsin role in irradiance coding within the thalamo-cortical visual system [63], sustained and transient response types were distinguished when measuring multiunit firing within the LGN in red cone knock-in mice. These animals have RGCs with normal projections pattern, a fully intact visual system but the cone spectral sensitivity is shifted towards red light, and

this allows to better identify the cone component of any response. To isolate melanopsin's contribution, long bright blue stimuli were compared to red ones. If transient cells showed equivalent responses to the two wavelengths, neurons with a sustained phenotype were more responsive to the blue stimulus. To further test the hypothesis of melanopsin contribution to the sustained activation of LGN in mice, Brown and colleagues also investigated the response to blue light stimulation for melanopsin knockout mice (they have intact rod/cone function but mRGCs are not intrinsically photosensitive). Both multiunit and single unit recordings revealed that the sustained component of light responses throughout the visual thalamus was mostly reduced. However, it should also be reminded that a previous study [105] found the surprising result of transient responses to light onset in the left thalamus and in two limbic areas, i.e. the amygdala and the hippocampus, and blue light elicited these responses more than green light. Different brain responses to different monochromatic stimulation were found both in LHON and in HC, but with opposite directions. A stronger response to blue light compared to red was present in LHON in particular in the prefrontal cortex, while in HC a stronger response to red light was observed in widespread cortical and subcortical areas. When both comparisons between wavelengths and comparisons between groups are considered, several cortical areas shows higher activation under blue with respect to red in LHON higher than HC. It could be thought that all these effects are driven by the stronger stimulation of red in HC, but also the different effects of lights in LHON are likely to play a role, as various brain areas show a positive brain response to blue while a negative or absent response to red.

As for the visual pattern paradigm, the characteristic aspect is that it constitutes a visual stimulation not with uniform light but with a moving pattern. However, it should be kept in mind that in this case it was not possible to have a control on the light spectrum: different colours just refers to different background on a screen, and not to monochromatic light. Therefore, even if the comparison between blue and red is intriguing, hypotheses on a possible involvement of melanopsin would be too hasty. With this paradigm as well we observed a reduced activation of visual cortex in LHON, and this is fully in line with the disease. While in HC both the primary visual cortex and the lateral occipital cortex are recruited, in LHON the activations in the primary visual cortex are missing while the lateral occipital areas are normally activated, both for transient and sustained responses to the visual stimuli. The lateral occipital cortex plays a key role in object recognition, in particular in analysing object shape [127]. The primary visual cortex is the cortical brain area that receive sensory stimuli, within the thalamus cortical visual system, and it is where damage to RGCs may mostly lead to degenerative changes. An intriguing effect that we observed for sustained brain response to the visual stimuli is an hyper-activation of thalamus in LHON patients,

that was not present for HC. In particular, the thalamic sub-areas we found activated were compatible with the location of the LGN and of the pulvinar nucleus, even if they cannot be distinguished in our MR images so it is an approximation. Both these thalamic regions play a key role in thalamo-cortical communications. The pulvinar in particular plays a key role in visual attention [128–130], and ventro-lateral pulvinar has been also shown to be necessary for both normal attention and sensory processing, and for keeping the cortex in an active state [130]. At the exploratory level of our investigations, we also considered effects of distinct line orientations (horizontal and vertical), and an interesting aspect is a different response of LHON visual areas, that showed a stronger stimulation when vertical lines were displayed. It would be captivating to relate this results with the specific pattern of degeneration of optic nerve fibres in LHON, or with their characteristic field defect of centrocaecal scotoma, but it would be probably too ventured, and more investigations in this sense would be appropriate. When the paradigm was repeated asking for a feedback about lines orientation, the results in visual areas were analogous while the thalamic recruitment for patients was absent. Moreover, many cortical areas were particularly active at the beginning of each period of visual stimuli, suggesting brain response to the necessity of more attention in order to give the answer. This cortical activation was interestingly present in both groups, without significance differences.

Among the fMRI paradigms we administered, the visual cognitive paradigm is the only one that has been already used in previous literature in cohort of healthy subjects or in patients. In both our groups, the brain areas that are recruited to perform the 3-back task (compared to the control condition, i.e. the 0-back task) are consistent with areas dealing with cognitive functions that are involved in this sustained attention task (parietal cortex, cingulate and premotor cortices, dorsolateral prefrontal cortex, middle frontal gyrus, cerebellum), and they are also in line with previous fMRI literature on this cognitive task, for which a meta-analysis exists [131]. This is a good proof of the quality of our data and acquisition, and it is also a positive confirmation of the fact that participants were actually involved in the cognitive task, along with their performances, that in all cases were higher than 75%. We evaluated responses to pure visual stimulation also in this paradigm, i.e. ignoring the cognitive part, in particular as far as the sustained response was concerned, because light periods were slightly longer than those used in the pure visual paradigms, and therefore it was possible to compare brain responses to visual stimulation with different durations. In this case, the different cortical brain responses to blue and red in healthy subjects were not observed. As for LHON, a stronger response to blue than to red was found in the occipital lobe, suggesting that with longer illumination periods it gets more clear the effects of a higher excitability of primary visual cortex with blue light compared to red. Differently from the pure visual

paradigm, in this case a significant effect in LHON group within visual cortex come up for both red and blue lights. When considering comparisons between populations, a significant differences, in particular a lower visual activation for LHON compared to HC, was observed only for red light, and not for the blue one. All these considerations, taken together also with results for the pure visual paradigm, build support to the hypothesis of a visual role of melanopsin, that shows a particular strong effect in chronic LHON considering their pattern of retinal degeneration: loss of RGCs, relative sparing of RGCs that express melanopsin and intact rod/cone system. These results come in the current literature view where the initially neglected possible role of melanopsin in visual processes is instead getting stronger and more widely accepted, thanks to a series of recent neurophysiological studies, mainly in rodents [21, 63, 64, 69, 66, 132, 67, 62]. Considered the LHON retinal degeneration, it is not possible to fully exclude the role of rods and cones. This is undeniably a limitation of this retinal model, especially if aiming to isolate the role of melanopsin in humans. When we considered the interactions between cognitive task and light stimulation, that is when we compared brain responses to the cognitive task when performed under blue light stimulation to brain responses when the same task was done under red light stimulation, no significant effects were found for healthy participants. This differs from previous studies that instead described brain activity modulation in healthy subjects under the exposure to blue light [54, 105]. Possible explanations to this discrepancy could be found in statistical power considerations, taking into account various aspects: our HC cohort was quite small, the field intensity we used was lower than what previously used (1.5T vs 3T), the corrections for multiple comparisons that we applied were those commonly used in the field but more stringent than those applied in our reference previous studies. Nevertheless, when looking at the LHON group, a significant modulation of brain activity due to different wavelength lights was observed, in cortical areas, cerebellum and brainstem, in good agreement with what was found by Vandewalle and colleagues in healthy subjects [54, 105]. Indeed, we found a higher brain activity under blue light exposure in the middle frontal gyrus, the insular cortex, the precuneus and lateral occipital cortices, the brainstem, in an area that is compatible with the locus ceruleus, the putamen and the cerebellum. Blue light has been also shown to trigger brain activity of prefrontal and thalamic brain regions during a working memory task in blind subjects [55], despite their loss of functionality of the rod /cone system. A possible explanation for this stronger effect we observed in LHON patients can be the different proportion of mRGCs, considering the general loss of RGCs that is observed in their retina and the relative sparing of mRGCs [81]. This findings gave a confirmation of the maintained functionality of mRGCs in LHON patients also from this point of view, i.e. brain activity modulation during attentive cognitive involvement.

Voxel-based morphometry (VBM) analysis in our group of LHON patients showed the presence of locally reduced grey matter (GM) density in the primary visual cortex. This is in line with the findings of the unique study that is currently present in literature about the VBM evaluation of GM atrophy in LHON [93]. Considering the small cohorts and the lack of previous literature, this is an important confirmatory result. It supports the hypothesis of an involvement of the posterior areas of the central nervous system in LHON, possibly due to neuronal degeneration secondary to the selective degeneration of retinal ganglion cells and optic nerve. Differently from Barcella and colleagues, we found no significant differences between patients and healthy controls for white matter (WM) VBM evaluation, therefore not confirming the WM tissue loss they found in the chiasm, the optic tracts and several areas located in the optic radiations. In both studies LHON patients are in a chronic stage of the disease, therefore this discrepancy in the result cannot be attributable to a different stage of the disease; a technical difference remains between the two studies, which is the magnetic field intensity (1.5T and 3T), even if the effects of a higher field on the quality of high-resolution T1-w images are not particularly striking. VBM analyses are typically discouraged for white matter, as the analysis protocol was optimised for grey matter [120], and more suitable MR methods exist to explore white matter integrity, such as diffusion weighted imaging, even if it can be argued that diffusion weighted imaging can give insights into the WM tissue integrity, and not into WM tissue loss. As for previous diffusion imaging studies, in the first evaluations no microscopic abnormalities were found [87], while later investigations revealed altered diffusivity parameters mainly within the optic tract and optic radiations [89–92]. From the metabolic point of view, both proton and phosphorus MR spectroscopy studies [133, 134, 96, 95] found alterations in the occipital normal appearing WM of LHON patients. The finding of a tissue loss in primary visual cortex raised the issue of an effect of atrophy in our fMRI results within the visual cortex, but when we repeated group comparisons for the visual paradigms by adding individual GM maps as covariate of no interest to control for this possible bias, the previous results were confirmed, and this support the fact that the group differences we found in fMRI activation within visual cortices were driven by functional differences and not by structural differences.

The present study has some limitations that should be taken into consideration. First, the subject cohort is small for the statistical point of view: it is slightly below the minimum number of subjects suggested as good practice for fMRI studies [135, 136]. Nevertheless, it should be considered in relation to the rarity of the disease and to the complexity of the protocol. Moreover, a 1.5T MR scanner has a relatively low field intensity when compared to current technologies especially for research purposes, and this leads to relatively low temporal and spatial fMRI resolution. Nonetheless, considering that this is the first fMRI

study with light stimulation in LHON, it is possible to obtain interesting exploratory results and first insights into the phenomenology. Finally, it was not feasible to acquire all the data in a short period of time during the year to avoid possible bias related to seasonality [109] and some of the subjects are slightly outside the reference cut-off for sleep quality and anxiety/depression assessment. Considering the rare disease we were interested in and the dense protocol, even if preferred it was not conceivable to exclude these subject from recruitment. As for the possible effects of seasonality, we tried to take them into account by adding the average hours of light per day at the time of MR acquisition as covariate of no interest in our group analyses.

Chapter 5

Conclusions and future developments

The present study gave the possibility to investigate brain responses in a population of LHON patients during monochromatic light stimulation. Despite the general loss of RGCs in LHON patients, mRGCs are relatively spared. With this study, the functional integrity of mRGCs in LHON was confirmed by fMRI. Indeed, light exposure modulates brain responses to a sustained attention cognitive task in LHON patients. Moreover, brain activities during purely visual light stimulation suggest a possible role of mRGCs in vision. This mounting evidence for a direct contribution of mRGCs to vision could pave the way for a possible avenue for interventions in particular in blind subjects where mRGCs are spared.

Combination of MRI results, both functional and structural, and clinical data of LHON patients might give more insights into the biological mechanisms underlying the effects we observed, therefore this combination will be further explored to get a more specific characterization of these results. From the brain structure point of view, our VBM evaluation was aimed to just explore possible structural differences between our groups and to keep under control possible related structural effects in the fMRI results. However, it could be of interest to further explore structural alterations, also with other advanced methodological approaches, such as the evaluation of cortical thickness, cortical area or cortex folding, or the study of the covariance between structural measures of different brain areas between groups. With the present study, the functionality of mRGCs has been tested in a population of LHON patients and they offered a peculiar paradigm of retinal degeneration, given their general loss of RGCs with a relative spare of mRGCs and their intact system of rods and cones. In order to add a second paradigm of retinal degeneration, it would be of particular interest to perform analogous investigations in a population of patients with inherited retinal dystrophy, that instead suffer of a selective loss of photoreceptors (rods, cones and pigmentary epithelium). The instrumental setup and the set of methodologies for acquisition and analyses that have been set up for this project constitute the technical starting point for similar future

investigations in other neurological diseases in which mRGCs may be affected, such as Alzheimer's disease [137].

Bibliography

- [1] Graham DM and Wong KY. Melanopsin-expressing, intrinsically photosensitive retinal ganglion cells (iprgcs).
- [2] Keeler CE. Iris movements in blind mice. *Am J Physiol*, 81:107–12, 1927.
- [3] Keeler CE. Normal and rodless retinae of the house mouse with respect to the electromotive force generated through stimulation by light. *Proc Natl Acad Sci U S A*, 14(6):477–84, 1928.
- [4] Provencio I, Jiang G, De Grip WJ, Hayes WP, and Rollag MD. Melanopsin: An opsin in melanophores, brain, and eye. *Proc Natl Acad Sci U S A*, 95(1):340–5, 1998.
- [5] Provencio I, Rodriguez IR, Jiang G, Hayes WP, Moreira EF, and Rollag MD. A novel human opsin in the inner retina. *J Neurosci*, 20(2):600–5, 2000.
- [6] Provencio I, Rollag MD, and Castrucci AM. Photoreceptive net in the mammalian retina. this mesh of cells may explain how some blind mice can still tell day from night. *Nature*, 415(6871):493, 2002.
- [7] Hannibal J, Hindersson P, Knudsen SM, Georg B, and Fahrenkrug J. The photopigment melanopsin is exclusively present in pituitary adenylate cyclase-activating polypeptide-containing retinal ganglion cells of the retinohypothalamic tract. *J Neurosci*, 22(1):RC191, 2002.
- [8] Berson DM, Dunn FA, and Takao M. Phototransduction by retinal ganglion cells that set the circadian clock. *Science*, 295(5557):1070–3, 2002.
- [9] Hattar S, Liao HW, Takao M, Berson DM, and Yau KW. Melanopsin-containing retinal ganglion cells: architecture, projections, and intrinsic photosensitivity. *Science*, 295(5557):1065–70, 2002.
- [10] Do MT, Kang SH, Xue T, Zhong H, Liao HW, Bergles DE, and Yau KW. Photon capture and signalling by melanopsin retinal ganglion cells. *Nature*, 457:281–7, 2009.
- [11] Dacey DM, Liao HW, Peterson BB, Robinson FR, Smith VC, Pokorny J, Yau KW, and Gamlin PD. Melanopsin-expressing ganglion cells in primate retina signal colour and irradiance and project to the lgn. *Nature*, 433(7027):749–54, 2005.
- [12] Tu DC, Zhang D, Demas J, Slutsky EB, Provencio I, Holy TE, and Van Gelder RN. Physiologic diversity and development of intrinsically photosensitive retinal ganglion cells. *Neuron*, 48(6):987–99, 2005.

- [13] Isoldi MC, Rollag MD, Castrucci AM, and Provencio I. Rhabdomic phototransduction initiated by the vertebrate photopigment melanopsin. *Proc Natl Acad Sci U S A*, 102:1217–21, 2005.
- [14] Panda S, Nayak SK, Campo B, Walker JR, Hogenesch JB, and Jegla T. Illumination of the melanopsin signaling pathway. *Science*, 307:600–4, 2005.
- [15] Melyan Z, Tarttelin EE, Bellingham J, Lucas RJ, and Hankins MW. Addition of human melanopsin renders mammalian cells photoresponsive. *Nature*, pages 741–5, 2005.
- [16] Graham DM, Wong KY, Shapiro P, Frederick C, Pattabiraman K, and Berson DM. Melanopsin ganglion cells use a membrane-associated rhabdomic phototransduction cascade. *J Neurophysiol*, 99:2522–32, 2008.
- [17] Mure LS, Rieux C, Hattar S, and Cooper HM. Melanopsin-dependent nonvisual responses: evidence for photopigment bistability in vivo. *J Biol Rhythms*, 22(5):411–24, 2007.
- [18] Mure LS, Cornut PL, Rieux C, Drouyer E, Denis P, Gronfier C, and Cooper HM. Melanopsin bistability: a fly’s eye technology in the human retina. *PLoS One*, 4(6):e5991, 2009.
- [19] Viney TJ, Balint K, Hillier D, Siegert S, Boldogkoi Z, Enquist LW, Meister M, Cepko CL, and Roska B. Local retinal circuits of melanopsin-containing ganglion cells identified by transsynaptic viral tracing. *Curr Biol*, 17(11):981–8, 2007.
- [20] Schmidt TM, Taniguchi K, and Kofuji P. Intrinsic and extrinsic light responses in melanopsin-expressing ganglion cells during mouse development. *J Neurophysiol*, 100:371–84, 2008.
- [21] Ecker JL, Dumitrescu ON, Wong KY, Alum NM, Chen SK, LeGates T, Renna JM, Prusky GT, Berson DM, and Hattar S. Melanopsin-expressing retinal ganglion-cell photoreceptors: cellular diversity and role in pattern vision. *Neuron*, 67:49–60, 2010.
- [22] Schmidt TM and Kofuji P. Functional and morphological differences among intrinsically photosensitive retinal ganglion cells. *J Neurosci*, 29:476–82, 2009.
- [23] Hu C, Hill DD, and Wong KY. Intrinsic physiological properties of the five types of mouse ganglion-cell photoreceptors. *J Neurophysiol*, 109:1876–89, 2013.
- [24] Zhao X, Stafford BK, Godin AL, King WM, , and Wong KY. Photoresponse diversity among the five types of intrinsically photosensitive retinal ganglion cells. *J Physiol*, 592:1619–36, 2014.
- [25] Reifler AN, Chervenak AP, Dolikian ME, Benenati BA, Meyers BS, Demertzis ZD, Lynch AM, Li BY, Wachter RD, Abufarha FS, Dulka EA, Pack W, Zhao X, and Wong KY. The rat retina has five types of ganglion-cell photoreceptors. *Exp Eye Res*, 130:17–28, 2015.

- [26] Estevez ME, Fogerson PM, Ilardi MC, Borghuis BG, Chan E, Weng S, Auferkorte ON, Demb JB, and Berson DM. Form and function of the m4 cell, an intrinsically photosensitive retinal ganglion cell type contributing to geniculocortical vision. *J Neurosci*, 32:13608–20, 2012.
- [27] Liao HW, Ren X, Peterson BB, Marshak DW, Yau KW, Gamlin PD, and Dacey DM. Melanopsin-expressing ganglion cells on macaque and human retinas form two morphologically distinct populations. *J Comp Neurol*, 524(14):2845–72, 2016.
- [28] Belenky MA, Smeraski CA, Provencio I, Sollars PJ, and Pickard GE. Melanopsin retinal ganglion cells receive bipolar and amacrine cell synapses. *J Comp Neurol*, 460(3):380–93, 2003.
- [29] Perez-Leon JA, Warren EJ, Allen CN, Robinson DW, and Brown RL. Synaptic inputs to retinal ganglion cells that set the circadian clock. *Eur J Neurosci*, 24(4):1117–23, 2006.
- [30] Wong KY, Dunn FA, Graham DM, and Berson DM. Synaptic influences on rat ganglion-cell photoreceptors. *J Physiol*, 582(Pt 1):279–96, 2007.
- [31] Weng S, Estevez ME, and Berson DM. Mouse ganglion-cell photoreceptors are driven by the most sensitive rod pathway and by both types of cones. *PLoS One*, 8:e66480, 2013.
- [32] Lall GS, Revell VL, Momij H, Enezi JA, Altimus CM, Güler AD, Aguilar C, Cameron MA, Allender S, Hankins MW, and Lucas RJ. Distinct contributions of rod, cone, and melanopsin photoreceptors to encoding irradiance. *Neuron*, 66(3):417–28, 2010.
- [33] Gooley JJ, Mien IH, St. Hilaire MA, Yeo S, Chua EC, van Reen E, Hanley CJ, Hull JT, Czeisler CA, and Lockley SW. Melanopsin and rod-cone photoreceptors play different roles in mediating pupillary light responses during exposure to continuous light in humans. *J Neurosci*, 32(41):14242–53, 2012.
- [34] Barrionuevo PA, McAnany NNJJ, Zele AJ, Gamlin P, and Cao D. Assessing rod, cone, and melanopsin contributions to human pupil flicker responses. *Invest Ophthalmol Vis Sci*, 55(2):719–727, 2014.
- [35] Vandewalle G, Maquet P, and Dijk DJ. Light as a modulator of cognitive brain function. *Trends Cogn Sci*, 13(10):429–38, 2009.
- [36] Hattar S, Kumar M, Park A, Tong P, Tung J, Yau KW, and Berson DM. Central projections of melanopsin-expressing retinal ganglion cells in the mouse. *J Comp Neurol*, 497(3):326–49, 2006.
- [37] Hannibal J, Kankipati L, Strang CE, Peterson BB, Dacey D, and Gamlin PD. Central projections of intrinsically photosensitive retinal ganglion cells in the macaque monkey. *J Comp Neurol*, 522:2231–48, 2014.
- [38] Panda S, Sato TK, Castrucci AM, Rollag MD, DeGrip WJ, Hogenesch JB, Provencio I, and Kay SA. Melanopsin (opn4) requirement for normal light-induced circadian phase shifting. *Science*, 298(5601):2213–6, 2002.

- [39] Brainard GC, Hanifin JP, Greeson JM, Byrne B, Glickman G, Gerner E, and Rollag MD. Action spectrum for melatonin regulation in humans: evidence for a novel circadian photoreceptor. *J Neurosci*, 21:6405–12, 2001.
- [40] Thapan K, Arendt J, and Skene DJ. An action spectrum for melatonin suppression: evidence for a novel non-rod, non-cone photoreceptor system in humans. *J Physiol*, 535:261–7, 2001.
- [41] Vartanian GV, Li BY, Chervenak AP, Walch OJ, Pack W, Ala-Laurila P, and Wong KY. Melatonin suppression by light in humans is more sensitive than previously reported. *J Biol Rhythms*, 30:351–4, 2015.
- [42] Lucas RJ, Freedman MS, Muñoz M, Garcia-Fernández JM, and Foster RG. Regulation of the mammalian pineal by non-rod, non-cone, ocular photoreceptors. *Science*, 284(5413):505–7, 1999.
- [43] Czeisler CA, Shanahan TL, Klerman EB, Martens H, Brotman DJ, Emens JS, Klein T, and Rizzo JF. Suppression of melatonin secretion in some blind patients by exposure to bright light. *N Engl J Med*, 332:6–11, 1995.
- [44] Zaidi FH, Hull JT, Peirson SN, Wulff K, Aeschbach D, Gooley JJ, Brainard GC, Gregory-Evans K, Rizzo JF, Czeisler CA, Foster RG, Moseley MJ, and Lockley SW. Short-wavelength light sensitivity of circadian, pupillary, and visual awareness in humans lacking an outer retina. *Curr Biol*, 17:2122–8, 2007.
- [45] Hattar S, Lucas RJ, Mrosovsky N, Thompson S, Douglas RH, Hankins MW, Lem J, Biel M, Hofmann F, Foster RG, and Yau KW. Melanopsin and rod-cone photoreceptive systems account for all major accessory visual functions in mice. *Nature*, 424(6944):76–81, 2003.
- [46] Lucas RJ, Hattar S, Takao M, Berson DM, Foster RG, and Yau KW. Diminished pupillary light reflex at high irradiances in melanopsin-knockout mice. *Science*, 299(5604):245–7, 2003.
- [47] Panda S, Provencio I, Tu DC, Pires SS, Rollag MD, Castrucci AM, Pletcher MT, Sato TK, Wiltshire T, Andahazy M, Kay SA, Van Gelder RN, and Hogenesch JB. Melanopsin is required for non-image-forming photic responses in blind mice. *Science*, 301(5632):525–7, 2003.
- [48] Mrosovsky N and Hattar S. Impaired masking responses to light in melanopsin-knockout mice. *Chronobiol Int*, 20(6):989–99, 2003.
- [49] Lupi D, Oster H, Thompson S, and Foster RG. The acute light-induction of sleep is mediated by opn4-based photoreception. *Nat Neurosci*, 11(9):1068–73, 2008.
- [50] Morin LP and Studholme KM. Separation of function for classical and ganglion cell photoreceptors with respect to circadian rhythm entrainment and induction of photosomnolence. *Neuroscience*, 199:213–24, 2011.
- [51] Altimus CM, Güler AD, Villa KL, McNeill DS, Legates TA, and Hattar S. Rods-cones and melanopsin detect light and dark to modulate sleep independent of image formation. *Proc Natl Acad Sci U S A*, 105-50:19998–20003, 2008.

- [52] Tsai JW, Hannibal J, Hagiwara G, Colas D, Ruppert E, Ruby NF, Heller HC, Franken P, and Bourgin P. Melanopsin as a sleep modulator: circadian gating of the direct effects of light on sleep and altered sleep homeostasis in *opn4(-/-)* mice. *PLoS Biol*, 7(6):e1000125, 2009.
- [53] Muindi F, Zeitzer JM, Colas D, and Heller HC. The acute effects of light on murine sleep during the dark phase: importance of melanopsin for maintenance of light-induced sleep. *Eur J Neurosci*, 37(11):1727–36, 2013.
- [54] Vandewalle G, Gais S, Schabus M, Baiteau E, Carrier J, Darsaud A, Sterpenich V, Albouy G, Dijk DJ, and Maquet P. Wavelength-dependent modulation of brain responses to a working memory task by daytime light exposure. *Cereb Cortex*, 17(12):2788–95, 2007.
- [55] Vandewalle G, Collignon O, Hull JT, Daneault V, Albouy G, Lepore F, Phillips C, Doyon J, Czeisler CA, Dumont M, Lockley SW, and Carrier J. Blue light stimulates cognitive brain activity in visually blind individuals. *J Cogn Neurosci*, 25(12):2072–85, 2013.
- [56] Viola AU, James LM, Schlangen LJ, and Dijk DJ. Blue-enriched white light in the workplace improves self-reported alertness, performance and sleep quality. *Scand J Work Environ Health*, 34(4):297–306, 2008.
- [57] Iyilikci O, Aydin E, and Canbeyli R. Blue but not red light stimulation in the dark has antidepressant effect in behavioral despair. *Behav Brain Res*, 203(1):65–8, 2009.
- [58] Meesters Y, Dekker V, Schlangen LJ, Bos EH, and Ruiters MJ. Low-intensity blue-enriched white light (750 lux) and standard bright light (10,000 lux) are equally effective in treating sad. a randomized controlled study. *BMC Psychiatry*, 11:17, 2011.
- [59] Nosedá R and Burstein R. Advances in understanding the mechanisms of migraine-type photophobia. *Curr Opin Neurol*, 24(3):197–202, 2011.
- [60] Sikka G, Hussmann GP, Pandey D, Cao S, Hori D, Park JT, Stepan J, Kim JH, Barodka V, Myers AC, Santhanam L, Nyhan D, Halushka MK, Koehler RC, Snyder SH, Shimoda LA, and Berkowitz DE. Melanopsin mediates light-dependent relaxation in blood vessels. *Proc Natl Acad Sci U S A*, 111(50):17977–82, 2014.
- [61] Danilenko KV and Sergeeva OY. Immediate effect of blue-enhanced light on reproductive hormones in women. *Neuro Endocrinol Lett*, 36(1):84–90, 2015.
- [62] Sonoda T and Schmidt TM. Re-evaluating the role of intrinsically photosensitive retinal ganglion cells: New roles in image-forming functions. *Integr Comp Biol*, 56(5):834–41, 2016.
- [63] Brown TM, Gias C, Hatori M, Keding SR, Semo M, Coffey PJ, Gigg J, Piggins HD, Panda S, and Lucas RJ. Melanopsin contributions to irradiance coding in the thalamo-cortical visual system. *PLoS Biol*, 8:e1000558, 2010.
- [64] Brown TM, Tsujimura S, Allen AE, Wynne J, Bedford R, Vickery G, Vugler A, and Lucas RJ. Melanopsin-based brightness discrimination in mice and humans. *Curr Biol*, 22(12):1134–41, 2012.

- [65] Allen AE, Storch R, Martial FP, Petersen RS, Montemurro MA, Brown TM, and Lucas RJ. Melanopsin-driven light adaptation in mouse vision. *Curr Biol.*, 24(21):2481–90, 2014.
- [66] Storch R, Milosavljevic N, Eleftheriou CG, Martial FP, Orłowska-Feuer P, Bedford RA, Brown TM, Montemurro MA, Petersen RS, and Lucas RJ. Melanopsin-driven increases in maintained activity enhance thalamic visual response reliability across a simulated dawn. *Proc Natl Acad Sci U S A*, 112(42):E5734–43, 2015.
- [67] Prigge CL, Yeh PT, Liou NF, Lee CC, You SF, Liu LL, McNeill DS, Chew KS, Hattar S, Chen SK, and Zhang DQ. M1 iprgcs influence visual function through retrograde signaling in the retina. *J Neurosci*, 36(27):7184–97, 2016.
- [68] Horiguchi H, Winawer J, Dougherty RF, and Wandell BA. Human trichromacy revisited. *Proc Natl Acad Sci U S A*, 110:E260–9, 2012.
- [69] Schmidt TM, Alam NM, Chen S, Kofuji P, Li W, Prusky GT, and Hattar S. A role for melanopsin in alpha retinal ganglion cells and contrast detection. *Neuron*, 82:781–8, 2014.
- [70] Man PYW, Turnbull DM, and Chinnery PF. Leber hereditary optic neuropathy. *J Med Genet*, 39(3):162–9, 2002.
- [71] Leber T. Über hereditäre and congenital-angelegte sehnerven-leiden. *Arch Ophthalmol*, 17:249–91, 1871.
- [72] Wallace DC, Singh G, Lott MT, Hodge JA, Schurr TG, Lezza AM, Elsas LJ, and Nikoskelainen EK. Mitochondrial dna mutation associated with leber’s hereditary optic neuropathy. *Science*, 242(4884):1427–30, 1988.
- [73] Carelli V, Ross-Cisneros FN, and Sadun AA. Mitochondrial dysfunction as a cause of optic neuropathies. *Prog Retin Eye Res*, 23(1):53–89, 2004.
- [74] Man PYW, Griffiths PG, Brown DT, Howell N, Turnbull DN, and Chinnery PF. The epidemiology of leber hereditary optic neuropathy in the north east of england. *Am J Hum Genet*, 72(2):333–9, 2003.
- [75] Puomila A, Hämäläinen P, Kivioja S, Savontaus ML, Koivumäki S, Huoponen K, and Nikoskelainen E. Epidemiology and penetrance of leber hereditary optic neuropathy in finland. *Eur J Hum Genet*, 15(10):1079–89, 2007.
- [76] Mascialino B, Leinonen M, and Meier T. Meta-analysis of the prevalence of leber hereditary optic neuropathy mtdna mutations in europe. *Eur J Ophthalmol*, 22(3):461–5, 2012.
- [77] Wakakura M and Yokoe J. Evidence for preserved direct pupillary light response in leber’s hereditary optic neuropathy. *Br J Ophthalmol*, 79(5):442–6, 1995.
- [78] Bremner FD, Shallo-Hoffmann J, Riordan-Eva P, and Smith SE. Comparing pupil function with visual function in patients with leber’s hereditary optic neuropathy. *Invest Ophthalmol Vis Sci*, 40(11):2528–34, 1999.

- [79] Sadun AA, La Morgia C, and Carelli V. Leber's hereditary optic neuropathy. *Curr Treat Options Neurol*, 13(1):109–17, 2011.
- [80] La Morgia C, Carbonelli M, Barboni P, Sadun AA, and Carelli V. Medical management of hereditary optic neuropathies. *Front Neurol*, 5:141, 2014.
- [81] La Morgia C, Ross-Cisneros FN, Sadun AA, Hannibal J, Munarini A, Mantovani V, Barboni P, Cantalupo G, Tozer KR, Sancisi E, Salomao SR, Moraes MN, Moraes-Filho MN, Heegaard S, Milea D, Kjer P, Montagna P, and Carelli V. Melanopsin retinal ganglion cells are resistant to neurodegeneration in mitochondrial optic neuropathies. *Brain*, 133(Pt 8):2426–38, 2010.
- [82] Kawasaki A, Herbst K, Sander B, and Milea D. Selective wavelength pupillometry in leber hereditary optic neuropathy. *Clin Exp Ophthalmol*, 38(3):322–4, 2010.
- [83] Moura AL, Nagy BV, La Morgia C, Barboni P, Oliveira AG, Salomão SR, Berezovsky A, de Moraes-Filho MN, Chicani CF, Belfort R Jr, Carelli V, Sadun AA, Hood DC, and Ventura DF. The pupil light reflex in leber's hereditary optic neuropathy: evidence for preservation of melanopsin-expressing retinal ganglion cells. *Invest Ophthalmol Vis Sci*, 54(7):4471–7, 2013.
- [84] Jezzard P, Matthews PM, and Smith SM. *Functional MRI an introduction to methods*. Oxford University Press, 2001.
- [85] Ogawa S, Lee TM, Kay AR, and Tank DW. Brain magnetic resonance imaging with contrast dependent on blood oxygenation. *Proc Natl Acad Sci U S A*, 87:9868 – 72, 1990.
- [86] Ogawa S, Menon RS, Tank DW, Kim SG, Merkle H, Ellermann JM, and Ugurbil K. Functional brain mapping by blood oxygenation level-dependent contrast magnetic resonance imaging. a comparison of signal characteristics with a biophysical model. *Biophysical Journal*, 68:803–12, 1993.
- [87] Inglese M, Rovaris M, Bianchi S, La Mantia L, Mancardi GL, Ghezzi A, Montagna P, Salvi F, and Filippi M. Magnetic resonance imaging, magnetisation transfer imaging, and diffusion weighted imaging correlates of optic nerve, brain, and cervical cord damage in leber's hereditary optic neuropathy. *J Neurol Neurosurg Psychiatry*, 70(4):444–9, 2001.
- [88] Inglese M, Rovaris M, Bianchi S, Comi G, and Filippi M. Magnetization transfer and diffusion tensor mr imaging of the optic radiations and calcarine cortex from patients with leber's hereditary optic neuropathy. *J Neurol Sci*, 188(1-2):33–36, 2001.
- [89] Milesi J, Rocca MA, Bianchi-Marzoli S, Petrolini M, Pagani E, Falini A, Comi G, and Filippi M. Patterns of white matter diffusivity abnormalities in leber's hereditary optic neuropathy: a tract-based spatial statistics study. *J Neurol*, 259(9):1801–7, 2012.
- [90] Rizzo G, Tozer KR, Tonon C, Manners D, Testa C, Malucelli E, Valentino ML, La Morgia C, Barboni P, Randhawa RS, Ross-Cisneros FN, Sadun AA, Carelli V, and Lodi R. Secondary post-geniculate involvement in leber's hereditary optic neuropathy. *PLoS One*, 7(11):e50230, 2012.

- [91] Ogawa S, Takemura H, Horiguchi H, Terao M, Haji T, Pestilli F, Yeatman JD, Tsuneoka H, Wandell BA, and Masuda Y. White matter consequences of retinal receptor and ganglion cell damage. *Invest Ophthalmol Vis Sci*, 55(10):6976–86, 2014.
- [92] Manners DN, Rizzo G, La Morgia C, Tonon C, Testa C, Barboni P, Malucelli E, Valentino ML, Caporali L, Strobbe D, Carelli V, and Lodi R. Diffusion tensor imaging mapping of brain white matter pathology in mitochondrial optic neuropathies. *Am J Neuroradiol*, 36(7):1259–65, 2015.
- [93] Barcella V, Rocca MA, Bianchi-Marzoli S, Milesi J, Melzi L, Falini A, Pierro L, and Filippi M. Evidence for retrochiasmatic tissue loss in leber’s hereditary optic neuropathy. *Hum Brain Mapp*, 31(12):1900–6, 2010.
- [94] d’Almeida OC, Mateus C, Reis A, Grazina MM, and Castelo-Branco M. Long term cortical plasticity in visual retinotopic areas in humans with silent retinal ganglion cell loss. *Neuroimage*, 81:222–30, 2013.
- [95] Ostojic J, Jancic J, Kozic D, Semnic R, Koprivsek K, Prvulovic M, and Kostic V. Brain white matter 1 h mrs in leber optic neuropathy mutation carriers. *Acta Neurol Belg*, 109(4):305–9, 2009.
- [96] Lodi R, Carelli V, Cortelli P, Iotti S, Valentino ML, Barboni P, and Pallotti F. Phosphorus mr spectroscopy shows a tissue specific in vivo distribution of biochemical expression of the g3460a mutation in leber’s hereditary optic neuropathy. *J Neurol Neurosurg Psychiatry*, 72(6):805–7, 2002.
- [97] Sadun AA, Carelli V, Bose S, Ross-Cisneros FN, Barboni P, and Ahrens ET. First application of extremely high-resolution magnetic resonance imaging to study microscopic features of normal and lhon human optic nerve. *Ophthalmology*, 109(6):1085–91, 2002.
- [98] Rocca MA, Valsasina P, Pagani E, Bianchi-Marzoli S, Milesi J, Falini A, Comi G, and Filippi M. Extra-visual functional and structural connection abnormalities in leber’s hereditary optic neuropathy. *PLoS One*, 6(2):e17081, 2011.
- [99] Vandewalle G, Archer SN, Wuillaume C, Balteau E, Degueldre C, Luxen A, Maquet P, and Dijk DJ. Functional magnetic resonance imaging-assessed brain responses during an executive task depend on interaction of sleep homeostasis, circadian phase, and per3 genotype. *J Neurosci*, 29(25):7948–56, 2009.
- [100] Gaggioni G, Maquet P, Schmidt C, Dijk DJ, and Vandewalle G. Neuroimaging, cognition, light and circadian rhythms. *Front Syst Neurosci*, 8:126, 2014.
- [101] Vandewalle G, Schwartz S, Grandjean D, Wuillaume C, Balteau E, Degueldre C, Schabus M, Phillips C, Luxen A, Dijk DJ, and Maquet P. Spectral quality of light modulates emotional brain responses in humans. *Proc Natl Acad Sci U S A*, 107(45):19549–54, 2010.
- [102] Vandewalle G, Hébert M, Beaulieu C, Richard L, Daneault V, Garon ML, Leblanc J, Grandjean D, Maquet P, Schwartz S, Dumont M, Doyon J, and Carrier J. Abnormal hypothalamic response to light in seasonal affective disorder. *Biol Psychiatry*, 70(10):954–61, 2011.

- [103] Perrin F, Peigneux P, Fuchs S, Verhaeghe S, Laureys S, Middleton B, Degueldre C, Del Fiore G, Vandewalle G, Balteau E, Poirrier R, Moreau V, Luxen A, Maquet P, and Dijk DJ. Nonvisual responses to light exposure in the human brain during the circadian night. *Curr Biol*, 14(20):1842–6, 2004.
- [104] Vandewalle G, Balteau E, Phillips C, Degueldre C, Moreau V, Sterpenich V, Albouy G, Darsaud A, Desseilles M, Dang-Vu TT, Peigneux P, Luxen A, Dijk DJ, and Maquet P. Daytime light exposure dynamically enhances brain responses. *Curr Biol*, 16(16):1616–21, 2006.
- [105] Vandewalle G, Schmidt C, Albouy G, Sterpenich V, Darsaud A, Rauchs G, Berken PY, Balteau E, Degueldre C, Luxen A, Maquet P, and Dijk DJ. Brain responses to violet, blue, and green monochromatic light exposures in humans: prominent role of blue light and the brainstem. *PLoS One*, 2(11):e1247, 2007.
- [106] Vandewalle G, Archer SN, Wuillaume C, Balteau E, Degueldre C, Luxen A, Dijk DJ, and Maquet P. Effects of light on cognitive brain responses depend on circadian phase and sleep homeostasis. *J Biol Rhythms*, 26(3):249–59, 2011.
- [107] Chellappa SL, Ly JQ, Meyer C, Balteau E, Degueldre C, Luxen A, Phillips C, Cooper HM, and Vandewalle G. Photic memory for executive brain responses. *Proc Natl Acad Sci U S A*, 111(16):6087–91, 2014.
- [108] Daneault V, Hébert M, Albouy G, Doyon J, Dumont M, Carrier J, and Vandewalle G. Aging reduces the stimulating effect of blue light on cognitive brain functions. *Sleep*, 37(1):85–96, 2014.
- [109] Meyer C, Muto V, Jaspard M, Kussé C, Lambot E, Chellappa SL, Degueldre C, Balteau E, Luxen A, Middleton B, Archer SN, Collette F, Dijk DJ, Phillips C, Maquet P, and Vandewalle G. Seasonality in human cognitive brain responses. *Proc Natl Acad Sci U S A*, 113(11):3066–71, 2016.
- [110] Schmidt C, Collette F, Reichert CF, Maire M, Vandewalle G, Peigneux P, and Cajochen C. Pushing the limits: Chronotype and time of day modulate working memory-dependent cerebral activity. *Front Neurol*, 6:199, 2015.
- [111] Vignatelli L, Plazzi G, Barbato A, Ferini-Strambi L, Manni R, Pompei F, and D’Alessandro R. Ginsen (gruppo italiano narcolessia studio epidemiologico nazionale). italian version of the epworth sleepiness scale: external validity. *Neurol Sci*, 26(3):295–300, 2003.
- [112] Buysse DJ, Reynolds CF, Monk TH, Berman SR, and Kupfer DJ. The pittsburgh sleep quality index: a new instrument for psychiatric practice and research. *Psychiatry Res*, 28(2):193–213, 1989.
- [113] Beck AT, Epstein N, Brown G, and Steer RA. An inventory for measuring clinical anxiety: psychometric properties. *J Consult Clin Psychol*, 56:893–897, 1988.
- [114] Beck AT, Ward CH, Mendelson M, Mock J, and Erbauch J. An inventory for measuring depression. *Arch Gen Psychiatry*, 4:561–71, 1961.

- [115] Horne JA and Ostberg O. A self-assessment questionnaire to determine morningness-eveningness in human circadian rhythms. *Int J Chronobiol*, 4(2):97–110, 1976.
- [116] Netzer NC, Stoohs RA, Netzer CM, Clark K, and Strohl KP. Using the berlin questionnaire to identify patients at risk for the sleep apnea syndrome. *Ann Intern Med*, 131(7):485–91, 1999.
- [117] International Commission on Non-Ionizing Radiation Protection. Icnirp (2013) guidelines on limits of exposure to incoherent visible and infrared radiation. *Health Phys*, 105(1):74–96, 2013.
- [118] Jenkinson M, Beckmann CF, Behrens TE, Woolrich MW, and Smith SM. Fsl. *Neuroimage*, 62:782–90, 2012.
- [119] Jenkinson M, Bannister P, Brady JM, and Smith SM. Improved optimisation for the robust and accurate linear registration and motion correction of brain images. *Neuroimage*, 17(2):825–41, 2002.
- [120] Ashburner J. Fast diffeomorphic image registration algorithm. *Neuroimage*, 38(1):95–113, 2007.
- [121] Johnson SC, Saykin AJ, Baxter LC, Flashman LA, Santulli RB, McAllister TW, and Mamourian AC. The relationship between fmri activation and cerebral atrophy: comparison of normal aging and alzheimer disease. *Neuroimage*, 11(3):179–87, 2000.
- [122] Oakes TR, Fox AS, Johnstone T, Chung MK, Kalin N, and Davidson RJ. Integrating vbm into the general linear model with voxelwise anatomical covariates. *Neuroimage*, 34:500–8, 2007.
- [123] Wang Z, Yan C, Zhao C, Qi Z, Zhou W, Lu J, He Y, and Li K. Spatial patterns of intrinsic brain activity in mild cognitive impairment and alzheimer’s disease: a resting-state functional mri study. *Hum Brain Mapp*, 32(10):1720–40, 2011.
- [124] Filippi M, Valsasina P, Misci P, Falini A, Comi G, and Rocca MA. The organization of intrinsic brain activity differs between genders: a resting-state fmri study in a large cohort of young healthy subjects. *Hum Brain Mapp*, 34:1330–43, 2013.
- [125] Premi E, Cauda F, Gasparotti R, Diano M, Archetti S, Padovani A, and Borroni B. Multimodal fmri resting-state functional connectivity in granulin mutations: the case of fronto-parietal dementia. *PLoS One*, 9(9):e106500, 2014.
- [126] Dukart J and Bertolino A. When structure affects function—the need for partial volume effect correction in functional and resting state magnetic resonance imaging studies. *PLoS One*, 9(12):e114227, 2014.
- [127] Grill-Spector K, Kourtzi Z, and Kanwisher N. The lateral occipital complex and its role in object recognition. . *Vision Res*, 41(10-11):1409–22, 2001.
- [128] Smith AT, Cotton PL, Bruno A, and Moutsiana C. Dissociating vision and visual attention in the human pulvinar. *J Neurophysiol*, 101(2):917–25, 2009.

- [129] Arcaro MJ, Pinsk MA, and Kastner S. The anatomical and functional organization of the human visual pulvinar. *J Neurosci*, 8:9848–71, 2015.
- [130] Zhou H, Schafer RJ, and Desimone R. Pulvinar-cortex interactions in vision and attention. *Neuron*, 89(1):209–20, 2016.
- [131] Owen AM, McMillan KM, Laird AR, and Bullmore E. N-back working memory paradigm: a meta-analysis of normative functional neuroimaging studies. *Hum Brain Mapp*, 25(1):46–59, 2005.
- [132] Procyk CA, Eleftheriou CG, Storchi R, Allen AE, Milosavljevic N, Brown TM, and Lucas RJ. Spatial receptive fields in the retina and dorsal lateral geniculate nucleus of mice lacking rods and cones. *J Neurophysiol*, 114(2):1321–30, 2015.
- [133] Barbiroli B, Montagna P, Cortelli P, Iotti S, Lodi R, Barboni P, Monari L, Lugaresi E, Frassinetti C, and Zaniol P. Defective brain and muscle energy metabolism shown by in vivo ³¹p magnetic resonance spectroscopy in nonaffected carriers of 11778 mtdna mutation. *Neurology*, 45:1364–1369, 1995.
- [134] Cortelli P, Montagna P, Avoni P, Sangiorgi S, Bresolin N, Moggio M, Zaniol P, Mantovani V, Barboni P, Barbiroli B, and Lugaresi E. Leber’s hereditary optic neuropathy: Genetic, biochemical, and phosphorus magnetic resonance spectroscopy study in an italian family. *Neurology*, 41:1211–15, 1991.
- [135] Friston KJ, Holmes AP, and Worsley KJ. How many subjects constitute a study? *Neuroimage*, 10(1):1–5, 1999.
- [136] Desmond JE and Glover GH. Estimating sample size in functional mri (fmri) neuroimaging studies: statistical power analyses. *J Neurosci Methods*, 118(2):115–28, 2002.
- [137] La Morgia C, Ross-Cisneros FN, Koronyo Y, Hannibal J, Gallassi R, Cantalupo G, Sambati L, Pan BX, Tozer KR, Barboni P, Provini F, Avanzini P, Carbonelli M, Pelosi A, Chui H, Liguori R, Baruzzi A, Koronyo-Hamaoui M, Sadun AA, and Carelli V. Melanopsin retinal ganglion cell loss in alzheimer disease. *Ann Neurol*, 79(1):90–109, 2016.

Acknowledgements

I would like to thank all the persons that made the realization of this project possible and gave their support at many different levels, from the conception of the project, to participants recruitment, from technical instrumentation setup to data acquisition and analysis.

Prof. Raffele Lodi, Prof Caterina Tonon, Dr. ssa Claudia Testa, Dr. David Neil Manners, Dr. Claudio Bianchini *Functional MR Unit, Policlinico S. Orsola-Malpighi, Bologna; Department of Biomedical and Neuromotor Sciences, University of Bologna*

Prof. Valerio Carelli, Dr. ssa Chiara La Morgia, *IRCSS Institute of Neurological Sciences of Bologna, Neurology Unit, Bellaria Hospital, Bologna; Department of Biomedical and Neuromotor Sciences, University of Bologna*

Dr. Gilles Vandewalle, *Cyclotron Research Centre, University of Liège*

We would like to acknowledge the financial support of Fondazione del Monte.